THE UNIVERSITY OF READING

DEPARTMENT OF MATHEMATICS

Higher Order Balance Conditions Using Hamiltonian Dynamics for Numerical Weather Prediction

by Steven James Fletcher

Dissertation submitted for the degree of

Doctor of Philosophy

Feb 2004

Acknowledgements

The first person I wish to thank is my mother, Christine, who without her continuous support, I would never have achieved so much.

My two sisters, Susan and Donna, I thank you for standing by me when things were bad. I also thank my niece Tyisha and the rest of my family.

Dr. Dave Stirling and Dr. Paul Glaister, I thank you both for taking a chance with me in 1995. I am also grateful for the teaching post that Dave recommended me for.

To my friends Cheryl, Karen, Gill, Dave, Steve, Philip and Grant you all saw me at my worst and helped me to recover. I am eternally grateful. To Annie, Liz, Bethan and especially Joy, thank you.

I would also like to thank Ros, you have been like a mum to me these last eight years.

I am grateful for all the support and advice from my supervisors Prof. Nancy Nichols and Dr. Ian Roulstone and thank them for this opportunity. I am also grateful for the advice from Dr. Amos Lawless, Dr. Marek Wlasak and Prof. Mike Baines.

I acknowledge the financial support that I have received from E.P.R.S.C. and the Met. Office.

Finally I dedicate this thesis to my Nan, Doris, who never saw it finished.

Table of Variables

Symbol	Meaning	Symbol	Meaning
ξ	Relative Vorticity	ξ^c	Constrained Relative Vorticity
Q	Potential Vorticity (PV)	Q_{sg}	Semi-Geostrophic PV
Q^c	Constrained PV	h	Height
ζ^c	Constrained Absolute Vorticity	δ	Divergence
ψ	Streamfunction	χ	Velocity Potential
$\mathbf{u}$	Horizontal Wind, $(u,v)^T$	$\mathbf{u}_g$	Geostrophic Wind, $(u_g,v_g)^T$
$\mathbf{u}^c$	Balanced Wind Field	$\bar{\mathbf{u}}_g$	Base State Geostrophic Wind
$\mathbf{u}'_g$	Perturbed Geostrophic Wind	w	Vertical Wind
Ω	Earth's Rotation Rate	f	Coriolis Parameter
f_0	Constant Coriolis Parameter	g	Gravity Acceleration
m	Mass	τ_i	Time Scales
t	Time	L_H	Horizontal Length Scale
V_H	Horizontal Velocity Scale	R_0	Rossby Number
L_R	Rossby Radius of Deformation	θ	Latitude
λ	Longitude	$\mathbf{x}$	Space Coordinates
$\mathbf{a}$	Particle Labels	a	Radius of the Earth
$\boldsymbol{X}$	Canonical Coordinates		

Contents

Chapter 1

Introduction

The process of modelling the Earth's atmosphere and the movement of weather systems is a large and complicated problem. The atmosphere is a non-linear system which becomes less predictable with time. Advancements in computing power and better understanding of the meteorology have made improvements in weather forecasting.

An advancement associated with the increasing computing power is in data assimilation. This process brings together observations and information from numerical models in a consistent way. In numerical weather prediction it is used as a means of providing representations of the weather but also initial conditions for atmospheric models to give accurate forecasts, [27].

The set of equations generally used to describe the evolution of the atmosphere are usually in terms of pressure, density, wind, temperature and

humidity. There are normally non-linear interactions between the variables, varying in time, [14], [17], [19], [34] and [56].

As an approximation to the atmosphere the 2-D non-linear shallow water equations on a rotating sphere are seen as a good choice. The equations support most of the motions that are present in the atmosphere and are the kernal of many atmospheric models, [55]. They describe the atmosphere as a thin layer of incompressible fluid defined on a 2-D surface with varying height and horizontal velocities, [19].

The atmosphere is continually adjusting towards an equilibrium state and as such the motions in the atmosphere are constrained, [34]. There is a broad spectrum of waves in the atmosphere; some travelling fast, such as sound waves, and those with slower motions, such as Rossby waves, [36]. The large-scale features are forced to travel more slowly due to the small amount of the total energy being used as kinetic energy, [34]. When these large-scale features are moving slowly then the quantities associated with them are said to be *balanced* with respect to each other. The fast waves are assumed to not have a direct effect on the large-scale flow.

As we have mentioned in this Introduction, data assimilation is a means of deriving a set of consistent initial conditions for the numerical models. It is desirable to have these initial conditions such that they will not excite spurious waves that introduce errors into the model.

The problem with data assimilation is the sparseness of observations of the atmosphere over certain areas of the Earth, mainly the oceans, does not provide initial conditions at the required operational resolution. This problem is overcome by using information about the atmospheric movements prior to the data assimilation and this requires the evaluation of the balanced and unbalanced parts of the flow. The decomposition is often referred to as a *control variable transform.*

Currently at the Met Office this decomposition is achieved by transforming the wind field, $\mathbf{u}$, into its rotational part, (relative vorticity), ξ, and divergent part, δ. From these there are two elliptic partial differential equations that are solved for a balanced stream function, ψ, given ξ and an unbalanced velocity potential, χ, given δ. The two variables, ψ and χ are the *control variables* where the third control variable is an unbalanced pressure and is calculated from the linear balance equation, [14].

This current decomposition only allows the flow that is rotational and divergence free to be considered as balanced. This is the case for certain types of flow, such as geostrophic flow on an f plane , but the atmosphere is not always in geostrophic balance.

Salmon in his three papers, [38], [39] and [41], through using Hamiltonian dynamics, is able to derive a sub-space in the phase space of the shallow water equations, this defines a balanced wind field that is divergent which

represents the semi-geostrophic part of the equations. Associated with this phase space is a set of canonical coordinates which turned out to be those derived by Hoskins in [21]. These coordinates have special features and have been used operationally, [15], but the semi-geostrophic equations are also seen as an important part of research in numerical weather modelling, [13], [45], [47] and [52].

McIntyre and Roulstone in [30] and [31] are able to extend the ideas derived by Salmon and are able to derive a relationship between the sub-space, (they refer to it as a constrained submanifold) and the canonical coordinates. The potential vorticity associated with the manifolds can be written as a Monge-Ampère equation between the canonical coordinates and the Lagrangian fluid particle coordinates.

If we consider the vertical component of the relative vorticity of the balanced wind field then this is related to the depth of the fluid by a Monge-Ampère equation for a balanced height. From this height we calculate the balanced wind field. This field is not divergence free, but is balanced as it defines the sub-space of the shallow water equations that does not excite the fast waves.

In this thesis we investigate this new wind field as a possible alternative for the current decomposition to rotational and divergent fields in the control variable transform. We start in Chapter 2 where we briefly introduce the

process of initialisation and the shallow water equations and summarise a method of initialising the equations so that the fast waves are not excited. We also introduce the time scale associated with the two types of motions and differentiate between *initialised* and *balanced*.

In Section 2.3 we introduce the 3-D primitive equations which are the set of equations regularly used to model the atmosphere and summarise a technique explained in [14] where we derive what is referred to as the ***non-linear balance equation***.

In Chapter 3 we introduce the basics of Hamiltonian dynamics, which are the tools that are used by Salmon, [38] [39] and [41], and McIntyre and Roulstone, [30] and [31], to derive a new expression for balanced wind fields. There are special properties associated with these fields and we review these also in Chapter 3 as well as summarising the wind field expressions including the two that we use for the research in this thesis. Associated with these balanced wind fields is a balanced height which we consider as a possible alternative for the current balanced variable in the Met Office's data assimilation scheme.

Because we are considering whether or not this new variable could be of any benefit in the Met Office's incremental data assimilation scheme, we derive the balanced wind field in spherical coordinates. We also require a linear equation for the height if this is to be used in the Met Office's

incremental VAR scheme. All of this is derived in Chapter 4, where we also introduce the spherical shallow water equations as these are the equations that we use to perform the numerical experiments with in Chapters 6 and 7.

The linearised equations that we derive are for a balanced height increment given either a relative vorticity (RV) or a potential vorticity (PV). In Section 4.4 we introduce a possible set of new control variables that would be associated with the balanced height.

As these are partial differential equations, there is theory associated with these problems that ensures that there are solutions to the equations. We introduce this theory and definition in Chapter 5 where we derive the condition necessary for the two differential equations to be elliptic for the continuous problem. We also introduce the theory for the discrete problem.

We also explain the numerical approximations that we apply to obtain the solutions to the elliptic equations and derive the approximations to calculate the new control variables as well as the new balanced wind field on the C grid. This is the grid that the Met Office's shallow water equations model runs on and is introduced in this chapter along with the Rossby-Haurwitz wave which we use in our idealised experiments. Finally in this chapter we introduce three test cases that we use throughout the remainder of the thesis.

In Chapter 6 we explain the experiments that we perform to test the ellipticity condition, which is the condition that ensures that there are solu-

tions to the elliptic equations, and compare these results with those from the constant coefficient equations to see if there is any extra information coming from the extra terms. We also perform a scale analysis at 72 hrs on the terms in the differential equation for the same reason.

The reason for these experiments is that the new equation requires a nine-point stencil to approximate it rather than the five-point for the Laplacian and as such if the Laplacian is the dominant term then it may not be economical to calculate the extra terms involving the variable coefficients. We also perform a scale analysis of the terms in the ellipticity conditions at 72 hrs to see if there are any terms that could be removed from the equations.

The second set of experiments involve the numerical solutions of the new elliptic equations where we consider, as a first choice, a zonal averaged base state and we examine the effects that this has when considered with the three test cases. We also test to see if the result about using the PV with a low Burger number flow regime, [57], carries over to the higher form of the PV that we derive in Chapter 4. We also test to see if the balanced wind field is divergent for a constant Coriolis parameter.

We finish the thesis with conclusions from the experiments and present suggestions for possible further work.

Chapter 2

Initialisation and Balance

As we mentioned in Chapter 1, there are large-scale movements in the atmosphere that are slow and the variables associated with these movements are said to be *balanced* with each other. In this chapter we give a more mathematical description of what is meant by *balanced* and *initialised* and we do this in the next section.

In Section 2.2 we introduce the shallow water equations in Cartesian coordinates and explain the motions that are present in this model. We also derive the potential vorticity, (PV), for the shallow water equations.

We then summarise a procedure derived by Hinkelmann and Phillips that defines a set of initial conditions for the shallow water equations that prevents the fast waves forming in the numerical solution.

In Section 2.3 we introduce the primitive equations and summarise a pro-

cedure to derive an initialisation that prevents the fast motions forming in the numerical solution. The result is a choice between two sets of conditions. The first is a set of initial conditions and the second is a Monge-Ampère equation that is referred to as a ***non-linear balance equation*** whose solution does not include the fast waves.

2.1 Atmospheric Motions

We begin with a quote from a letter that appears in [14] from Jule Charney to Phillip Thompson. Charney has the following description for the atmosphere:

" *We might say that the atmosphere is a musical instrument on which one can play many tunes. High notes are the sound waves, low notes are long inertial waves, and nature is a musician more of the Beethoven than of the Chopin type. He much prefers the low notes and only occasionally plays arpeggios in the treble and then only with a light hand. The oceans and the continents are the elephants in Saint-Saens' animal suite, marching in a slow cumbrous rhythm, one step every day or so. Of course, there are overtones; sound waves, billow clouds (gravity waves), inertial oscillations, etc., but these are unimportant.*"

In his 1955 paper, [7], Charney discusses the characteristics of atmospheric motion by making the following assumption: he assumes that the

atmosphere is statically stable, by this he is assuming that the horizontal scale, L_H, is larger than the vertical, L_Z. He takes L_Z to be of the order of one atmospheric height, 10km, and the horizontal scale to be 100km. The effect of this is that the atmospheric motions are in *quasi-hydrostatic balance* and are of planetary scale, [34].

A consequence of the hydrostatic assumption is that there are no sound waves and the equations that govern such an atmosphere are the primitive equations, which we introduce in Section 2.3.

In [14], Daley defines two types of time scales that are observed in this type of atmosphere. These are given by

$$\tau_1 = \frac{1}{f}, \qquad \tau_2 = \frac{L_H}{V_H}, \tag{2.1}$$

where f is the Coriolis parameter and V_H is a characteristic horizontal velocity. These two time scales are referred to as the 'inertial' and 'advective' time scales respectively. The Rossby number associated with these scales is given by the ratio

$$R_0 = \frac{\tau_1}{\tau_2} = \frac{V_H}{L_H f}. \tag{2.2}$$

In the atmosphere R_0 is usually small. This implies that the advective time scale is much larger that the inertial time scale. The time scale τ_1 is usually a few hours whereas τ_2 is considered to be longer than a day.

There are two kinds of atmospheric motions that can be identified as

normal modes of the primitive equations, linearised about a simple base state, [14]. The first kinds of motions are known as ***inertia-gravity waves*** and have time scales $\leq \tau_1$ with velocities of propagation considerably larger than V_H. The second kind of motions have time scales similar to τ_2 and velocity propagation similar to V_H. With a few exceptions, it is the motions of the second type that are of primary meteorological significance.

In the tropics we have $f \to 0$ and so τ_1 is almost the same order as τ_2 and therefore R_0 is no longer small. Thus at low latitudes we have the problem that inertia-gravity waves can not be separated from the other flows on the basis of the characteristic time scale.

The consequence is the motions where the advective time scales dominate the synoptic and planetary scales of the atmosphere and the inertia-gravity waves are considered to be a small part of the flow. It is the advective motions that are considered to be ***balanced***. The question is how do we model these balanced flows in our numerical models?

Later in Charney's letter there is a remark that the atmosphere is like a transmitter and the computers like the receivers. He assumes that the computer does not introduce any substantial noise. He goes on to say that the noise is coming from the input. To overcome this he says

"*Now there are two ways to eliminate the noise in the input. The first is to make sure that the input is free from objectionable noise, and the second*

is to employ a filtering system in the receiver. Translating, the first method implies that the unwanted harmonics shall be eliminated from the raw data by some type of harmonic analysis; the second that you transform the equations of motion and make the approximations in such a way that the bad harmonics are automatically eliminated."

Charney is saying that there are two methods in which to perform the numerical modelling to prevent inertia-gravity waves,

1. Integrate a model that does not permit inertia-gravity wave motion.

2. Integrate a primitive equations model but modify the initial state in such a way that the inertia-gravity waves are not excited.

It is the second method that is of interest in modern numerical weather prediction and is referred to as ***initialisation***.

2.1.1 Initialisation

The benefit of an initialisation to the primitive equations is that the initial conditions do not excite spurious inertia-gravity waves. In effect because the models only approximate the atmosphere, then the atmospheric multivariate relationships are not duplicated exactly. This results in inconsistent,

unbalanced initial conditions for the model and a large projection onto the inertia-gravity mode of the equations.

An important thing to note is the atmosphere cannot be initialised but can be in balance. Initialisation is a process and can result in a balanced set of initial conditions.

In the next section we look at a way of initialising the shallow water equations to prevent the formation of inertia-gravity waves that are supported in this model.

2.2 Shallow Water Theory

In this section we give a brief description of the shallow water model and the equations associated with this model. We also introduce the PV for this model and show that is materially invariant. Finally we give a review of an initialisation performed by Hinkelmann and Phillips to the shallow water equations.

2.2.1 Shallow Water Model

The underlying assumptions, as described in [34], for the shallow water model are that the flow is a sheet of fluid with constant and uniform density with a free surface height, h, where the fluid is assumed to be inviscid and in

rotation. The flow is also assumed to be incompressible. A diagram of the model is in Figure 2.1.

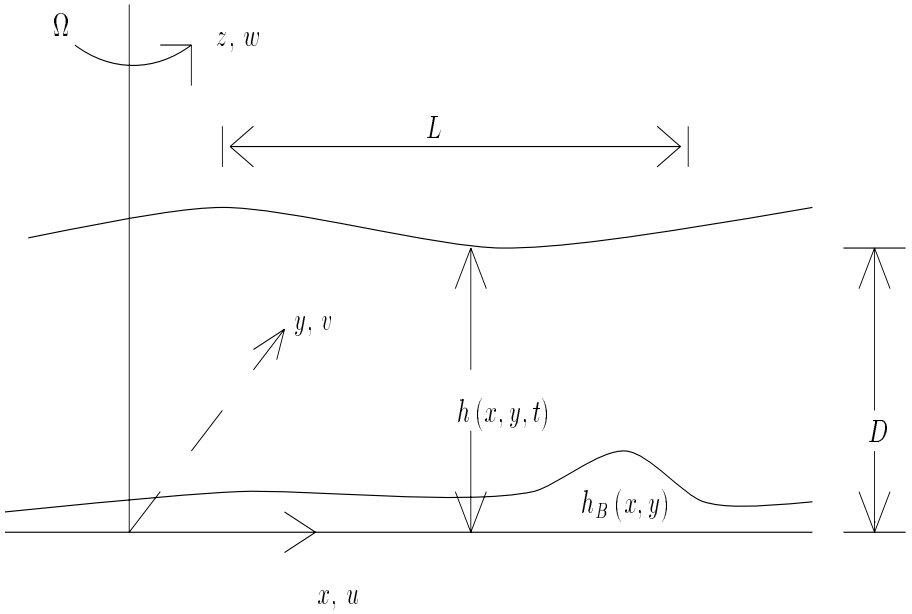

Figure 2.1: Diagram of the Shallow Water Model.

In Figure 2.1 the variable h is the height above a reference level $z = 0$ and is a function of the horizontal coordinates, x and y and time t, Ω is the rotation rate, u and v are the horizontal winds that are parallel to the horizontal coordinates, z is the vertical coordinate, w is the vertical wind which is parallel to the vertical axis, and h_B is the rigid bed of the fluid. Hence D is the depth, given by $h - h_B$, which does vary with time. For the scale analysis that allows us to consider these equations as a substitute for the atmosphere, we choose a sensible characteristic value. The characteristic horizontal length scale is given by L, and the parametric condition which

characterises shallow water theory is

$$\frac{D}{L} \ll 1. \tag{2.3}$$

Therefore we require the horizontal length scale to be considerably larger than the vertical scale.

2.2.2 Shallow Water Equations

The set of equations that govern this model is comprised of two momentum equations, one for each of the horizontal directions, and a continuity equation. These are given by

$$\frac{\partial u}{\partial t} + u\frac{\partial u}{\partial x} + v\frac{\partial u}{\partial y} - fv + g\frac{\partial h}{\partial x} = 0, \tag{2.4}$$

$$\frac{\partial v}{\partial t} + u\frac{\partial v}{\partial x} + v\frac{\partial v}{\partial y} + fu + g\frac{\partial h}{\partial y} = 0, \tag{2.5}$$

$$\frac{\partial h}{\partial t} + u\frac{\partial h}{\partial x} + v\frac{\partial h}{\partial y} + h\left(\frac{\partial u}{\partial x} + \frac{\partial v}{\partial y}\right) = 0, \tag{2.6}$$

where u is the wind component in the eastward direction, v is the wind component in the northward direction, h is the height of the free surface, g is the acceleration due to gravity and is taken to be $9.81ms^{-1}$, f is the Coriolis parameter, given by $2\Omega \sin\theta$, and θ is the angle of latitude. For the theory that is described in Section 2.2.3 we assume a constant value for f of f_0, this is referred to as the f-plane approximation, [34]. Equations (2.4) - (2.6) are

in their Eulerian form. The Lagrangian counterpart is given by

$$\frac{D\mathbf{u}}{Dt} + f\mathbf{k} \times \mathbf{u} = -g\nabla h, \tag{2.7}$$

$$\frac{Dh}{Dt} = -h\nabla \cdot \mathbf{u}, \tag{2.8}$$

where

$$\frac{D}{Dt} = \frac{\partial}{\partial t} + \mathbf{u} \cdot \nabla,$$

$\mathbf{k}$ is the z direction unit vector and $\nabla \cdot \mathbf{u}$ is the horizontal divergence.

An interesting feature of the shallow water equations, (SWE), is that the model supports gravity waves. The speed at which these waves travel is given by $c = \sqrt{gh}$. These waves will always break after a time of order $\frac{c}{U}$ where U is some typical flow speed.

Another variable that is associated with the shallow water model is the potential vorticity, (PV). We now derive the PV for the shallow water equations and show that it is materially invariant.

We start by considering the vertical component of the relative vorticity, (RV), as we are only working in two dimensions in the shallow water equations. This then is

$$\xi \equiv \mathbf{k} \cdot (\nabla \times \mathbf{u}) = \frac{\partial v}{\partial x} - \frac{\partial u}{\partial y}. \tag{2.9}$$

If we now take the curl of (2.7) then we obtain

$$\frac{D}{Dt}(\xi + f) + (\xi + f)\,\delta = 0, \tag{2.10}$$

where δ represents the horizontal divergence. Rearranging (2.8) we obtain

$$\delta = -\frac{1}{h}\frac{Dh}{Dt}. \tag{2.11}$$

Substituting (2.11) into (2.10) gives

$$\frac{D}{Dt}(\xi + f) - \frac{(\xi + f)}{h}\frac{Dh}{Dt} = 0. \tag{2.12}$$

This can be written in the form

$$\frac{D}{Dt}\left(\frac{\xi + f}{h}\right) = 0. \tag{2.13}$$

This last equation gives the information that the potential vorticity,

$$Q \equiv \frac{f + \xi}{h} = \frac{f + \frac{\partial v}{\partial x} - \frac{\partial u}{\partial y}}{h}, \tag{2.14}$$

is conserved following the motion of the vertical fluid columns. We will use the shallow water equations' potential vorticity in many of the following chapters but we now review an initialisation to the shallow water equations to stop the excitation of the gravity waves.

2.2.3 Initialisation of the Shallow Water Equations.

The initialisation that we summarise here is given in more detail in [14]. We start with the SWE in Cartesian coordinates, (2.4) - (2.6), and linearise about a constant wind, U, which is independent of x, y and t. There is also

a base state geopotential, $\bar{\Phi} = g\bar{h}$, which is only a function of y, where U is related to $\bar{\Phi}$ geostrophically through

$$U = -\frac{1}{f_0}\frac{\partial \bar{\Phi}}{\partial y}.$$

It is also assumed that the perturbations with respect to the velocity and the geopotential are only functions of x. When these assumptions are applied to equations (2.4) - (2.6) then the result is a much simpler set of equations.

Next stage in this process is to introduce the Helmholtz theorem that allows the wind field, $\mathbf{u}$, to be written in terms of derivatives of a stream function, ψ, and velocity potential, χ. This is given by

$$\mathbf{u} = \mathbf{k} \times \nabla\psi + \nabla\chi,$$

which in component form is

$$u = -\frac{\partial \psi}{\partial y} + \frac{\partial \chi}{\partial x}, \qquad v = \frac{\partial \psi}{\partial x} + \frac{\partial \chi}{\partial y}. \tag{2.15}$$

This can be used to write equations (2.4) - (2.6) in terms of ψ, χ and Φ. Next a wave solution is assumed for each of the three variables of the form

$$\begin{vmatrix} \psi(x,t) \\ \chi(x,t) \\ \Phi(x,t) \end{vmatrix} = \begin{vmatrix} \hat{\psi}_0(t) \\ \hat{\chi}_o(t) \\ \hat{\Phi}_0(t) \end{vmatrix} \exp\left[\frac{imx}{a} - \frac{iUmt}{a}\right], \tag{2.16}$$

where m is the x wave number, a is the radius of the Earth and the subscript denotes the variable at the initial time. These are then substituted into the

reduced equations and a Laplace transform is then applied to each of the three variables. The transfer function for χ is given by

$$L\left(\hat{\chi}\right) = \frac{\hat{\chi}_0\left(s^2 + s\left(f_0\hat{\psi}_0 - \hat{\Phi}_0\right)/\hat{\chi}_0 - if_0^2\sigma_2\hat{\psi}_0/\hat{\chi}_0\right)}{s^3 + sf_0^2\sigma_1^2 - if_0^3\sigma_2}, \tag{2.17}$$

where $i = \sqrt{-1}$, $\sigma_1 = \sqrt{1 + m^2\tilde{\Phi}/a^2f_0^2}$ and $\sigma_2 = Um/af_0$.

The σ_1 and σ_2 are nondimensional frequencies. The first being that of inertia-gravity wave frequency with time scale τ_1 and σ_2, that of the advective time scale, τ_2.

The denominator is then factorised so that the transform can be inverted using standard results for Laplace transforms. Hinkelmann and Phillips then make a simplification to the denominator by ignoring the term $if_0^3\sigma_2$ which is assumed to be small relative to the other two terms. The consequences of this are explained in [14].

The result for the inverse transform of (2.17) is

$$\begin{aligned}\hat{\chi}\left(t\right)e^{-if_0\sigma_2 t} = &\left(\frac{-i\sigma_2\hat{\psi}_0}{\sigma_1^2} + \left(\hat{\chi}_0 + \frac{i\sigma_2\hat{\psi}_0}{\sigma_1^2}\right)\cos f_0\sigma_1 t\right.\\ &\left. + \left(\frac{f_0\hat{\psi}_0 - \hat{\Phi}_0}{f_0\sigma_1}\right)\sin f_0\sigma_1 t\right)e^{-if_0\sigma_2 t}.\end{aligned} \tag{2.18}$$

This is a solution in the form of an inertia-gravity wave with characteristic frequency, σ_1, modulated by the slower advective frequency, σ_2. To prevent these gravity waves from forming then, there are two situations. The first is the degenerate case where a term in the reduced continuity equation is set

to zero. This removes the term $\frac{i\sigma_2\hat{\psi}_0}{\sigma_1^2}$ from (2.17) and in that case for there to be no inertia-gravity waves we must have the coefficients of the sine and cosine terms initially zero. This then gives the conditions

$$\hat{\chi}_0 = 0 \qquad \text{and} \qquad f_0\hat{\psi}_0 - \hat{\Phi}_0 = 0. \tag{2.19}$$

This condition is seen as a zeroth order initialisation state as it is saying that the initial state should be in geostrophic balance and that there should be a zero initial velocity potential.

If we now allow all the terms to stay in the reduced equations then this gives

$$\hat{\chi}_0 + \frac{i\sigma_2\hat{\psi}_0}{\sigma_1^2} = 0 \qquad \text{and} \qquad f_0\hat{\psi}_0 - \hat{\Phi}_0 = 0. \tag{2.20}$$

This is seen as a first order set of conditions, as we require more than just geostrophy and a zero initial velocity potential.

This then gives two different sets of initial conditions with which to start the numerical integration of the linearised shallow water equations that will not generate inertia gravity waves; the first, (2.19), is giving a set of non-divergent conditions whereas (2.20), is a set of divergent conditions, [14].

As we mentioned in Chapter 1, the shallow water equations provide an approximation to the movements in the horizontal direction in the atmosphere. These equations also support inertia-gravity waves and as such if we can remove these from the shallow water equations then we hope to also to re-

move these from the more sophisticated models in 3-D, namely the primitive equations, (PE) and we do this in the next section.

2.3 Primitive Equation Model

In the last section we summarised a technique to derive an initialisation to the 2-D non-linear shallow water equations to remove the inertia-gravity waves from the numerical model.

In this section we introduce the 3-D primitive equations and summarise a technique that initialises the PE such that the gravity waves are removed but also briefly look at the limitations of the method.

2.3.1 Primitive Equations

The primitive equations comprise of the equations of motion, (2.21), hydrostatic equation, (2.22), conservation of mass, (2.23), and the thermodynamic equation, (2.24). These are

$$\frac{\partial \mathbf{u}}{\partial t} + \mathbf{u}\cdot\nabla\mathbf{u} + \omega\frac{\partial \mathbf{u}}{\partial P} + f\mathbf{k}\times\mathbf{u} + \nabla\Phi = \mathbf{F}, \tag{2.21}$$

$$\frac{\partial \Phi}{\partial P} + \frac{RT}{P} = 0, \tag{2.22}$$

$$\nabla\cdot\mathbf{u} + \frac{\partial \omega}{\partial P} = 0, \tag{2.23}$$

$$\left(\frac{\partial}{\partial t} + \mathbf{u}\cdot\nabla\right)\frac{\partial \Phi}{\partial P} + \omega\Gamma = -\frac{RQ}{C_p P}, \tag{2.24}$$

where P is the pressure and is used as the vertical coordinate system, $\omega \equiv \mathrm{d}P/\mathrm{d}t$ is the vertical velocity, R is the gas constant, C_P is the specific heat at constant pressure, T is the temperature and Φ is the geopotential, $\mathbf{F}$, is the frictional force per unit mass, Q here is the time rate of heating per unit mass, Γ is the static stability, ∇ is the gradient operator as defined in Appendix A and $\mathbf{u} = (u, v)^T$ is the horizontal wind field.

Firstly we nondimensionalise (2.21)-(2.24) using the following scales

- L_H is the horizontal scale (m)
- L_Z is the vertical scale (m)
- Π is the vertical pressure scale (mb)
- V_H is the horizontal winds speed (ms^{-1})
- N_0 is the Brunt-Väisälä frequency (s^{-1})
- $\frac{L_H}{V_H}$ is the advective time scale (s)
- g is the gravitational constant (ms^{-2})

The variables are nondimensionalised as follows

$$\begin{aligned} \mathbf{u}^* = V_H^{-1}\mathbf{u}, \qquad \nabla^* &= L_H\nabla, \qquad t^* = V_H L_H^{-1} t, \\ (x^*, y^*) = L_H^{-1}(x, y), \qquad P^* &= \Pi^{-1}P, \qquad \omega^* = L_H\Pi^{-1}V_H^{-1}\omega. \end{aligned} \tag{2.25}$$

The Coriolis parameter is approximated through a beta-plane as defined in Pedlosky, [34], given by

$$f^* = \frac{f}{2\Omega} = \left(f_0^* + \frac{L_H}{a}\beta^* y^* \right), \tag{2.26}$$

where $f_0^* = \sin\theta_0$ and $\beta^* = \cos\theta_0$, where θ_0 is a reference latitude. Next Q and $\mathbf{F}$ are ignored to make the equations homogenous. This then gives

$$\frac{\partial \mathbf{u}^*}{\partial t} + \mathbf{u}^* \nabla \mathbf{u}^* + \omega \frac{\partial \mathbf{u}^*}{\partial P^*} + R_0^{-1} \left(\left(f_0^* + L_H a^{-1} \beta^* y^* \right) \mathbf{k} \times \mathbf{u}^* + \nabla^* \Phi^* \right) = 0, \tag{2.27}$$

$$\nabla^* \cdot \mathbf{u}^* + \frac{\partial \omega^*}{\partial P^*} = 0, \tag{2.28}$$

$$\left(\frac{\partial}{\partial t^*} + \mathbf{u} \cdot \nabla \right) \frac{\partial \Phi^*}{\partial P^*} + \frac{L_H^2}{R_0 L_H^2} \omega^* \tilde{\Gamma}^* + \omega^* \Gamma^* = 0, \tag{2.29}$$

where the Rossby number is given by

$$R_0 = \frac{V_H}{2\Omega L_H}, \tag{2.30}$$

and the Rossby radius of deformation is

$$L_R = \frac{N_0 L_Z}{2\Omega}. \tag{2.31}$$

Both of these two quantities are nondimensional.

Before we move onto the next step of the derivation we give a brief explanation of the quasi-geostrophic approximation that will be used in the analysis of the nondimensionalised equations, (2.27) - (2.29).

Holton, [17], derives the relationship that defines a flow to be *geostrophic* through applying a scale analysis to (2.21) using typical synoptic scales for

the mid-latitudes. The result is that the leading terms, in magnitude, are the Coriolis term and the geopotential gradients,

$$-fv \approx -\frac{\partial \Phi}{\partial x}, \qquad fu \approx -\frac{\partial \Phi}{\partial y}. \tag{2.32}$$

The two conditions in (2.32) are seen as first order approximations to the flow and is only valid for small Rossby numbers as explained in [17]. Therefore a flow is said to be *quasi-geostrophic* if the motion is nearly geostrophic.

To apply this approximation to (2.27) - (2.29) we require the parameters R_0, L_R and $\frac{L_H}{a} \ll 1$. If we consider

$$L_H = 10^6\text{m}, \quad L_Z = 10^4\text{m}, \quad V_H = 10\text{ms}^{-1}, \quad g = 10\text{ms}^{-2},$$

$$\Omega = 10^{-4}\text{s}^{-1}, \quad a = 10^7\text{m}, \quad N_0 = 10^{-2}\text{s}^{-1}, \quad L_R = 10^6\text{m},$$

to be typical values for the mid-latitudes, [14], then we see that the three parameters R_0, L_R and $\frac{L_H}{a}$ are around 0.1. We now introduce a small parameter, ε, that is the same magnitude as the Rossby number. This makes the three dimensionless numbers $O(\epsilon)$. We will use this information to initialise the model.

2.3.2 Quasi-Geostrophic Initialisation

Two possible methods to derive the quasi-geostrophic equations are; firstly expand the dependent variables u, v and Φ in an asymptotic series in terms

of the small parameter, ϵ. This is detailed in [34]. The second method uses a bounded derivative method as detailed in [4] and [24] but is also explained in [14]. It is the latter that we review here.

The method works by noticing that the scales that were chosen to nondimensionalise with have the time scale the size of the advective scale. Therefore the time derivatives are $O(1)$ and as such all subsequent time derivatives must be of the same order otherwise different time scales would be introduced. For the first time derivative to be $O(1)$ then the following must hold

$$\frac{\partial \Phi}{\partial x} - f_0 v = \varepsilon G_u(x, y, P, t), \tag{2.33}$$

$$\frac{\partial \Phi}{\partial y} + f_0 u = \varepsilon G_v(x, y, P, t), \tag{2.34}$$

$$\omega = \varepsilon G_\Phi(x, y, p, t), \tag{2.35}$$

where G_u, G_v and G_Φ are $O(1)$ functions. Then we introduce the Helmholtz theorem for the horizontal velocities and scale the divergent wind by ϵ,

$$\mathbf{u} = \mathbf{k} \times \nabla \psi + \epsilon \nabla \chi = \mathbf{u}_\psi + \epsilon \mathbf{u}_\chi. \tag{2.36}$$

The first order set of initial conditions to ensure motions of the advective scale is to set all terms that are $O(\epsilon)$ to zero. This gives

$$u = -\frac{1}{f_0}\frac{\partial \Phi}{\partial y}, \quad v = \frac{1}{f_0}\frac{\partial \Phi}{\partial x}, \quad \omega = 0. \tag{2.37}$$

The first two terms are the geostrophic balance given in (2.32).

To derive a higher order set of conditions, we require the second time derivatives of u, v and Φ to be order one functions in ϵ. After many manipulations, for more details see [14], the final outcome is a version of the ***non-linear balance equation***, given by

$$\nabla^2\Phi - f\xi = -\varepsilon\left(\beta u_\psi + \nabla\cdot(\mathbf{u}_\psi\cdot\nabla\mathbf{u}_\psi)\right), \tag{2.38}$$

where u_ψ is the u component of $\mathbf{u}_\psi$.

The important feature of this equation is that it relates the stream function to the geopotential, through a Monge-Ampère type equation, to prevent motions of the same size as the inertia-gravity waves forming in the model. Therefore the initial data that satisfy (2.38) is balanced and integrating a primitive equations model with this data will not excite gravity waves.

We now consider briefly the limitations of the quasi-geostrophic initialisations to both the shallow water and primitive equations models before a final summary of the whole chapter.

2.3.3 Limitations of Quasi-Geostrophic Initialisation

The scaling that was performed to the primitive equations assumed mid-latitudinal values for the variables and as such ensured that the Rossby number was small. A result of this was that the flow was nearly geostrophic.

This meant

$$R_0 = \frac{V_H}{2\Omega L_H}, \qquad \frac{L_H}{a}, \qquad \frac{R_0 L_H^2}{L_R^2},$$

were order ε. The main problem occurs when we start to enter the lower latitudes and the Rossby number is growing and as such the rotational flow associated with geostrophic flows is not correctly modelling the flow here. This restrains this type of initialisation to the mid-latitudes for best results.

2.4 Summary

In this chapter was we have introduced the motivation and techniques for the removal of inertia-gravity waves from either a shallow water or primitive equations model.

There were two different techniques used to derive the initialisation. The first uses a Laplace transform and the other a bounded derivative method. The main result that arose from both approaches was that a simple geostrophic condition would prevent the fast motions but this is often felt to be too severe a restriction, [35].

Applying the bounded derivative method to the non-dimensionalised primitive equations resulted in a non-linear partial differential equation whose solution is considered 'balanced' and as such if used in the model will not excite the gravity waves.

In the next chapter we consider a different approach to this problem by considering Hamiltonian dynamics and derive a different non-linear partial differential equation that also prevents these fast motions.

Chapter 3

Balance Via Hamiltonian Dynamics

In the previous chapter we reviewed two initialisation techniques: one for the shallow water equations and the other for the primitive equations. For the primitive equations the process resulted in a non-linear balance equation, (2.38), where the stream function was related to the geopotential through a Monge-Ampère equation.

In this chapter we review other mathematical techniques to derive a balance equation. We start by introducing the basics of Hamiltonian dynamics, which will be used to derive a different balance equation. We then show how the shallow water equations can be derived in Hamiltonian dynamics through a variational principle. This is important as from this different balance equa-

tions are derived.

We then move onto a higher order balance from geostrophy to semi-geostrophy where we review the consequences of semigeostrophy and define a new version for the semi-geostrophic PV in terms of a new form for the horizontal wind field derived by Roulstone and Sewell in [37]. We then review briefly the geostrophic coordinates discovered by Hoskins in 1975, [21]. In the next section we give a brief summary of the results by Salmon from the three papers, [38], [39] and [41], where he makes approximations to the Lagrangian that describes the shallow water equations in order to derive a set of balance conditions.

The final section is a review of the work by McIntyre and Roulstone, [30] and [31], where they extend the ideas by Salmon to define a balanced wind field, $\mathbf{u}^c$, which captures the balanced divergent flow. They also define an extension to the geostrophic coordinates. It is from these $\mathbf{u}^c$ that we are able to define a different balance equation which the remainder of the thesis is concerned with.

3.1 Hamiltonian Dynamics

We start by considering the shallow water equations by considering a fluid as a continuum, which is a continuous distribution of mass in space, [40].

There are two different ways of describing the continuum motion. The first is the Eulerian where the independent variables are the space coordinates, $\boldsymbol{x} = (x, y)$, and the time, t. The dependent variables are the height field, $h(x, y, t)$, and the velocities, $\mathbf{u}(x, y, t)$.

In the Lagrangian description, the independent variables are a set of particle labels $\mathbf{a} = (a, b)$, and the time τ. The dependent variables are the coordinates

$$x(a, b, \tau), \quad y(a, b, \tau), \tag{3.1}$$

at time τ, of the fluid parcel identified by (a, b). The particle labels vary continuously throughout the fluid, but the values of (a, b) on each fluid particle remain fixed as the fluid particle moves from place to place. Also the use of τ to denote time is to make clear that $\partial/\partial\tau$ means (a, b) are being held fixed. For the Eulerian description $\partial/\partial t$ means that (x, y) are held fixed.

A way to view these descriptions is to think of a label space with coordinates (a, b) and a location space with coordinates (x, y). The fluid motion is a time dependent mapping between these two spaces.

The derivative with respect to Eulerian and Lagrangian coordinates are related by the chain rule

$$\frac{\partial F}{\partial \tau} = \frac{\partial F}{\partial t}\frac{\partial t}{\partial \tau} + \frac{\partial F}{\partial x}\frac{\partial x}{\partial \tau} + \frac{\partial F}{\partial y}\frac{\partial y}{\partial \tau}, \tag{3.2}$$

where F is a function of (x, y, t) or (a, b, τ). This leads to

$$\frac{\partial F}{\partial \tau} = \frac{\partial F}{\partial t} + u\frac{\partial F}{\partial x} + v\frac{\partial F}{\partial y} = \frac{\partial F}{\partial t} + \mathbf{u} \cdot \nabla F. \tag{3.3}$$

which is the form used in Section 2.2.1. A detailed derivation is given in [42].

With the basic description of fluid motions described here in terms of Lagrangian and Eulerian framework we now show how these are used in derivation of motions using Hamilton's principle.

3.1.1 Hamilton's Principle

Hamilton's principle states that the *action*

$$A \equiv \int_{t_1}^{t_2} L \mathrm{d}t, \tag{3.4}$$

is stationary, where L is called the *Lagrangian* and is given by

$$L \equiv T - V, \tag{3.5}$$

where T is the kinetic energy and V is the potential energy. We will briefly give two examples of how this is formulated. The first is for a system comprised of point masses and the second a fluid continuum.

For the first example we consider a system composed of N point-particles each with masses, m_i, $(i = 1 \text{ to } N)$, and locations, $\mathbf{x}_i\,(t)$. Now let $V\,(\mathbf{x}_1, \ldots, \mathbf{x}_N)$ be the potential energy of the system. The kinetic energy is given by

$$T = \frac{1}{2}\sum_{i=1}^{N} m_i \frac{\mathrm{d}\mathbf{x}_i}{\mathrm{d}t} \cdot \frac{\mathrm{d}\mathbf{x}_i}{\mathrm{d}t}. \tag{3.6}$$

Hamilton's principle states that the first variation of the action, δA, satisfies

$$\delta A \equiv \delta \int_{t_1}^{t_2} \left(\frac{1}{2} \sum_{i=1}^{N} m_i \frac{\mathrm{d}\mathbf{x}_i}{\mathrm{d}t} \cdot \frac{\mathrm{d}\mathbf{x}_i}{\mathrm{d}t} - V \right) \mathrm{d}t = 0, \tag{3.7}$$

for arbitrary, independent variations $\{\delta x_i(t), \delta y_i(t)\}$ that vanish at t_1 and t_2. Therefore we must have $\delta \mathbf{x}_i(t_1) = \delta \mathbf{x}_i(t_2) = 0$. From applying variational techniques we obtain

$$0 = \int_{t_1}^{t_2} \left(-m_i \frac{\mathrm{d}^2 \mathbf{x}_i}{\mathrm{d}t^2} - \frac{\mathrm{d}V}{\mathrm{d}\mathbf{x}_i} \right) \cdot \delta \mathbf{x}_i \mathrm{d}t. \tag{3.8}$$

As a result of the arbitrariness of the variations the quantity inside the brackets must be zero. The result is Newton's second law.

For the second example we consider a barotropic fluid. The difference between the system of point masses and the fluid continuum is that the masses are distributed continuously in space in the continuum. Therefore, instead of a summation to represent the masses we have

$$\iiint \mathrm{d}m = \iiint \mathrm{d}a\mathrm{d}b\mathrm{d}c, \tag{3.9}$$

as derived in [42]. The kinetic energy is given by

$$T = \frac{1}{2} \iiint \mathrm{d}a\mathrm{d}b\mathrm{d}c \frac{\partial \mathbf{x}}{\partial \tau} \cdot \frac{\partial \mathbf{x}}{\partial \tau}. \tag{3.10}$$

For the potential energy we assume that this arises from external and interparticle forces that depend on the particle location $\mathbf{x}(a, b, c, \tau)$. The potential energy is

$$V = \iiint \mathrm{d}a\mathrm{d}b\mathrm{d}c \left(E(\alpha) + \phi(\mathbf{x}) \right), \tag{3.11}$$

where α is the specific volume and is given by

$$\alpha \equiv \frac{1}{\rho} = \frac{\partial(x,y,z)}{\partial(a,b,c)} = \begin{vmatrix} \frac{\partial x}{\partial a} & \frac{\partial x}{\partial b} & \frac{\partial x}{\partial c} \\ \frac{\partial y}{\partial a} & \frac{\partial y}{\partial b} & \frac{\partial y}{\partial c} \\ \frac{\partial z}{\partial a} & \frac{\partial z}{\partial b} & \frac{\partial z}{\partial c} \end{vmatrix} = \frac{\partial(\mathbf{x})}{\partial(\mathbf{a})},$$

ρ is the density and $E(\alpha)$ is the specific internal energy and is a function of α, and $\phi(\mathbf{x}(\mathbf{a},t))$ is the external potential and is dependent on the fluid-particle locations.

This then gives the *action* for this system as

$$\int \mathrm{d}\tau\,(T-V) = \int \mathrm{d}\tau \iiint \mathrm{d}\mathbf{a}\left(\frac{1}{2}\frac{\partial \mathbf{x}}{\partial \tau}\cdot\frac{\partial \mathbf{x}}{\partial \tau} - E\left(\frac{\partial(\mathbf{x})}{\partial(\mathbf{a})}\right) - \phi(\mathbf{x}(\mathbf{a},\tau))\right), \tag{3.12}$$

which must be stationary with respect to the arbitrary variations $\delta\mathbf{x}(a,b,c,\tau)$, in the location of the fluid particles. A full derivation of the resulting equations can be found in [42].

We now extend these ideas to the shallow water equations, where in the next section we will define the Lagrangian for the shallow water equations as shown in [39] and derive the shallow water equations from this.

3.2 Hamiltonian Form for the Shallow Water Equations

In Salmon's 1983 and 1985 papers, [38] and [39], he shows that Hamilton's principle for a mechanical system with N degrees of freedom can be written in the form

$$\delta \int \mathrm{d}\tau \left(\sum_i p_i \frac{\partial q_i}{\partial \tau} - H\left(q_1, p_1, \ldots, q_N, p_N\right) \right) = 0, \tag{3.13}$$

where the variables q_i are the generalised coordinates, p_i are the corresponding momenta, H is the Hamiltonian and δ denotes the first variation with respect to the arbitrary variations

$$\delta q_i\left(\tau\right), \quad \delta p_i\left(\tau\right),$$

at fixed time τ.

We are considering the shallow water equations as a layer of inviscid homogeneous fluid. We are using the definition for the height as the Jacobian of the mapping between the particle labels and the coordinates such that the conservation of mass is given by

$$\mathrm{d}a\mathrm{d}b = \frac{\mathrm{d}m}{\rho} = h\mathrm{d}x\mathrm{d}y, \tag{3.14}$$

where

$$h = \frac{\partial\left(a,b\right)}{\partial\left(x,y\right)} = \begin{vmatrix} \frac{\partial x}{\partial a} & \frac{\partial x}{\partial b} \\ \frac{\partial y}{\partial a} & \frac{\partial y}{\partial b} \end{vmatrix}. \tag{3.15}$$

In [38] the Lagrangian for the shallow water momentum equations is given by

$$L = \int\int \mathrm{d}a\mathrm{d}b \left((u - R) \frac{\partial x}{\partial \tau} + (v + P) \frac{\partial y}{\partial \tau} \right) - H, \tag{3.16}$$

where H is the *Hamiltonian* and is given by

$$H = \frac{1}{2} \int\int \mathrm{d}a\mathrm{d}b \left(u^2 + v^2 + gh \right), \tag{3.17}$$

and the functions $R(x, y)$ and $P(x, y)$ are representing the effect of rotation and have the property

$$\frac{\partial R}{\partial y} + \frac{\partial P}{\partial x} = f(x, y), \tag{3.18}$$

where f is the Coriolis parameter. Applying variations to x, y, u and v results in the following Euler-Lagrange equations

$$\delta x \quad : \quad \frac{\partial u}{\partial \tau} - f \frac{\partial y}{\partial \tau} = -g \frac{\partial h}{\partial x}, \tag{3.19}$$

$$\delta y \quad : \quad \frac{\partial v}{\partial \tau} + f \frac{\partial x}{\partial \tau} = -g \frac{\partial h}{\partial y}, \tag{3.20}$$

$$\delta u \quad : \quad u = \frac{\partial x}{\partial \tau}, \tag{3.21}$$

$$\delta v \quad : \quad v = \frac{\partial y}{\partial \tau}. \tag{3.22}$$

Substituting equations (3.21) and (3.22) into (3.19) and (3.20) and recalling (3.3) then (3.19) and (3.20) are the shallow water momentum equations, (2.4) and (2.5) respectively. The continuity equation arises from applying a variation to h in (3.16) given (3.17).

We shall return to the shallow water Lagrangian in Section 3.4 but we first describe an approximation made to (3.19) and (3.20). This approximation results in the *semi-geostrophic equations*. We look at this approximation in the next section and review certain properties that arise from this and extended these in Section 3.5.

3.3 Semi-Geostrophic Theory

In this section we will look at how the semi-geostrophic equations are derived from (3.19) and (3.20). We also look at the PV that is associated with these equations. We then give a review of the geostrophic coordinates that were devised by Hoskins, [21]. We finish this section with a summary of the Monge-Ampère equation that connects the Cartesian and geostrophic coordinates.

3.3.1 Semi-Geostrophic Approximation

We start by noticing that the equations (3.19) and (3.20) can be written in terms of $(\ddot{x}, \ddot{y})$, where $(\dot{})$ represents $\frac{\partial}{\partial \tau}$. This then enables (3.19) and (3.20) to be written as

$$\ddot{x} + g\frac{\partial h}{\partial x} - \dot{y}f = 0, \quad \ddot{y} + g\frac{\partial h}{\partial y} + \dot{x}f = 0. \tag{3.23}$$

The semi-geostrophic approximation is to replace the acceleration terms, $(\ddot{x}, \ddot{y})$, with the material derivatives of $\mathbf{u}_g = (u_g, v_g)$, which are the geostrophic

winds, (2.32). This then leads to the equations

$$\dot{u}_g + g\frac{\partial h}{\partial x} - \dot{y}f = 0, \quad \dot{v}_g + g\frac{\partial h}{\partial y} + \dot{x}f = 0. \tag{3.24}$$

These are referred to as the semi-geostrophic equations when they are combined with the continuity equation, (2.6).

This system has the Hamiltonian

$$\mathrm{H} = V + \int_{\mathcal{D}} \frac{1}{2}|\mathbf{u}_g|^2 \mathrm{d}m, \tag{3.25}$$

where $\mathcal{D}$ is the domain of interest and $\mathrm{d}m$ is the mass element, and

$$V = \int_{\mathcal{D}} \frac{1}{2} gh \mathrm{d}m, \tag{3.26}$$

is the potential energy of the mass configuration. There is a conserved quantity like potential vorticity associated with this model, which is given by

$$Q_{sg} = \frac{1}{h}\left(f + \frac{\partial v_g}{\partial x} - \frac{\partial u_g}{\partial y} + \frac{1}{f}\frac{\partial\left(u_g, v_g\right)}{\partial\left(x, y\right)}\right). \tag{3.27}$$

This potential vorticity is materially invariant i.e. $\frac{DQ_{sg}}{Dt} = 0$, [31].

3.3.2 Geostrophic Coordinates

Hoskins in his paper in 1975, [21], shows that the semi-geostrophic equations, (3.24), could be simplified through the following variable transform

$$X = x + \frac{\partial \phi}{\partial x}, \quad Y = y + \frac{\partial \phi}{\partial y}, \tag{3.28}$$

where ϕ is defined by

$$\phi(x,y,t) = \frac{g}{f^2} h(x,y,t). \tag{3.29}$$

This choice of ϕ enables us to write the definition of geostrophic winds, (2.32), as

$$u_g = -f\frac{\partial \phi}{\partial y}, \quad v_g = f\frac{\partial \phi}{\partial x}. \tag{3.30}$$

This transformation, $\boldsymbol{x} \mapsto \boldsymbol{X}$, is referred to as the geostrophic momentum transformation and when we assume f is constant then (X, Y) are referred to as the momentum coordinates and have the property

$$\dot{X} = u_g, \quad \dot{Y} = v_g. \tag{3.31}$$

When $h(x,y,t)$, or corresponding $\phi(x,y,t)$, is regarded as a known function of x, y with t fixed, then (3.28) specifies a transformation,

$$X = X(x,y,t), \quad Y = Y(x,y,t) \quad (t \text{ fixed}), \tag{3.32}$$

which at each time step is assumed to have an inverse of the form

$$x = x(X,Y,t), \quad y = y(X,Y,t). \tag{3.33}$$

We introduce a new variable dependent on the new coordinates,

$$\Phi(X,Y,t) = \phi + \frac{1}{2}(X-x)^2 + (Y-y)^2. \tag{3.34}$$

This has the derivatives

$$\frac{\partial \Phi}{\partial X} = \frac{\partial \phi}{\partial x} = X - x, \quad \frac{\partial \Phi}{\partial y} = \frac{\partial \phi}{\partial y} = Y - y. \tag{3.35}$$

This then enables us to write the material derivative of the geostrophic coordinates in terms of Φ as

$$\dot{X} = -f\frac{\partial \Phi}{\partial Y}, \quad \dot{Y} = f\frac{\partial \Phi}{\partial X}. \tag{3.36}$$

It is shown in [31] that

$$\begin{aligned} Q_{sg} &= \frac{1}{h}\left(f + \frac{\partial v^g}{\partial x} - \frac{\partial u^g}{\partial y} + \frac{1}{f}\frac{\partial\left(u^G, v^G\right)}{\partial\left(x, y\right)}\right) \\ &= \frac{g}{f\psi}\left(\frac{\partial X}{\partial x}\frac{\partial Y}{\partial y} - \frac{\partial X}{\partial y}\frac{\partial Y}{\partial x}\right) \\ &= \frac{g}{f^2\phi}\frac{\partial\left(X, Y\right)}{\partial\left(x, y\right)} > 0, \end{aligned} \tag{3.37}$$

Therefore we are able to obtain the PV in terms of the new coordinates, but in the form of a Jacobian. This means that the semi-geostrophic evolution can be described in terms of this Jacobian.

In the next subsection we look at the mathematical form of the equation that is defining the PV and the conditions for its solution.

3.3.3 Monge-Ampère Equations

In the previous subsection we summarised the derivation of the PV in terms of the geostrophic coordinates. The result was that the PV could be written as the Jacobian of the mapping between the two coordinate systems, (3.37).

The original equation for the PV, (3.27), when the definitions for the

geostrophic winds are substituted in, gives

$$Q_{sg} = \frac{1}{h}\left(f + \left(\frac{\partial^2\phi}{\partial x^2} + \frac{\partial^2\phi}{\partial y^2}\right) - \frac{1}{2f}\left(\frac{\partial^2\phi}{\partial x^2}\frac{\partial^2\phi}{\partial y^2} - \left(\frac{\partial^2\phi}{\partial x \partial y}\right)^2\right)\right). \tag{3.38}$$

This partial differential equation is referred to as a ***Monge-Ampère Equation***. There is a condition on the equation to ensure solvablility but first we give the general form of the Monge-Ampère equation as expressed in [31] and then give this condition.

The general form of the Monge-Ampère equation is

$$A + Br + 2Cs + Dt + E\left(rt - s^2\right) = 0, \tag{3.39}$$

where for (x, y) space we can define p, q, r, s and t to be

$$p = \frac{\partial\phi}{\partial x},\ \ q = \frac{\partial\phi}{\partial y},\ \ r = \frac{\partial^2\phi}{\partial x^2},\ \ s = \frac{\partial^2\phi}{\partial x \partial y},\ \ t = \frac{\partial^2\phi}{\partial y^2}, \tag{3.40}$$

where A, B, C, D and E are given functions of (x, y, ϕ, p, q). It must be noted that p and q are the general notation used in [31]. The solvability condition for non-linear second order partial differential equations is

$$BD - C^2 - AE > 0, \tag{3.41}$$

and is referred to as the ellipticity condition, [31]. This comes from the following theorem, [11].

Theorem 1 *The non-linear Monge-Ampère equation, (3.39), has at most two solutions in the interior of the domain and satisfies the boundary condi-*

tions if

$$BD - C^2 - AE > 0,$$

and the coefficients in (3.39) are all continuous in the domain.

Returning to (3.38) then, after we have multiplied throughout by $\frac{h}{f}$, we have the following coefficients $B = D = 1, C = 0, E = 1$ and $A = 1 - \frac{Q_{sg}h}{f}$. Then evaluating (3.41) gives us the condition $Q_{sg} > 0$ which was assumed in Section 3.3.2. In [31] they derive the condition for the transformed variable and arrive at the same condition for the PV.

In Section 3.5 we derive another Monge-Ampère equation whose solutions gives a balanced height field. Before this we return to the Hamiltonian dynamics to explain a series of approximations to the shallow water Lagrangian that were performed by Salmon, [38], [39], which results in an initialisation through Hamiltonian dynamics.

3.4 Salmon's L_0 and L_1 Dynamics

In Section 3.2 we introduced the Lagrangian for the shallow water equations, (3.16), as derived in [38]. We now summarise two approximations that Salmon makes to this functional which result in sets of initial conditions for the shallow water equations, and yet have a Hamiltonian structure associated

with them. We start with what Salmon refers to as L_0 dynamics, [38] and [39].

3.4.1 L_0 Dynamics

Salmon is concerned with approximations to (3.16). The first approximation that he makes is to set $u = v = 0$. He labels this L_0, where L_0 is given by

$$L_0 = \int\int \mathrm{d}a\mathrm{d}b \left(-R\left(x,y\right)\frac{\partial x}{\partial \tau} + P\left(x,y\right)\frac{\partial y}{\partial \tau} - \frac{g}{2}\frac{\partial\left(a,b\right)}{\partial\left(x,y\right)} \right), \tag{3.42}$$

which is only dependent on the particle locations. If we now apply variations to x, y and h we obtain

$$\begin{aligned} \delta x \quad &: \quad -f\frac{\partial y}{\partial \tau} = -g\frac{\partial h}{\partial x}, \\ \delta y \quad &: \quad f\frac{\partial x}{\partial \tau} = -g\frac{\partial h}{\partial y}. \end{aligned}$$

Through the set up of the dynamics, the conservation of mass is implicit and so the resulting dynamical equations are

$$-fv = -g\frac{\partial h}{\partial x}, \tag{3.43}$$

$$fu = -g\frac{\partial h}{\partial y}, \tag{3.44}$$

$$\frac{\partial h}{\partial t} + \frac{\partial}{\partial x}\left(uh\right) + \frac{\partial}{\partial y}\left(vh\right) = 0, \tag{3.45}$$

where the last equation arises from δh. As Salmon comments in [39], we have neglected the relative accelerations, which he sees as too severe to model

geophysical fluid dynamics. He suggests not dropping the wind field but to replace them with the geostrophic winds. He labels this approximation L_1.

3.4.2 L_1 Dynamics

We return to the full Lagrangian for the shallow water equations, where Salmon now uses the geostrophic winds, (u_g, v_g), which are dependent on the height field, as an approximation to the full wind fields. The resulting Lagrangian is labelled L_1 and is given by

$$L_1 = \int\int \mathrm{d}a\mathrm{d}b \left((u_g - R) \frac{\partial x}{\partial \tau} + (v_g + P) \frac{\partial y}{\partial \tau} - \frac{1}{2} \left(u_g^2 + v_g^2 + g \frac{\partial (a,b)}{\partial (x,y)} \right) \right). \tag{3.46}$$

L_1 is still dependent only on the particle locations as the geostrophic winds are determined by the mass distribution.

To apply Hamilton's principle to L_1, Salmon introduces variations to x, y, u_g, v_g, h, R and P. Substituting these quantities into (3.46) and ignoring terms of $O(\delta^2)$ gives

$$\int\int \mathrm{d}a\mathrm{d}b \, (u_g - R) \frac{\partial \delta x}{\partial \tau} + (v_g + P) \frac{\partial \delta y}{\partial \tau} - \dot{x}\delta R + \dot{y}\delta P + (\dot{\mathbf{x}} - \mathbf{u}_G) \cdot \delta \mathbf{u}_g - \frac{1}{2} g \delta h. \tag{3.47}$$

Salmon now introduces the ageostrophic velocity, which he defines to be

$$\mathbf{u}_{ag} \equiv \frac{\partial \mathbf{x}}{\partial \tau} - \mathbf{u}_g. \tag{3.48}$$

The next step is to integrate (3.47) and then substitute (3.48). This then results in

$$\int\int \left(-\dot{u}_g + f\dot{y}\right)\delta x + \left(-\dot{v}_g - f\dot{x}\right)\delta y + \mathbf{u}_{ag}\cdot\delta\mathbf{u}_g - \frac{1}{2}g\delta h. \tag{3.49}$$

The final stage of the derivation to the equations is shown in Appendices A and B in [39]. The resulting equations in an Eulerian framework are the momentum equations

$$h\left(\frac{\partial}{\partial t}\mathbf{u}_g + \mathbf{u}_g\cdot\nabla\mathbf{u}_g + \mathbf{u}_{ag}\cdot\nabla\mathbf{u}_g + \mathbf{u}_{ag}\cdot\nabla\mathbf{u}_g\right) + f\mathbf{k}\times h\left(\mathbf{u}_g + \mathbf{u}_{ag}\right) + g\nabla\left(\frac{1}{2}h^2\right)$$
$$= -g\nabla\left(h^2\mathbf{k}\cdot\nabla\times\left(\frac{\mathbf{u}_{ag}}{f}\right)\right) - g\nabla\left(\frac{1}{2}h^2\right)\left(\mathbf{u}_{ag}\times\nabla\left(\frac{1}{f}\right)\right)\cdot\mathbf{k}, \tag{3.50}$$

and a continuity equation

$$\frac{\partial h}{\partial t} + \nabla\cdot\left(\left(\mathbf{u}_g + \mathbf{u}_{ag}\right)h\right) = 0. \tag{3.51}$$

To simplify equations (3.50) and (3.51) Salmon uses the information that every Hamiltonian system is precisely defined by the two geometrical objects: the Poisson-bracket operator and the Hamiltonian itself, [39], [41]. We will not go into how Salmon manages to derive the results but there is a full explanation in [39].

Salmon notices that it is possible to define a set of canonical coordinates that enables the Poisson-bracket operator to take its simplest form. He then applies these coordinates to the shallow water Lagrangian and then applies the variations with respect to these coordinates. The result is the coordinates

derived by Hoskins, [21], and the resulting dynamical equations are the semi-geostrophic equations in 2-D for a constant f, which show that the potential vorticity for these equations, (3.27), is conserved.

One final remark from [39] is the description that Salmon has for the reduced dynamics. Salmon says that the approximations $L \approx L_0$ and $L \approx L_1$ can be viewed as projections of the fluid state vector in the infinite dimensional phase space spanned by $\{x, y, u, v\}$ onto the subspace spanned by $\{x, y\}$. For L_0 the projected coordinates $\{u, v\}$ are set to zero whereas for L_1 these are replaced by the geostrophic values, (u_g, v_g).

In [41] Salmon gives a mathematical interpretation for the approximations that he has applied. In the paper he shows that the semi-geostrophic approximation is a specific projection onto the phase space manifold corresponding to geostrophic balance. Associated with these is a set of canonical coordinates. He goes on to derive the expression for the balanced part of the phase space in terms of the approximation to the wind field, $\mathbf{u}$, and he shows that for the semi-geostrophic approximation the subspace in the phase space is given by

$$\mathbf{u}_s^c \equiv \mathbf{u}_g - \frac{1}{2f} \left(\mathbf{u}_g \cdot \nabla\right) \left(\mathbf{k} \times \mathbf{u}_g\right). \tag{3.52}$$

In [41], Salmon comments that it would be possible to make further approximations of higher order to the wind field that would also have a subspace

associated with them. McIntyre and Roulstone extend this theory from the semi-geostrophic subspace to link the coordinates with the subspace, [30] and [31]. We summarise their work in the next section.

3.5 McIntyre and Roulstone

In the previous section we summarised the work undertaken by Salmon in [38], [39] and [41]. The important result that arises from these papers is the ability to define a subspace in the phase space of the shallow water equations that captures the balanced flow.

Salmon found that for the shallow water equations the semi-geostrophic equations could be found from applying the canonical coordinates that Hoskins found, (3.28), to (3.16). From this he was able to find the expression that defined the subspace in the phase space, (3.52). He commented that there is a family of these subspaces depending on the type of balance that is required to be enforced on the flow. In this section we look at the work that was undertaken by McIntyre and Roulstone in [30] and [31] where they are able to define a general expression that links the canonical coordinates to the subspaces.

We are interested in how it would be possible to use this subspace to define a balanced variable to be used in the data assimilation scheme. The

result is a Monge-Ampère equation, where the solution is a balanced height field. From this we are able to construct the wind field, $\mathbf{u}^c$ which is the subspace in the full phase space which, from the work done by Salmon, is the balanced component of the flow.

We begin with a result from a paper by Roulstone and Sewell, [37], where they are able to link the PV for the semi-geostophic case to the manifold defined by (3.52).

3.5.1 Wind Field Constraints

We recall the form for the semi-geostrophic PV, (3.27), given by

$$Q_{sg} = \frac{1}{h}\left(f + \frac{\partial v_g}{\partial x} - \frac{\partial u_g}{\partial y} + \frac{1}{f}\frac{\partial\left(u_g, v_g\right)}{\partial\left(x, y\right)}\right).$$

In the Lagrangian description then the conserved PV is

$$Q = \frac{1}{h}\left(f + \frac{\partial \dot{y}}{\partial x} - \frac{\partial \dot{x}}{\partial y}\right). \tag{3.53}$$

Roulstone and Sewell noticed that instead of replacing the terms $(\dot{x}, \dot{y})$ with the geostrophic winds if you used what they refer to as a *constrained* wind field, $\mathbf{u}_s^c$, as it is a restriction to a sub-manifold of the phase space,

$$\mathbf{u}_s^c = \mathbf{u}_g - \frac{1}{2f}\mathbf{u}_g \cdot \nabla\left(\mathbf{k} \times \mathbf{u}_g\right). \tag{3.54}$$

We are then able to write the PV as

$$Q = \frac{1}{h}\left(f + \frac{\partial v_{sg}}{\partial x} - \frac{\partial u_{sg}}{\partial y}\right) = Q_{sg}, \tag{3.55}$$

which is of the same form as in Section 2.2.2.

The constrained wind field $\mathbf{u}_s^c$ is the expression given for the subspace for the semi-geostrophic balance, (3.52). Equation (3.55) is the same as (3.27).

We next describe the work undertaken by McIntyre and Roulstone where they extend the ideas by Salmon.

3.5.2 Higher Order Balance

In [31], McIntyre and Roulstone note that the constrained wind field, $\mathbf{u}_s^c$, that Salmon derived for the slow manifold, (3.52), is both a field and a mass-configuration functional. They denote this by

$$\mathbf{u}^c \equiv \mathbf{u}^c\left(\mathbf{x}; h\left(\cdot\right)\right). \tag{3.56}$$

They make useful comments on how to view the constraint as a splitting of the parent velocity field, $\mathbf{u}^p$, into two different fields. The first of these being $\mathbf{u}^c$ itself which has the property of entering into the conservation relations, importantly the PV relation

$$Q^c = \frac{1}{h}\left(f + \frac{\partial v^c}{\partial x} - \frac{\partial u^c}{\partial y}\right) = \frac{1}{h}\left(f + \xi^c\right). \tag{3.57}$$

The second is the particle velocity $\dot{\mathbf{x}} = \mathbf{u}^p$, where the term $\mathbf{u}^p$ is the full wind field. Its difference from $\mathbf{u}^c$ is taken to be $\mathbf{u}^s = \mathbf{u}^p - \mathbf{u}^c$, where $\mathbf{u}^s$ is referred to as the *velocity split*, [31].

McIntyre and Roulstone then derive an extension to the canonical coordinates that Salmon uses to derive the semi-geostrophic equations form. They are able to derive a set of set of canonical coordinates so that the PV can be written in the form

$$Q^c = \frac{f}{h}\frac{\partial(X,Y)}{\partial(x,y)}, \tag{3.58}$$

where the canonical coordinates are given by

$$\boldsymbol{X} = \mathbf{x} + \nabla\phi - i\gamma\mathbf{k}\times\nabla\psi, \tag{3.59}$$

where $i = \sqrt{-1}$ and $\gamma = \sqrt{(2\alpha+1)}$. They show that the α in (3.59) is related to the sub-spaces by

$$\mathbf{u}^c = \frac{1}{2}f\mathbf{k}\times\mathbf{x} + \mathbf{u}_g + \frac{\alpha}{f}\mathbf{u}_g\cdot\nabla\left(\mathbf{k}\times\mathbf{u}_g\right). \tag{3.60}$$

To obtain the form for the semi-geostrophic model, (3.52), we substitute $\alpha = -\frac{1}{2}$ in (3.60) and ignore the first term. This extra term in (3.60) arises in [30] and [31] as when we take $\mathbf{k}\cdot\nabla\times\mathbf{u}^c$ using (3.60) then we obtain the balanced absolute vorticity, ζ^c, rather than the balanced relative vorticity with (3.52). The canonical coordinates associated with $\alpha = -\frac{1}{2}$ are those derived by Hoskins, [21].

If we take $\alpha = 0$, ignoring the first part in (3.60) then $\mathbf{u}^c \equiv \mathbf{u}_g$ and so we are constraining the flow to be solely geostrophic. Finally if we take $\alpha = 1$

then the resulting balanced wind field is

$$\mathbf{u}^c \equiv \mathbf{u}_g + \frac{1}{f}\mathbf{u}_g \cdot \nabla \left(\mathbf{k} \times \mathbf{u}_g\right), \tag{3.61}$$

where we have again ignored the first term in (3.60). Equation (3.61) is consistent with a Rossby number expansion for the velocity [31], when this number is small and is a higher order balance condition than geostrophic balance which is only $O(\epsilon)$.

McIntyre and Roulstone noticed that the substitution of the canonical coordinates into (3.58) gives a general Monge-Ampère equation,

$$1 + \nabla^2\phi + \left(1 - \gamma^2\right) \mathrm{hess}_{xy}(\phi) = \frac{\zeta^c}{f}, \tag{3.62}$$

where

$$\mathrm{hess}_{xy}(\psi) = \begin{vmatrix} \dfrac{\partial^2\phi}{\partial x^2} & \dfrac{\partial^2\phi}{\partial x \partial y} \\ \dfrac{\partial^2\phi}{\partial x \partial y} & \dfrac{\partial^2\phi}{\partial y^2} \end{vmatrix},$$

ζ^c is the constrained absolute vorticity given by

$$\zeta^c = f + \frac{\partial v^c}{\partial x} - \frac{\partial u^c}{\partial y}.$$

The coefficients for the ellipticity condition are now, $A = 1 - \frac{\zeta^c}{f}$, $B = D = 1$, $C = 0$ and $E = (1 - \gamma^2)$. This then gives the condition

$$\left(\gamma^2 - 1\right)\frac{\zeta^c}{f} < c^2, \tag{3.63}$$

and is always satisfied for the L_1 dynamics, $\alpha = 0$, $\gamma = 1$. For the semi-geostrophic case then we satisfy this condition if $\frac{\zeta^c}{f} > 0$ which is the same as

the condition derived in Section 3.3.3. For the third situation we have $\alpha = 1$ and $\gamma = \sqrt{3}$ and as such the equation is elliptic if $\frac{\zeta^c}{f} < \frac{3}{2}$ which is satisfied provided that the sub-space actually approximates the slow moving manifold and this is so only when we have the Rossby number small.

The balanced wind field defined by (3.61) has the property that for constant f this is not divergence free. Therefore if we could use this to find a balanced height then the associated $\mathbf{u}^c$ with this would be a divergent rotational balanced wind.

This is possible by calculating the relative vorticity from $\mathbf{u}^c$ and we do that here

$$\begin{aligned}
\xi^c &= \mathbf{k}\cdot\nabla\times\mathbf{u}^c = \mathbf{k}\cdot\nabla\times\mathbf{u}_g + \frac{1}{f}\mathbf{k}\cdot\nabla\times(\mathbf{u}_g\cdot\nabla)(\mathbf{k}\times\mathbf{u}_g)\\
&= \frac{g}{f}\nabla^2 h + \frac{1}{f}\mathbf{k}\cdot\nabla\times\left(-\left(u_g\frac{\partial v_g}{\partial x} + v_g\frac{\partial v_g}{\partial y}\right)\mathbf{i} + \left(u_g\frac{\partial u_g}{\partial x} + v_g\frac{\partial u_g}{\partial y}\right)\mathbf{j}\right)\\
&= \frac{g}{f}\nabla^2 h + \frac{1}{f}\left(\frac{\partial}{\partial x}\left(u_g\frac{\partial u_g}{\partial x} + v_g\frac{\partial u_g}{\partial y}\right)\frac{\partial}{\partial y}\left(u_g\frac{\partial v_g}{\partial x} + v_g\frac{\partial v_g}{\partial y}\right)\right)\\
&= \frac{g}{f}\left(\frac{\partial^2 h}{\partial x^2} + \frac{\partial^2 h}{\partial y^2}\right) - \frac{2g^2}{f^3}\left(\frac{\partial^2 h}{\partial x^2}\frac{\partial^2 h}{\partial y^2} - \left(\frac{\partial^2 h}{\partial x\partial y}\right)^2\right), \qquad (3.64)
\end{aligned}$$

which has the following coefficients for the ellipticity condition: $A = \frac{f^3\xi^c}{2g^2}$, $B = D = -\frac{f^2}{2g^2}$, $C = 0$ and $E = 1$. This then gives a condition of $\frac{f}{2} > \xi^c$.

It is from this last Monge-Ampère equation and the equation arising from forming ξ^c when $\alpha = 0$ that the rest of the thesis is concerned with.

3.6 Summary

We started this chapter with a brief introduction to Hamiltonian dynamics and summarised how a fluid motion could be described with respect to a Eulerian or Lagrangian framework. From this we then showed Hamilton's principle for point masses and for a continuous flow. In section 3.2 we described the Lagrangian that Salmon defines for the shallow water equations.

In Section 3.3 we introduced the semi-geostrophic approximation that is made to the shallow water equations along with the semi-geostrophic PV , (3.27) which differed from the expression in Section 2.2.2 where we now have the Jacobian term. In Section 3.3.2 we reviewed the canonical coordinates that were introduced by Hoskins in [21] which have the property of enabling the PV to be written in terms of a Jacobian between the canonical and Cartesian coordinates, (3.37) which is a Monge-Ampère equation.

In Section 3.4 we summarised results from [38], [39] and [41] where approximations to $\mathbf{u}$ in the Lagrangian (3.16) are made. The first approximation is to set $\mathbf{u} = 0$. The resulting dynamical equations were geostrophic balance, (3.43) and (3.44). The second approximation uses $\mathbf{u} = \mathbf{u}_g$. The resulting equation, (3.50), was simplified by Salmon in [39] by introducing a general canonical coordinate system which has to satisfy strict equalities. These were the semi-geostrophic equations and Hoskin's coordinate system

associated with these.

In [41], Salmon gives a mathematical structure to the approximations he makes in [38] and [39] by deriving an expression for a balanced wind field, (3.52), which he shows defines a slow moving manifold in the phase space of the shallow water equations.

In Section 3.5 we summarised a result by Roulstone and Sewell, [37], where they show that the balanced wind field, (3.52), when used in the PV for the semi-geostrophic case, removes the Jacobian term and has the same appearance as (2.14).

In Section 3.5.2 we reviewed the extensions to Salmon's ideas by McIntyre and Roulstone, [30] and [31], where they derive a set of submanifolds and the canonical coordinates associated with these. They also show that the balance relation for the semi-geostrophic case was a specific case for their general formula.

In the remainder of the thesis we develop the balanced wind field, (3.61), as a possible alternative for the current balanced wind field which is only the rotational part of the flow. We started this development by deriving the Monge-Ampère equation, (3.64), for the balanced height for a given ξ^c.

In the next chapter we derive the spherical version of the balanced wind field and the practical aspects of how it could be used in an incremental data assimilation scheme.

Chapter 4

Balance Equations on the Sphere

Before we start the development of the balanced wind on the sphere we summarise the different methods used so far to eliminate the fast motions in either the shallow water equations or the 3-D primitive equations.

In Section 2.2.3 we summarised a method by Hinkelmann and Phillips where they arrived at two possible initialisations, (2.19) and (2.20), for the non-linear shallow water equations.

The conditions were arrived at by setting the terms in the solution for the velocity potential, (2.18), that were multiples of the inertial time scale, σ_1, to zero. The first set of conditions involved a form of geostrophic balance, [14], and a zero initial velocity potential, (2.19). The second set of conditions,

(2.20), required again some form of geostrophic balance but now with a non-zero velocity potential. These are seen as differing in that the second conditions allow for an initial divergence.

In Section 2.3 we reviewed a method that nondimensionalised the primitive equations so that the time scale was that of the advective scale. To these equations a bounded derivative method was applied. Through bounding the first time derivatives to be $O(1)$ we arrived at (2.37), which is the geostrophic balance condition. By bounding the second derivatives we arrive at an equation that links the geopotential to the stream function, (2.38). This is referred to as a non-linear balance equation, [14], [54].

In Section 3.3 we introduce a form of balance that is referred to as semi-geostrophic. This is where, in equation (3.24), the acceleration term is replaced by the time derivative of the geostrophic winds. These equations have the property that there exists a set of canonical coordinates, (3.28), which enable the PV to be written as the Jacobian of the canonical coordinates with respect to the Cartesian coordinates, (3.37).

In Section 3.4 we looked at Salmon's approximations to Lagrangian of the shallow water equations, (3.16). His first approximation was to set $u = v = 0$, the result was the geostrophic balance relation, (3.43) and (3.44). His second approximation was to substitute the geostrophic winds for the full fields. The result was a balance equation for the ageostrophic wind, (3.50). Through

using information about the structure of Hamiltonian dynamics, Salmon is able to define a subspace in the phase space of the shallow water equations where the semi-geostrophic motions lie, (3.52).

In Section 3.5 we reviewed [30] and [31] where McIntyre and Roulstone extend the subspace to a more generalised form as Salmon suggests in [41], to link a set of sub-spaces that represent the slow motions in the shallow water equations to a set of canonical coordinates, (3.59) with (3.60), and enables the PV to be written in the Jacobian form, (3.58).

One of these sub-spaces is given by

$$\mathbf{u}^c = \mathbf{u}_g + \frac{1}{f}\left(\mathbf{u}_g \cdot \nabla\right)\left(\mathbf{k} \times \mathbf{u}_g\right),$$

(3.61, which is the same as the Rossby number expansion for the wind fields correct to second order, [31], [47]. This is also defining a balanced wind.

In this chapter we develop the mathematics necessary to calculate a balanced height through the same approach that we described at the end of Section 3.5.2, but on the sphere. We also derive the spherical component form for the balanced wind and the spherical version of the Monge-Ampère equation given in Cartesian coordinates by (3.64).

We then modify this technique to be able to use this with an incremental data assimilation scheme. We achieve this by linearising the spherical definition of the balanced wind field and following the same procedure for

calculating ξ^c as in Section 3.5.2.

We also derive a linearised version of Q^c associated with (3.61) for the sphere. The result is a variable coefficient Poisson equation for the relative vorticity and a variable coefficient Helmholtz equation for the PV. The solution of these equations is a balanced height increment from which we can reconstruct the balanced wind field. If $\alpha = 1$ in the spherical version of (3.61) then the resulting wind field is divergent for constant f.

As we are concerned with the possibility of using this variable in a variational data assimilation scheme, we briefly describe the current control variable transforms employed in the Met. Office's incremental 3-D variational data assimilation scheme, (3D VAR), and then explain how the balanced height could be used as an alternative to the stream function and introduce two new unbalanced variables in the last section.

We begin with a brief derivation of the shallow water equations as this model is used to calculate the linearisation states for (3.61) and then review a derivation from [22], which results in the dimensional spherical version of (2.38).

4.1 Spherical SWE and Balance

The aim of this section is to introduce the spherical shallow water equations and then to derive the spherical version of the non-linear balance equation. This is the equivalent to the Cartesian version that can be found following the derivation in [34]. To arrive at the spherical version we follow the proof set out in [22].

4.1.1 Spherical Shallow Water Equations

We recall the vectorial version of the Cartesian form of the shallow water equations in Section 2.2.2, (2.7) and (2.8). We start with (2.7),

$$\frac{D\mathbf{u}}{Dt} + f\mathbf{k} \times \mathbf{u} = -g\nabla h.$$

Writing in component form gives, using Appendix A,

$$\begin{aligned} \frac{\partial u}{\partial t} + \frac{u}{a\cos\theta}\frac{\partial u}{\partial \lambda} + \frac{v}{a}\frac{\partial u}{\partial \theta} - \frac{\tan\theta}{a}vu - fv &= -\frac{g}{a\cos\theta}\frac{\partial h}{\partial \lambda}, \qquad (4.1) \\ \frac{\partial v}{\partial t} + \frac{u}{a\cos\theta}\frac{\partial v}{\partial \lambda} + \frac{v}{a}\frac{\partial v}{\partial \theta} + \frac{\tan\theta}{a}u^2 + fu &= -\frac{g}{a}\frac{\partial h}{\partial \theta}, \qquad (4.2) \end{aligned}$$

where a is the Earth's radius, $f = 2\Omega\sin\theta$, θ is the angle of latitude and has the values $\theta \in \left[-\frac{\pi}{2}, \frac{\pi}{2}\right]$, λ is the angle of longitude and has the value $\lambda \in [0, 2\pi]$.

Using the information from Appendix A gives the spherical version of the

continuity equation, (2.6), as

$$\frac{\partial h}{\partial t} + \frac{u}{a\cos\theta}\frac{\partial h}{\partial \lambda} + \frac{v}{a}\frac{\partial h}{\partial \theta} + \frac{h}{a\cos\theta}\left(\frac{\partial u}{\partial \lambda} + \frac{\partial\left(\cos\theta v\right)}{\partial \theta}\right) = 0. \qquad (4.3)$$

Therefore, equations (4.1), (4.2) and (4.3) are the spherical version of the shallow water equations.

4.1.2 Spherical Non-Linear Balance Equation

In Section 2.3 we summarised an initialisation technique that resulted in a non-dimensional non-linear balance equation, (2.38). To derive the dimensional spherical version of (2.38) we consider the spherical version of the equations of motion for the 3-D primitive equations model, (2.21). We make the assumption of homogeneity and ignore the vertical wind, [54]. The remaining terms are similar to the spherical version of the shallow water equations, (4.1) and (4.2), but with geopotential gradients rather than height gradients.

We start by taking the divergence of the equations and ignoring the time derivative of the divergence. The reason for this is that the removal of this term 'filters' the inertia-gravity waves, [54]. The remaining terms are

$$\nabla\cdot\left(\left(\mathbf{u}\cdot\nabla\right)\mathbf{u}\right) + \nabla^2\Phi + \nabla\cdot\left(f\mathbf{k}\times\mathbf{u}\right) = 0. \qquad (4.4)$$

Expanding the term $\nabla\cdot\left(\mathbf{u}\cdot\nabla\right)\mathbf{u}$ using the spherical definitions in Ap-

pendix A gives

$$\frac{1}{a^2\cos^2\theta}\left(\left(\frac{\partial u}{\partial\lambda}\right)^2+u\frac{\partial^2 u}{\partial\lambda^2}\right)+\frac{1}{a^2\cos\phi}\left(2\frac{\partial v}{\partial\lambda}\frac{\partial u}{\partial\theta}+u\frac{\partial^2 v}{\partial\theta\partial\lambda}+v\frac{\partial^2 u}{\partial\lambda\partial\theta}\right)$$
$$-\frac{\tan\phi}{a^2\cos\theta}\left(v\frac{\partial u}{\partial\lambda}+2u\frac{\partial v}{\partial\lambda}\right)-\frac{\tan\theta}{a^2}v\frac{\partial v}{\partial\theta}+\left(\frac{1}{a^2\cos\theta}-\frac{\tan^2\theta}{a^2}\right)u^2$$
$$+\frac{1}{a^2}\left(\left(\frac{\partial v}{\partial\theta}\right)^2+v\frac{\partial^2 v}{\partial\theta^2}+\frac{2\tan\theta}{a^2}u\frac{\partial u}{\partial\theta}\right)=\nabla\cdot(\mathbf{u}\cdot\nabla)\,\mathbf{u}. \quad (4.5)$$

In the next step we use the trigonometric identity $\sec^2\theta=\tan^2\theta+1$. We now use the Helmholtz theorem for the wind field,

$$\mathbf{u}=\mathbf{k}\times\nabla\psi+\nabla\chi,$$

which in spherical coordinates, where we are only considering the balanced component,

$$u=-\frac{1}{a}\frac{\partial\psi}{\partial\theta},\qquad v=\frac{1}{a\cos\theta}\frac{\partial\psi}{\partial\lambda}. \quad (4.6)$$

Substituting (4.6) into (4.5) gives

$$\nabla\cdot(\mathbf{u}\cdot\nabla)\,\mathbf{u}=\frac{1}{a^4\cos^2\theta}\left(2\left(\frac{\partial^2\psi}{\partial\theta\partial\lambda}\right)^2-2\frac{\partial^2\psi}{\partial\lambda^2}\frac{\partial^2\psi}{\partial\theta^2}+4\tan\theta\frac{\partial\psi}{\partial\lambda}\frac{\partial^2\psi}{\partial\theta\partial\lambda}\right.$$
$$\left.+\left(2\tan^2\theta+1\right)\left(\frac{\partial\psi}{\partial\theta}\right)^2\right)+\frac{1}{a^4}\left(\frac{\partial\psi}{\partial\theta}\right)^2+\frac{2\tan\theta}{a^4}\frac{\partial\psi}{\partial\theta}\frac{\partial^2\psi}{\partial\theta^2}. \quad (4.7)$$

In (4.7) the third order terms have cancelled. We now consider the divergence of the Coriolis term, which gives

$$\nabla\cdot(f\mathbf{k}\times\mathbf{u})=\frac{1}{a\cos\theta}\frac{\partial}{\partial\lambda}(-fv)-\frac{\tan\theta}{a}(fu)+\frac{1}{a}\frac{\partial}{\partial\theta}(fu). \quad (4.8)$$

Substituting (4.6) for the wind field and differentiating the Coriolis parameter gives

$$\nabla \cdot (f\mathbf{k} \times \mathbf{u}) - \frac{1}{a^2 \cos^2\theta} f \frac{\partial^2 \psi}{\partial \lambda^2} + \frac{\tan\theta}{a^2} f \frac{\partial \psi}{\partial \theta} - \frac{\beta}{a^2} \frac{\partial \psi}{\partial \theta} - f \frac{\partial^2 \psi}{\partial \theta^2}, \tag{4.9}$$

where

$$\beta = \frac{\partial f}{\partial \theta}.$$

Collecting all the terms and using the following notation

$$r = \frac{\partial^2 \psi}{\partial \lambda^2}, \qquad s = \frac{\partial^2 \psi}{\partial \lambda \partial \theta}, \qquad t = \frac{\partial^2 \psi}{\partial \theta^2},$$

as used in Houghton [22] then (4.4) becomes

$$\begin{aligned} &\frac{2}{a^4 \cos\theta}\left(rt - s^2\right) - \frac{4\tan\theta}{a^4 \cos^2\theta}\psi_\lambda s + \left(\frac{f}{a^2} - \frac{2\tan\theta}{a^4}\psi_\theta\right) t + \frac{f}{a^2 \cos^2\theta} r \\ &\quad = \left(\frac{f\tan\theta}{a^2} - \frac{\beta}{a}\right)\psi_\theta + \nabla^2\Phi + \frac{2\tan^2\theta}{a^4 \cos^2\theta}\psi_\lambda^2 + \frac{1}{a^4}\left(\psi_\theta^2 + \frac{\psi_\lambda^2}{\cos^2\theta}\right). \end{aligned} \tag{4.10}$$

Therefore, equation (4.10) is a spherical version of a non-linear balance equation for ψ given Φ and can be considered as the dimensional spherical version of (2.38). Therefore, the solutions ψ do not include inertia gravity waves. The differential equation for ψ is another Monge-Ampère equation.

In the next section we derive a general spherical Monge-Ampère equation from the spherical version of (3.60) by calculating $\xi^c = \mathbf{k} \cdot \nabla \times \mathbf{u}^c$. This then gives a Monge-Ampère equation whose solution is a balanced height. We also derive a non-linear equation from the balanced potential vorticity, Q^c from the balanced wind field for h.

4.2 New Non-Linear Balance Equation

In this section we derive an alternative balance equation to (4.10) to find a balanced height. We derive the equation from the general form of the balanced wind field, (3.60) with the first term ignored, and then find the form of the equation for $\alpha = 0$ and 1.

We begin by recalling the general form of the balanced wind field, (3.60),

$$\mathbf{u}^c = \mathbf{u}_g + \frac{\alpha}{f}\mathbf{u}_g \cdot \nabla \left(\mathbf{k} \times \mathbf{u}_g\right), \tag{4.11}$$

where we have removed the first term to calculate the relative vorticity. To find its spherical form we use the spherical expression given in Appendix A. Therefore, in component form this is

$$u^c = u_g - \frac{\alpha}{f}\left(\frac{u_g}{a\cos\theta}\frac{\partial v_g}{\partial \lambda} + \frac{v_g}{a}\frac{\partial v_g}{\partial \theta} + \frac{\tan\theta}{a}u_g^2\right), \tag{4.12}$$

$$v^c = v_g + \frac{\alpha}{f}\left(\frac{u_g}{a\cos\theta}\frac{\partial u_g}{\partial \lambda} + \frac{v_g}{a}\frac{\partial u_g}{\partial \theta} - \frac{\tan\theta}{a}u_g v_g\right). \tag{4.13}$$

To form ξ^c we take the vertical component of the curl of (4.12) and (4.13). This gives

$$\xi^c \equiv \frac{1}{a\cos\theta}\left(\frac{\partial v^c}{\partial \lambda} - \frac{\partial}{\partial \theta}\left(\cos\theta u^c\right)\right), \tag{4.14}$$

which in component form is

$$\begin{aligned}\xi^c = & \frac{1}{a\cos\theta}\left(\frac{\partial}{\partial \lambda}\left(v_g + \frac{\alpha}{f}\left(\frac{u_g}{a\cos\theta}\frac{\partial u_g}{\partial \lambda} + \frac{v_g}{a}\frac{\partial u_g}{\partial \theta} - \frac{\tan\theta}{a}u_g v_g\right)\right)\right. \\ & \left. + \frac{\partial}{\partial \theta}\left(-\cos\theta u^c + \frac{\alpha}{f}\left(\frac{u_g}{a}\frac{\partial v_g}{\partial \lambda} + \frac{\cos\theta v_g}{a}\frac{\partial v_g}{\partial \theta} + \frac{\sin\theta}{a}u_g^2\right)\right)\right).\end{aligned} \tag{4.15}$$

We now introduce the height version of the geostrophic winds in spherical coordinates. These are

$$u_g \equiv -\frac{g}{f}\frac{\partial h}{\partial \theta}, \qquad v_g \equiv \frac{g}{fa\cos\theta}\frac{\partial h}{\partial \lambda}. \tag{4.16}$$

To derive the Monge-Ampère equation we substitute (4.16) into (4.15). The result is

$$\begin{aligned}\xi^c = \frac{g}{fa^2}\left(\frac{1}{\cos^2\theta}\frac{\partial^2 h}{\partial\lambda^2} + \frac{\partial^2 h}{\partial\theta^2} - \tan\theta\frac{\partial h}{\partial\theta}\right) + \frac{2g^2\alpha}{f^3a^4\cos^2\theta}\left(\left(\frac{\partial^2 h}{\partial\theta\partial\lambda}\right)^2\right.\\ -\frac{\partial^2 h}{\partial\lambda^2}\frac{\partial^2 h}{\partial\theta^2} + 2\tan\theta\frac{\partial h}{\partial\lambda}\frac{\partial^2 h}{\partial\theta\partial\lambda} + 2\tan^2\theta\left(\frac{\partial h}{\partial\lambda}\right)^2 + \sin\theta\cos\theta\frac{\partial h}{\partial\theta}\frac{\partial^2 h}{\partial\theta^2}\\ \left.+\frac{1}{2}\left(\left(\frac{\partial h}{\partial\lambda}\right)^2 + \cos^2\theta\left(\frac{\partial h}{\partial\theta}\right)^2\right)\right).\end{aligned} \tag{4.17}$$

In the expression above all the third order terms have cancelled out. To obtain this expression we have assumed a constant f. This is often referred to the f plane approximation, [54], which is often used as a first stage of testing of new model variables.

If we consider the geostrophic sub-space, $\alpha = 0$, then (4.17) simplifies to

$$\xi^c = \frac{g}{fa^2}\left(\frac{1}{\cos^2\theta}\frac{\partial^2 h}{\partial\lambda^2} + \frac{\partial^2 h}{\partial\theta^2} - \tan\theta\frac{\partial h}{\partial\theta}\right), \tag{4.18}$$

which is a spherical Poisson equation. If we take $\alpha = 1$ then the result is

$$\begin{aligned}\xi^c = \frac{g}{fa^2}\left(\frac{1}{\cos^2\theta}\frac{\partial^2 h}{\partial\lambda^2} + \frac{\partial^2 h}{\partial\theta^2} - \tan\theta\frac{\partial h}{\partial\theta}\right) + \frac{2g^2}{f^3a^4\cos^2\theta}\left(\left(\frac{\partial^2 h}{\partial\theta\partial\lambda}\right)^2\right.\\ -\frac{\partial^2 h}{\partial\lambda^2}\frac{\partial^2 h}{\partial\theta^2} + 2\tan\theta\frac{\partial h}{\partial\lambda}\frac{\partial^2 h}{\partial\theta\partial\lambda} + 2\tan^2\theta\left(\frac{\partial h}{\partial\lambda}\right)^2 + \sin\theta\cos\theta\frac{\partial h}{\partial\theta}\frac{\partial^2 h}{\partial\theta^2}\\ \left.+\frac{1}{2}\left(\left(\frac{\partial h}{\partial\lambda}\right)^2 + \cos^2\theta\left(\frac{\partial h}{\partial\theta}\right)^2\right)\right).\end{aligned}$$

We now consider an extension to ξ^c to form the constrained potential vorticity, Q^c. We start from the definition

$$Q^c \equiv \frac{f+\xi^c}{h} \equiv \frac{\zeta^c}{h}, \tag{4.19}$$

where we would substitute the right hand side of (4.17) into (4.19) for ξ^c. This then gives

$$\begin{aligned} Q^c \equiv \frac{1}{h}\Bigg(f + \frac{g}{fa^2}\Bigg(\frac{1}{\cos^2\theta}\frac{\partial^2 h}{\partial\lambda^2} + \frac{\partial^2 h}{\partial\theta^2} - \tan\theta\frac{\partial h}{\partial\theta}\Bigg) + \frac{2g^2\alpha}{f^3a^4\cos^2\theta}\Bigg(\Bigg(\frac{\partial^2 h}{\partial\theta\partial\lambda}\Bigg)^2 \\ - \frac{\partial^2 h}{\partial\lambda^2}\frac{\partial^2 h}{\partial\theta^2} + 2\tan\theta\frac{\partial h}{\partial\lambda}\frac{\partial^2 h}{\partial\theta\partial\lambda} + 2\tan^2\theta\Bigg(\frac{\partial h}{\partial\lambda}\Bigg)^2 + \sin\theta\cos\theta\frac{\partial h}{\partial\theta}\frac{\partial^2 h}{\partial\theta^2} \\ + \frac{1}{2}\Bigg(\Bigg(\frac{\partial h}{\partial\lambda}\Bigg)^2 + \cos^2\theta\Bigg(\frac{\partial h}{\partial\theta}\Bigg)^2\Bigg)\Bigg)\Bigg)\Bigg). \end{aligned} \tag{4.20}$$

To use this in an incremental variational data assimilation scheme we would require a linear equation for the height. In the next section we introduce a linearisation to (4.11) and derive a linearised Monge-Ampère equation for the height increment.

4.3 Linearisation

In this section we introduce a linearisation to (4.11) about a geostrophic base state. From the linearised version of the balanced wind field we derive a linearised Monge-Ampère equation for the height increment.

From this we follow the extension to form the PV from Section 4.2, (4.19).

However, we do not use (4.19) to define the PV but a linearised form that we derive in Section 4.3.3.

4.3.1 Linearised Balanced Wind Field

The non-linear aspect of the balanced wind field, (3.61), arises from the term $\mathbf{u}_g \cdot \nabla (\mathbf{k} \times \mathbf{u}_g)$. To linearise this we introduce a base state for the height and consider increments to this. We start by expressing the height field, h, as $h = \bar{h} + h'$, where $\bar{h}$ is a base state height and h' is an increment. The geostrophic wind then becomes

$$\mathbf{u}_g = \bar{\mathbf{u}}_g + \mathbf{u}'_g, \tag{4.21}$$

where

$$u'_g \equiv -\frac{g}{af}\frac{\partial h'}{\partial \theta}, \qquad v'_g \equiv \frac{g}{af\cos\theta}\frac{\partial h'}{\partial \lambda}, \tag{4.22}$$

$$\bar{u}_g \equiv -\frac{g}{af}\frac{\partial \bar{h}}{\partial \theta}, \qquad \bar{v}_g \equiv \frac{g}{af\cos\theta}\frac{\partial \bar{h}}{\partial \lambda}. \tag{4.23}$$

Substituting (4.21) into (4.11) gives the increment to $\mathbf{u}^c$ as

$$\mathbf{u}^{c\prime} \equiv \mathbf{u}'_g + \frac{\alpha}{f}\left(\bar{\mathbf{u}}_g \cdot \nabla\left(\mathbf{k} \times \mathbf{u}'_g\right) + \mathbf{u}'_g \cdot \nabla\left(\mathbf{k} \times \bar{\mathbf{u}}_g\right)\right). \tag{4.24}$$

In component form this is given by

$$u^{c\prime} \equiv u'_g - \frac{\alpha}{f}\left(\frac{u'_g}{a\cos\theta}\frac{\partial \bar{v}_g}{\partial \lambda} + \frac{\bar{u}_g}{a\cos\theta}\frac{\partial v'_g}{\partial \lambda} + \frac{v'_g}{a}\frac{\partial \bar{v}_g}{\partial \theta} + \frac{\bar{v}_g}{a}\frac{\partial v'_g}{\partial \theta} + 2\frac{\tan\theta}{a}u'_g\bar{u}_g\right), \tag{4.25}$$

$$v^{c\prime} \equiv v'_g + \frac{\alpha}{f}\left(\frac{u'_g}{a\cos\theta}\frac{\partial \bar{u}_g}{\partial\lambda} + \frac{\bar{u}_g}{a\cos\theta}\frac{\partial u'_g}{\partial\lambda} + \frac{v'_g}{a}\frac{\partial \bar{u}_g}{\partial\theta} + \frac{\bar{v}_g}{a}\frac{\partial u'_g}{\partial\theta} - \frac{\tan\theta}{a}\left(u'_g\bar{v}_g + \bar{u}_g v'_g\right)\right). \quad (4.26)$$

As in Section 4.2, we can construct a balance equation for the height, given either the constrained relative or potential vorticity. Over the next two subsections we derive two linear partial differential equations from both variables.

4.3.2 Relative Vorticity Approach (RV)

We now consider constructing a 'balance equation' from $\mathbf{u}^{c\prime}$ by forming the relative vorticity associated with $\mathbf{u}^{c\prime}$. This is achieved by considering the vertical component of $\nabla \times \mathbf{u}^{c\prime}$. Applying this to equation (4.24) results in

$$\begin{aligned}\xi^{c\prime} &\equiv \mathbf{k}\cdot\nabla\times\mathbf{u}^{c\prime} = \mathbf{k}\cdot\nabla\times\mathbf{u}'_g + \frac{\alpha}{f}\left(\mathbf{k}\cdot\left(\nabla\left(\times\bar{\mathbf{u}}_g\cdot\nabla\left(\mathbf{k}\times\mathbf{u}'_g\right)\right)\right)\right. \quad (4.27)\\ &+ \left.\mathbf{k}\cdot\left(\nabla\times\left(\mathbf{u}'_g\cdot\nabla\left(\mathbf{k}\times\bar{\mathbf{u}}_g\right)\right)\right)\right) + \mathbf{k}\cdot\left(\nabla\left(\frac{\alpha}{f}\right)\times\left(\bar{\mathbf{u}}_g\cdot\nabla\left(\mathbf{k}\times\mathbf{u}'_g\right) + \mathbf{u}'_g\cdot\nabla\left(\mathbf{k}\times\bar{\mathbf{u}}_g\right)\right)\right),\end{aligned}$$

where we have used the vector identity, [12],

$$\nabla\times f\boldsymbol{G} = f\nabla\times\boldsymbol{G} + \nabla f\times\boldsymbol{G},$$

to obtain the second line in (4.27).

The first term in (4.27) is

$$\mathbf{k}\cdot\nabla\times\mathbf{u}'_g = \frac{1}{a\cos\theta}\left(\frac{\partial v'_g}{\partial\lambda} - \frac{\partial}{\partial\theta}\left(\cos\theta u'_g\right)\right) = \frac{g}{f}\nabla^2 h' + \frac{g}{a^2}\frac{\partial h}{\partial\theta}\Gamma_1, \quad (4.28)$$

where, for convenience, we use Γ_1 to represent the first derivative of f^{-1} and Γ_2, the second derivative with respect to θ. Therefore these are

$$\Gamma_1 = \frac{\partial}{\partial\theta}\left(\frac{1}{f}\right), \qquad \Gamma_2 = \frac{\partial^2}{\partial\theta^2}\left(\frac{1}{f}\right). \tag{4.29}$$

The next term in (4.27) is $\mathbf{k}\cdot\nabla\times\left(\bar{\mathbf{u}}_g\cdot\nabla\left(\mathbf{k}\times\mathbf{u}'_g\right)\right)$. Evaluating $\bar{\mathbf{u}}_g\cdot\nabla\left(\mathbf{k}\times\mathbf{u}'_g\right)$ gives

$$\bar{\mathbf{u}}_g\cdot\nabla\left(\mathbf{k}\times\mathbf{u}'_g\right) = \frac{\bar{u}_g}{a\cos\theta}\frac{\partial}{\partial\lambda}\left(-\mathbf{i}v'_g+\mathbf{j}u'_g\right)+\frac{\bar{v}_g}{a}\frac{\partial}{\partial\theta}\left(-\mathbf{i}v'_g+\mathbf{j}u'_g\right).$$

Taking the differential operators through gives

$$\begin{aligned}\bar{\mathbf{u}}_g\cdot\nabla\left(\mathbf{k}\times\mathbf{u}'_g\right) &= -\left(\frac{\bar{u}_g}{a\cos\theta}\frac{\partial v'_g}{\partial\lambda}+\frac{\bar{u}_g}{a}\frac{\partial v'_g}{\partial\theta}+\frac{\tan\theta}{a}\bar{u}_g u'_g\right)\mathbf{i}\\ &\quad+\left(\frac{\bar{u}_g}{a\cos\theta}\frac{\partial u'_g}{\partial\lambda}+\frac{\bar{v}_g}{a}\frac{\partial u'_g}{\partial\theta}-\frac{\tan\theta}{a}\bar{u}_g v'_g\right)\mathbf{j}.\end{aligned} \tag{4.30}$$

For convenience we will write (4.30) as $\gamma_1\mathbf{i}+\gamma_2\mathbf{j}$, where

$$\gamma_1 = \left(\frac{\bar{u}_g}{a\cos\theta}\frac{\partial v'_g}{\partial\lambda}+\frac{\bar{u}_g}{a}\frac{\partial v'_g}{\partial\theta}+\frac{\tan\theta}{a}\bar{u}_g u'_g\right), \tag{4.31}$$

$$\gamma_2 = \left(\frac{\bar{u}_g}{a\cos\theta}\frac{\partial u'_g}{\partial\lambda}+\frac{\bar{v}_g}{a}\frac{\partial u'_g}{\partial\theta}-\frac{\tan\theta}{a}\bar{u}_g v'_g\right). \tag{4.32}$$

The final step is to form $\mathbf{k}\cdot\nabla\times(-\gamma_1\mathbf{i}+\gamma_2\mathbf{j})$. This is

$$\frac{1}{a^2\cos\theta}\begin{vmatrix} a\cos\theta\mathbf{i} & a\mathbf{j} & \mathbf{k}\\ \frac{\partial}{\partial\lambda} & \frac{\partial}{\partial\theta} & \frac{\partial}{\partial r}\\ -a\cos\theta\gamma_1 & a\gamma_2 & 0\end{vmatrix} = \frac{1}{a\cos\theta}\left(\frac{\partial\gamma_2}{\partial\lambda}+\frac{\partial\cos\theta\gamma_1}{\partial\theta}\right). \tag{4.33}$$

Substituting (4.31) and (4.32) into the right hand side of (4.33) gives

$$\mathbf{k}\cdot\nabla\times\left(\mathbf{u}_g'\cdot\nabla\left(\mathbf{k}\times\bar{\mathbf{u}}_g\right)\right)=\frac{1}{a\cos\theta}\left(\overbrace{\frac{\partial}{\partial\lambda}\left(\frac{\bar{u}_g}{a\cos\theta}\frac{\partial u_g'}{\partial\lambda}\right)}^{T_1}+\overbrace{\frac{\partial}{\partial\lambda}\left(\frac{\bar{v}_g}{a}\frac{\partial u_g'}{\partial\theta}\right)}^{T_2}\right.$$

$$\left.-\underbrace{\frac{\partial}{\partial\lambda}\left(\frac{\tan\theta}{a}\bar{u}_g v_g'\right)}_{T_3}+\underbrace{\frac{\partial}{\partial\theta}\left(\frac{\bar{u}_g}{a}\frac{\partial v_g'}{\partial\lambda}\right)}_{T_4}+\underbrace{\frac{\partial}{\partial\theta}\left(\frac{\cos\theta}{a}\bar{v}_g\frac{\partial v_g'}{\partial\theta}\right)}_{T_5}+\underbrace{\frac{\partial}{\partial\theta}\left(\frac{\sin\theta}{a}\bar{u}_g u_g'\right)}_{T_6}\right). \tag{4.34}$$

For the remainder of the derivation of $\mathbf{k}\cdot\left(\nabla\times\left(\bar{\mathbf{u}}_g\cdot\nabla\left(\mathbf{k}\times\mathbf{u}_g'\right)\right)\right)$ we substitute (4.22) for the incremental height and use the variables, h, u_g, v_g, to represent $h', \bar{u}_g, \bar{v}_g$ respectively.

The first term, T_1, in (4.34) is

$$T_1=\frac{\partial}{\partial\lambda}\left(\frac{u_g}{a\cos\theta}\frac{\partial}{\partial\lambda}\left(-\frac{g}{af}\frac{\partial h}{\partial\theta}\right)\right)=-\frac{g}{a^2 f\cos\theta}\left(\frac{\partial u_g}{\partial\lambda}\frac{\partial^2 h}{\partial\lambda\partial\theta}+u_g\frac{\partial^3 h}{\partial\lambda^2\partial\theta}\right). \tag{4.35}$$

The second term, T_2, becomes

$$T_2=\frac{\partial}{\partial\lambda}\left(\frac{v_g}{a}\frac{\partial}{\partial\theta}\left(-\frac{g}{af}\frac{\partial h}{\partial\theta}\right)\right)=$$
$$-\frac{g}{a^2 f}\left(\frac{\partial v_g}{\partial\lambda}\frac{\partial^2 h}{\partial\theta^2}+v_g\frac{\partial^3 h}{\partial\theta^2\partial\lambda}\right)-\frac{g\Gamma_1}{a^2}\left(\frac{\partial v_g}{\partial\lambda}\frac{\partial h}{\partial\theta}+v_g\frac{\partial^2 h}{\partial\theta\partial\lambda}\right). \tag{4.36}$$

The third term, T_3, is

$$T_3=-\frac{\tan\theta}{a}\frac{\partial}{\partial\lambda}\left(u_g\left(\frac{g}{af\cos\theta}\frac{\partial h}{\partial\lambda}\right)\right)=-\frac{g\tan\theta}{a^2 f\cos\theta}\left(\frac{\partial u_g}{\partial\lambda}\frac{\partial h}{\partial\lambda}+u_g\frac{\partial^2 h}{\partial\lambda^2}\right). \tag{4.37}$$

The fourth term, T_4, involves the derivative of $\sec\theta$ which is $\tan\theta\sec\theta$. Using this information and Γ_1 from (4.29) makes

$$T_4 = \frac{\partial}{\partial\theta}\left(\frac{gu_g}{a^2 f\cos\theta}\frac{\partial^2 h}{\partial\lambda^2}\right) = \frac{g}{a^2 f\cos\theta}\frac{\partial u_g}{\partial\theta}\frac{\partial^2 h}{\partial\lambda^2} + \frac{u_g}{a^2}\frac{\partial}{\partial\theta}\left(\frac{g}{f\cos\theta}\frac{\partial^2 h}{\partial\lambda^2}\right) = \frac{g}{a^2 f\cos\theta}\left(\frac{\partial u_g}{\partial\theta}\frac{\partial^2 h}{\partial\lambda^2} + \tan\theta u_g\frac{\partial^2 h}{\partial\lambda^2} + u_g\frac{\partial^3 h}{\partial\lambda^2\partial\theta}\right) + \frac{\Gamma_1}{a^2\cos\theta}u_g\frac{\partial^2 h}{\partial\lambda^2}. \quad (4.38)$$

The fifth term, T_5, is broken down into three parts. The first, T_{5a}, is

$$T_{5a} = \frac{\cos\theta}{a}\frac{\partial v_g}{\partial\theta}\frac{\partial}{\partial\theta}\left(\frac{g}{af\cos\theta}\frac{\partial h}{\partial\lambda}\right) = \frac{g\tan\theta}{a^2 f}\frac{\partial v_g}{\partial\theta}\frac{\partial h}{\partial\lambda} + \frac{g}{a^2 f}\frac{\partial v_g}{\partial\theta}\frac{\partial^2 h}{\partial\lambda\partial\theta} + \frac{g\Gamma_1}{a^2 f}\frac{\partial v_g}{\partial\theta}\frac{\partial h}{\partial\lambda}. \quad (4.39)$$

The second part, T_{5b}, is

$$T_{5b} = -\frac{\sin\theta v_g}{a}\frac{\partial}{\partial\theta}\left(\frac{g}{af\cos\theta}\frac{\partial h}{\partial\lambda}\right) = -\frac{g\tan^2\theta}{a^2 f}v_g\frac{\partial h}{\partial\lambda} - \frac{g\tan\theta}{a^2 f}v_g\frac{\partial^2 h}{\partial\theta\partial\lambda} - \frac{g\tan\theta\Gamma_1}{a^2}v_g\frac{\partial h}{\partial\lambda}. \quad (4.40)$$

The third part, T_{5c}, is the largest and most complicated. The first part of the derivation is

$$T_{5c} = \frac{\cos\theta v_g}{a}\frac{\partial^2}{\partial\theta^2}\left(\frac{g}{af\cos\theta}\frac{\partial h}{\partial\lambda}\right) = \frac{g\cos\theta v_g}{a^2}\frac{\partial}{\partial\theta}\left(\frac{\Gamma_1}{\cos\theta}\frac{\partial h}{\partial\lambda} + \frac{\tan\theta}{f\cos\theta}\frac{\partial h}{\partial\lambda} + \frac{1}{f\cos\theta}\frac{\partial^2 h}{\partial\theta\partial\lambda}\right).$$

This can be simplified by the identity $\sec^2\theta = \tan^2\theta + 1$. This result in

$$T_{5c} = \frac{gv_g}{a^2 f}\left(\left(2\tan^2\theta + 1\right)\frac{\partial h}{\partial\lambda} + 2\tan\theta\frac{\partial^2 h}{\partial\theta\partial\lambda} + \frac{\partial^3 h}{\partial\theta^2\partial\lambda}\right) + \frac{gv_g}{a^2\cos\theta}\left(\Gamma_2\frac{\partial h}{\partial\lambda} + 2\tan\theta\Gamma_1\frac{\partial h}{\partial\lambda} + 2\Gamma_1\frac{\partial^2 h}{\partial\theta\partial\lambda}\right). \quad (4.41)$$

The sixth term, T_6, from (4.34) result in

$$T_6 = -\frac{\partial}{\partial\theta}\left(\sin\theta u_g \frac{g}{a^2 f}\frac{\partial h}{\partial\theta}\right) =$$
$$\frac{g}{a^2 f}\left(\cos\theta u_g \frac{\partial h}{\partial\theta} - \sin\theta\frac{\partial u_g}{\partial\theta}\frac{\partial h}{\partial\theta} - \sin\theta u_g\frac{\partial^2 h}{\partial\theta^2}\right) - \frac{\sin\theta u_g\Gamma_1}{a^2}\frac{\partial h}{\partial\theta}. \qquad (4.42)$$

We can simplify $\frac{\partial v_g}{\partial\theta}$ in (4.39) by using the following identity

$$\frac{\partial v_g}{\partial\theta} = \tan\theta v_g - \frac{1}{\cos\theta}\frac{\partial u_g}{\partial\lambda} + f v_g\Gamma_1. \qquad (4.43)$$

A derivation of this is in Appendix B. Collecting the terms, $T_1, \ldots, T_6$, equations (4.35) - (4.42), with (4.43) substituted into (4.39) results in

$$\mathbf{k}\left(\cdot\nabla\times\left(\bar{\mathbf{u}}_g\cdot\nabla\left(\mathbf{k}\times\mathbf{u}_g'\right)\right)\right) = -\frac{g}{f^2 a^3\cos^2\theta}\left(u_{g\lambda}h_{\theta\lambda} + u_g h_{\theta\lambda\lambda} + \cos\theta v_g h_{\theta\theta}\right.$$
$$+\cos\theta v_g h_{\theta\theta\lambda} + \tan\theta u_g h_{\lambda\lambda} + \tan\theta u_{g\lambda}h_\lambda - u_{g\theta}h_{\lambda\lambda} - \tan\theta u_g h_{\lambda\lambda} - u_g h_{\theta\lambda\lambda}$$
$$-\tan\theta\sin\theta v_g h_\lambda + \tan\theta u_{g\lambda}h_\lambda - \sin\theta v_g h_{\theta\lambda} + u_{g\lambda}h_{\lambda\theta} + \tan\theta\sin\theta v_g h_\lambda$$
$$+\sin\theta v_g h_{\lambda\theta} - \left(2\tan\theta\sin\theta + \cos\theta\right)v_g h_\lambda - 2\sin\theta v_g h_{\theta\lambda} - \cos\theta v_g h_{\theta\theta\lambda}$$
$$\left.+\cos^2\theta u_g h_\theta + \sin\theta\cos\theta\left(u_{g\theta}h_\theta + u_g h_{\theta\theta}\right)\right).$$

This simplifies to

$$\mathbf{k}\cdot\left(\nabla\times\left(\bar{\mathbf{u}}_g\cdot\nabla\left(\mathbf{k}\times\mathbf{u}_g'\right)\right)\right) = -\frac{g}{a^3 f^2\cos^2\theta}\left(2u_{g\lambda}h_{\theta\lambda} + \cos\theta v_{g\lambda}h_{\theta\theta} - u_{g\theta}h_{\lambda\lambda}\right.$$
$$+2\tan\theta u_{g\lambda}h_\lambda - \cos\theta v_g h_\lambda - 2\tan\theta\sin\theta v_g h_\lambda - 2\sin\theta v_g h_{\theta\lambda} + \cos^2\theta u_g h_\theta$$
$$\left.+\sin\theta\cos\theta\left(u_{g\theta}h_\theta + u_g h_{\theta\theta}\right)\right). \qquad (4.44)$$

We now derive $\mathbf{k}\cdot\left(\nabla\times\left(\mathbf{u}_g'\cdot\nabla\left(\mathbf{k}\times\bar{\mathbf{u}}_g\right)\right)\right)$ from (4.27). The result is

$$\mathbf{k}\cdot\left(\nabla\times\left(\mathbf{u}_g'\cdot\nabla\left(\mathbf{k}\times\bar{\mathbf{u}}_g\right)\right)\right)=\frac{1}{a\cos\theta}\left(\overbrace{\frac{\partial}{\partial\lambda}\left(\frac{u_g'}{a\cos\theta}\frac{\partial\bar{u}_g}{\partial\lambda}\right)}^{T_1}+\overbrace{\frac{\partial}{\partial\lambda}\left(\frac{v_g'}{a}\frac{\partial\bar{u}_g}{\partial\theta}\right)}^{T_2}\right.$$

$$\left.-\underbrace{\frac{\partial}{\partial\lambda}\left(\frac{\tan\theta}{a}u_g'\bar{v}_g\right)}_{T_3}+\underbrace{\frac{\partial}{\partial\theta}\left(\frac{u_g'}{a}\frac{\partial\bar{v}_g}{\partial\lambda}\right)}_{T_4}+\underbrace{\frac{\partial}{\partial\theta}\left(\frac{\cos\theta}{a}v_g'\frac{\partial\bar{v}_g}{\partial\theta}\right)}_{T_5}+\underbrace{\frac{\partial}{\partial\theta}\left(\frac{\sin\theta}{a}u_g'\bar{u}_g\right)}_{T_6}\right), \tag{4.45}$$

where we use the same T notation to represent the terms in (4.45). We again represent $h',\bar{u}_g$ and $\bar{v}_g$ by h,u_g and v_g respectively. The first term, T_1, is

$$T_1=\frac{1}{a\cos\theta}\frac{\partial}{\partial\lambda}\left(-\frac{g}{af}\frac{\partial h}{\partial\theta}\frac{\partial u_g}{\partial\lambda}\right)=-\frac{g}{a^2f\cos\theta}\left(\frac{\partial^2h}{\partial\lambda\partial\theta}\frac{\partial u_g}{\partial\lambda}+\frac{\partial h}{\partial\theta}\frac{\partial^2u_g}{\partial\lambda^2}\right). \tag{4.46}$$

The second term, T_2, becomes

$$T_2=\frac{\partial}{\partial\lambda}\left(\frac{g}{a^2f\cos\theta}\frac{\partial h}{\partial\lambda}\frac{\partial u_g}{\partial\theta}\right)=\frac{g}{a^2f\cos\theta}\left(\frac{\partial^2h}{\partial\lambda^2}\frac{\partial u_g}{\partial\theta}+\frac{\partial h}{\partial\lambda}\frac{\partial^2u_g}{\partial\theta\partial\lambda}\right). \tag{4.47}$$

The third term, T_3, is

$$T_3=\frac{\partial}{\partial\lambda}\left(\frac{g\tan\theta}{a^2f}\frac{\partial h}{\partial\theta}v_g\right)=\frac{g\tan\theta}{a^2f}\left(\frac{\partial^2h}{\partial\theta\partial\lambda}v_g+\frac{\partial h}{\partial\theta}\frac{\partial v_g}{\partial\lambda}\right). \tag{4.48}$$

The fourth term, T_4, becomes

$$T_4=-\frac{\partial}{\partial\theta}\left(\frac{g}{a^2f}\frac{\partial h}{\partial\theta}\frac{\partial v_g}{\partial\lambda}\right)=-\frac{g}{a^2f}\left(\frac{\partial^2h}{\partial\theta^2}\frac{\partial v_g}{\partial\lambda}+\frac{\partial h}{\partial\theta}\frac{\partial^2v_g}{\partial\theta\partial\lambda}\right)-\frac{g\Gamma_1}{a^2}\frac{\partial h}{\partial\theta}\frac{\partial v_g}{\partial\lambda}. \tag{4.49}$$

The fifth term, T_5, at the moment, is

$$T_5 = \frac{\partial}{\partial\theta}\left(\frac{g}{a^2 f}\frac{\partial h}{\partial\lambda}\frac{\partial v_g}{\partial\theta}\right) = \frac{g}{a^2 f}\left(\frac{\partial^2 h}{\partial\lambda\partial\theta}\frac{\partial v_g}{\partial\theta} + \frac{\partial h}{\partial\lambda}\frac{\partial^2 v_g}{\partial\theta^2}\right) + \frac{g\Gamma_1}{a^2}\frac{\partial h}{\partial\lambda}\frac{\partial v_g}{\partial\theta}. \quad (4.50)$$

The sixth term, T_6, is given by

$$T_6 = -\frac{\partial}{\partial\theta}\left(\frac{g\sin\theta}{a^2 f}u_g\frac{\partial h}{\partial\theta}\right) = \frac{g}{a^2 f^2}\left(-\cos\theta u_g\frac{\partial h}{\partial\theta} - \sin\theta\frac{\partial h}{\partial\theta}\frac{\partial u_g}{\partial\theta} - \sin\theta u_g\frac{\partial^2 h}{\partial\theta^2}\right) + \frac{g\Gamma_1\sin\theta}{a^2}u_g\frac{\partial h}{\partial\theta}. \quad (4.51)$$

Returning to equations (4.49) and (4.50) these are currently dependent on $\frac{\partial v_g}{\partial\theta}$, $\frac{\partial^2 v_g}{\partial\theta^2}$ or $\frac{\partial^2 v_g}{\partial\theta\partial\lambda}$. We have an identity for the first derivative, (4.43), and can extend this to obtain identities for the second derivatives. These are as follows, where the derivations are in Appendix B,

$$\frac{\partial^2 v_g}{\partial\theta\partial\lambda} = \tan\theta\frac{\partial v_g}{\partial\lambda} - \frac{1}{\cos\theta}\frac{\partial^2 u_g}{\partial\lambda^2} + f\frac{\partial v_g}{\partial\lambda}\Gamma_1, \quad (4.52)$$

$$\frac{\partial^2 v_g}{\partial\theta^2} = \left(2\tan^2\theta + 1\right)v_g - 2\frac{\tan\theta}{\cos\theta}\frac{\partial u_g}{\partial\lambda} - \frac{1}{\cos\theta}\frac{\partial^2 u_g}{\partial\theta\partial\lambda} + 2f\tan\theta v_g\Gamma_1 - \frac{2f}{\cos\theta}\frac{\partial u_g}{\partial\lambda}\Gamma_1 + f v_g\Gamma_2. \quad (4.53)$$

Substituting (4.43), (4.52) and (4.53) into equations (4.49) and (4.50) then collect all the terms, $T_1, \ldots, T_6$, equations (4.46) - (4.51), gives

$$-\frac{g}{a^3 f^2\cos^2\theta}\left(2u_{g\lambda}h_{\theta\lambda} + h_\theta u_{g\lambda\lambda} - u_{g\theta}h_{\lambda\lambda} - h_\lambda u_{g\theta\lambda} - \sin\theta v_g h_{\theta\lambda} - \sin\theta h_\theta v_{g\lambda}\right.$$
$$+\cos\theta v_{g\lambda}h_{\theta\theta} + \sin\theta v_{g\lambda}h_\theta - u_{g\lambda\lambda}h_\theta - \sin\theta v_g h_{\theta\lambda} - \left(2\tan\theta\sin\theta + \cos\theta\right)v_g h_\lambda$$
$$\left.+2\tan\theta u_{g\lambda}h_\lambda + u_{\theta\lambda}h_\lambda + \cos^2\theta u_g h_\theta + \sin\theta\cos\theta\left(u_{g\theta}h_\theta + u_g h_{\theta\theta}\right)\right).$$

After cancellations the final result is (4.44) again.

We now consider the second line of (4.27), where we have ∇f^{-1}. As f is only a function of θ we have the vector $\nabla f^{-1} = (0, \Gamma_1, 0)^T$. Therefore

$$\mathbf{k} \cdot \nabla \left(\frac{\alpha}{f} \right) \times \left(\bar{\mathbf{u}}_g \cdot \nabla \left(\mathbf{k} \times \mathbf{u}'_g \right) + \mathbf{u}'_g \cdot \nabla \left(\mathbf{k} \times \bar{\mathbf{u}}_g \right) \right) =$$
$$\frac{\alpha \Gamma_1}{a} \left(\frac{1}{a \cos\theta} \left(\bar{u}_g \frac{\partial v'_g}{\partial \lambda} + u'_g \frac{\partial \bar{v}_g}{\partial \lambda} \right) + \frac{1}{a} \left(\bar{v}_g \frac{\partial v'_g}{\partial \theta} + v'_g \frac{\partial \bar{v}_g}{\partial \theta} \right) + 2 \frac{\tan\theta}{a} \bar{u}_g u'_g \right) \quad (4.54)$$

If we were modeling with a constant f then $\mathbf{k} \cdot \nabla \times \mathbf{u}^{c\prime}$ gives

$$\xi^{c\prime} \equiv \mathbf{k} \cdot \nabla \times \mathbf{u}^{c\prime} \equiv \frac{g}{f} \nabla^2 h' - \frac{2\alpha g}{a^3 f^2 \cos^2\theta} \left(2 u_{g\lambda} h_{\theta\lambda} + \cos\theta v_{g\lambda} h_{\theta\theta} - u_{g\theta} h_{\lambda\lambda} \right.$$
$$+ 2 \tan\theta u_{g\lambda} h_\lambda - \cos\theta v_g h_\lambda - 2 \tan\theta \sin\theta v_g h_\lambda - 2 \sin\theta v_g h_{\theta\lambda} + \cos^2\theta u_g h_\theta$$
$$\left. + \sin\theta \cos\theta \left(u_{g\theta} h_\theta + u_g h_{\theta\theta} \right) \right). \quad (4.55)$$

Currently (4.55) is an equivalence and not an equation.To form an equation for (4.55) we approximate the balanced relative vorticity, $\xi^{c\prime}$, by an increment to the full relative vorticity, $\xi^{c\prime} \approx \xi' = \xi - \bar{\xi}$, where $\bar{\xi}$ is a base state relative vorticity.

If we allow for a variable f then we have (4.55) plus the extra terms

$$-\frac{\alpha g \Gamma_1}{f^2 a^3 \cos^2\theta} \left(\cos\theta \frac{\partial v_g}{\partial \lambda} \frac{\partial h}{\partial \theta} + \cos\theta v_g \frac{\partial^2 h}{\partial \theta \partial \lambda} - u_g \frac{\partial^2 h}{\partial \lambda^2} + \frac{\partial u_g}{\partial \lambda} \frac{\partial h}{\partial \lambda} \right.$$
$$\left. - 2 \cos\theta v_g \frac{\partial^2 h}{\partial \theta \partial \lambda} - 2 \sin\theta v_g \frac{\partial h}{\partial \lambda} + \sin\theta \cos\theta u_g \frac{\partial h}{\partial \theta} \right) + \frac{g \Gamma_2}{a^3 \cos^2\theta} \cos\theta v_g \frac{\partial h}{\partial \lambda}$$
$$+ \frac{\alpha \Gamma_1 g}{f a^3 \cos^2\theta} \left(u_g \frac{\partial^2 h}{\partial \lambda^2} - \cos\theta \frac{\partial h}{\partial \theta} \frac{\partial v_g}{\partial \lambda} + 2 \sin\theta v_g \frac{\partial h}{\partial \lambda} + \cos\theta v_g \frac{\partial^2 h}{\partial \theta \partial \lambda} + \cos\theta \Gamma_1 v_g \frac{\partial h}{\partial \lambda} \right.$$
$$\left. - \frac{\partial h}{\partial \lambda} \frac{\partial u_g}{\partial \lambda} + f \frac{\partial h}{\partial \lambda} f v_g - 2 \frac{\sin\theta}{a} \frac{\partial h}{\partial \theta} u_g \right). \quad (4.56)$$

If we recall the values for α that are of interest to us, 0 and 1, then substituting these into equation (4.55) we obtain a spherical Poisson equation

for h when $\alpha = 0$ and (4.55) with α replaced with 1. This gives two elliptic equations whose solutions are balanced increments to the height field.

We now consider a different method of using the balanced wind field to derive an equation for the balanced height increment where instead of using the relative vorticity we now consider the potential vorticity.

4.3.3 Potential Vorticity Approach (PV)

In this section we derive a generalised version of the balance equation from the potential vorticity of shallow water equations model. The resulting elliptic partial differential equation is a variable coefficient Helmholtz equation. We then find the specific form of the equation for $\alpha = 0$ and $\alpha = 1$.

We start by considering the potential vorticity of the shallow water model given by

$$Q \equiv \frac{f + \xi}{h}, \tag{4.57}$$

where $\xi \equiv \mathbf{k} \cdot \nabla \times \mathbf{u}$. To form the balanced potential vorticity, (3.57), we make the substitution of the balanced relative vorticity, ξ^c, for ξ in (4.57). This now gives us the balanced PV as

$$Q^c \equiv \frac{f + \xi^c}{h}. \tag{4.58}$$

Equation (4.58) is a non-linear equation for h as $\xi^c \equiv \mathbf{k} \times \mathbf{u}^c$ where $\mathbf{u}^c$ is dependent on h. To linearise (4.58) we linearise $\mathbf{u}^c$ by $\mathbf{u}^c = \bar{\mathbf{u}}^c + \mathbf{u}^{c\prime}$. This

then gives us a base state for ξ^c. This is denoted by $\bar{\xi}^c$. We apply the same linearisation to the height field, $h = \bar{h} + h'$, and we still have $\mathbf{u}^{c\prime}$ defined by (4.24), but $\bar{\mathbf{u}}^c$ is defined by

$$\bar{\mathbf{u}}^c \equiv \bar{\mathbf{u}}_g + \frac{2\alpha}{f}\bar{\mathbf{u}}_g \cdot \nabla \left(\mathbf{k} \times \bar{\mathbf{u}}_g\right). \tag{4.59}$$

This is written in component form as

$$\bar{u}^c \equiv \bar{u}_g - \frac{2\alpha}{f}\left(\frac{\bar{u}_g}{a\cos\theta}\frac{\partial \bar{v}_g}{\partial \lambda} + \frac{\bar{v}_g}{a}\frac{\partial \bar{v}_g}{\partial \theta} + \frac{\tan\theta}{a}\bar{u}_g^2\right), \tag{4.60}$$

$$\bar{v}^c \equiv \bar{v}_g + \frac{2\alpha}{f}\left(\frac{\bar{u}_g}{a\cos\theta}\frac{\partial \bar{u}_g}{\partial \lambda} + \frac{\bar{v}_g}{a}\frac{\partial \bar{u}_g}{\partial \theta} - \frac{\tan\theta}{a}\bar{u}_g\bar{v}_g\right). \tag{4.61}$$

In the next step we follow standard procedures for linearisation

$$\begin{aligned} Q^{c\prime} &= \frac{f + \mathbf{k}\cdot\nabla\times\left(\bar{\mathbf{u}}^c + \mathbf{u}^{c\prime}\right)}{\bar{h} + h'} - \frac{f + \mathbf{k}\cdot\nabla\times\bar{\mathbf{u}}^c}{\bar{h}} \\ &= \frac{\bar{h}\left(f + \mathbf{k}\cdot\nabla\times\left(\bar{\mathbf{u}}^c + \mathbf{u}^{c\prime}\right)\right) - \left(\bar{h} + h'\right)\left(f + \mathbf{k}\cdot\nabla\times\bar{\mathbf{u}}^c\right)}{\bar{h}\left(\bar{h} + h'\right)} \\ &= \frac{\mathbf{k}\cdot\nabla\times\mathbf{u}^{c\prime}}{\bar{h} + h'} - \frac{\left(f + \mathbf{k}\cdot\nabla\times\bar{\mathbf{u}}^c\right)h'}{\bar{h}\left(\bar{h} + h'\right)}. \end{aligned} \tag{4.62}$$

However, this equation is still non-linear. Applying a binomial expansion,

$$\frac{1}{\bar{h}}\left(1 + \frac{h'}{\bar{h}}\right)^{-1} = \frac{1}{\bar{h}} - \frac{h'}{\bar{h}^2} + \frac{h'^2}{2\bar{h}^3} + \cdots, \tag{4.63}$$

from which we only require the first term as higher terms introduce non-linear terms. The final result is

$$Q^{c\prime} = \frac{\mathbf{k}\cdot\nabla\times\mathbf{u}^{c\prime}}{\bar{h}} - \frac{\left(f + \mathbf{k}\cdot\nabla\times\bar{\mathbf{u}}^c\right)}{\bar{h}^2}h'. \tag{4.64}$$

The right hand side of (4.64) is a variable coefficient Helmholtz equation for the balanced height increment, h'.

To complete the balance equation we require a linearisation to the left hand side of (4.57) as we use this to approximate the balanced PV. We achieve this by introducing a linearisation to the full wind, $\mathbf{u} = \bar{\mathbf{u}} + \mathbf{u}'$. This then enables us to linearise the relative vorticity as

$$\xi \equiv \mathbf{k} \cdot \nabla \times \mathbf{u} = \mathbf{k} \cdot \nabla \times (\bar{\mathbf{u}} + \mathbf{u}') = \bar{\xi} + \xi'. \tag{4.65}$$

We follow the same procedure set out to derive the linearised balanced PV, (4.62), but now substitute (4.65) into (4.57). The result is

$$Q' \equiv \frac{\bar{\xi}}{\bar{h}} - \frac{f + \xi'}{\bar{h}^2} h'_f, \tag{4.66}$$

where h'_f is the full height increment.

The result is another elliptic partial differential equation, which is a balance equation for the height increment but now using the potential vorticity rather than the relative vorticity to derive the equation. The pde is

$$\frac{\xi'}{\bar{h}} - \frac{f + \bar{\xi}}{\bar{h}^2} h'_f = \frac{\xi^{c\prime}}{\bar{h}} - \frac{\left(f + \bar{\xi}^c\right)}{\bar{h}^2} h' \tag{4.67}$$

To complete the derivation of the variable coefficient Helmholtz equation we require a definition for $\bar{\xi}^c$. Following the derivation set out in Section 4.3.2 for $\xi^{c\prime}$ using (4.59) gives

$$\bar{\xi}^c \equiv \mathbf{k} \cdot \nabla \times \bar{\mathbf{u}}^c = \frac{1}{a \cos\theta} \left(\frac{\partial \bar{v}_g}{\partial \lambda} - \frac{\partial}{\partial \theta} \left(\cos\theta \bar{u}_g \right) \right) + \frac{2\alpha}{a^2 f \cos^2\theta} \left(2 \left(\frac{\partial \bar{u}_g}{\partial \lambda} \right)^2 \right.$$

$$+ \quad 2\cos\theta\frac{\partial\bar{v}_g}{\partial\lambda}\frac{\partial\bar{u}_g}{\partial\theta} - 4\sin\theta\bar{v}_g\frac{\partial\bar{u}_g}{\partial\lambda} + \left(2\sin^2\theta + \cos^2\theta\right)\bar{v}_g^2$$
$$+ \quad \cos^2\theta\bar{u}_g^2 + 2\sin\theta\cos\theta\bar{u}_g\frac{\partial\bar{u}_g}{\partial\theta}\Bigg). \tag{4.68}$$

Equation (4.67) is quite substantially different from (4.55) yet the variable coefficient Helmholtz equation is dependent on $\xi^{c\prime}$. Therefore we can again choose either 0 or 1 for α. Although the classification of the equation will still be the same, i.e. a variable coefficient Helmholtz equation, the variability coming from the division by $\bar{h}$, the ellipticity conditions will be different and we discuss this in Chapter 5.

The motivation for this chapter so far has been to try and derive a possible use of these balanced wind fields to enable a better approximation to the balanced flow in an incremental variational data assimilation scheme. We have derived four balance equations, (4.55) with $\alpha = 0$ or 1, and (4.67) with $\alpha = 0$ or 1. All four solutions are a balanced height increment, h'.

As we mention in Chapter 1, currently the wind field is decomposed into a balanced and an unbalanced variable through considering the vorticity and divergence of $\mathbf{u}$. In the next section we briefly describe the current control variable transforms used in the 3D VAR scheme at the Met Office before we give a set of alternative control variables and describe their transforms.

4.4 Alternative Control Variables

In this section we briefly describe the transforms that are currently used to move between the state variables and the control variables before we describe an alternative set of control variables and transforms using h' as the balanced variable.

4.4.1 Current T and U Transforms

The current set of control variables used at the Met Office are comprised of a streamfunction, ψ, velocity potential, χ, and an unbalanced pressure, ${}^{A}P$. In this section we explain the current transforms from the model variable to the control variables, (T transform), and the transform from the control variables back to the model variables, (U transform).

We start with a brief description of the main aim of an incremental 3D VAR scheme. This is to minimise the following cost functional

$$\begin{aligned} J(\delta\mathbf{x}) = &(\delta\mathbf{x} - \delta\mathbf{x}^b)^T \quad \mathrm{B}^{-1} \quad (\delta\mathbf{x} - \delta\mathbf{x}^b) \\ &+ (\boldsymbol{y} - \mathrm{H}(\delta\mathbf{x}))^T \quad \mathrm{R}^{-1} \quad (\boldsymbol{y} - \mathrm{H}(\delta\mathbf{x})), \end{aligned} \tag{4.69}$$

where $\delta\mathbf{x}$ is the increment to the model state vector, $\delta\mathbf{x}^b$ are the increments to a background states, $\boldsymbol{y}$ is the vector of observations, H is an interpolation operator, B is the background error covariance matrix and R is the observation error covariance matrix.

Currently, the model at the Met Office uses around 10^7 model variables across the whole grid and around 10^6 observations. Therefore the two inverse matrices in (4.69) are large and full, although they are never stored.

One advantage of the T transform is it allows a simplification to be made to B. It transforms the matrix into block diagonal as the three control variables are assumed to be uncorrelated, [54]. This then makes the minimisation problem

$$\begin{aligned} J(\delta\mathbf{z}) = (\delta\mathbf{z} - \delta\mathbf{z}^b)^T \quad & \hat{\mathrm{B}}^{-1} \quad (\delta\mathbf{z} - \delta\mathbf{z}^b) \\ + (\boldsymbol{y} - \mathrm{H}(T\delta\mathbf{z}))^T \quad & \mathrm{R}^{-1} \quad (\boldsymbol{y} - \mathrm{H}(T\delta\mathbf{z})), \end{aligned} \tag{4.70}$$

where we have applied a transform matrix, T, such that $\mathbf{z} = T\mathbf{x}$ and this gives $\delta\mathbf{z} = T\delta\mathbf{x}$, $\delta\mathbf{z}^b = T\delta\mathbf{x}^b$ and $\hat{\mathrm{B}} = T\mathrm{B}T^T$.

The current T transform is defined as follows to calculate the stream-function and velocity potential increments, where we shall now use the prime notation that we have used for increment in the thesis so far,

$$\xi' = \nabla \times \mathbf{u}' = \nabla^2\psi', \tag{4.71}$$

$$\delta' = \nabla \cdot \mathbf{u}' = \nabla^2\chi'. \tag{4.72}$$

The transform to calculate the unbalanced pressure involves the solution of a linear balance equation, [54], and statistical regression which we shall not go into here.

The inverse transform from ψ and χ to $\mathbf{u}$ is achieved through a Helmholtz decomposition similar to the one in Section 2.3, (2.36) with $\varepsilon = 1$. This then gives

$$\mathbf{u}' = \mathbf{k} \times \nabla\psi' + \nabla\chi'. \tag{4.73}$$

This then gives the wind field, $\mathbf{u}$, expressed as the sum of its balanced component, $\mathbf{k} \times \nabla\psi$, and its unbalanced part given by $\nabla\chi$, where the balanced wind field is simply rotational flow.

We now give an alternative set of T and U transforms involving $\mathbf{u}^{c\prime}$, $\mathbf{u}^{s\prime}$, which we define in the next section, and h'.

4.4.2 Alternative T and U Transforms

The T transform that would be used to calculate the alternative balanced control variable, h', would either be (4.55) or (4.67), given either an increment to the relative or potential vorticity.

To calculate the two unbalanced variables we would have to reconstruct $\mathbf{u}^{c\prime}$ through (4.25) and (4.26) and then subtract this from the full wind field increment. This then gives

$$\mathbf{u}^{s\prime} = \mathbf{u}' - \mathbf{u}^{c\prime}, \tag{4.74}$$

where $\mathbf{u}^{s\prime}$ is the unbalanced wind field, the velocity split or the generalised ageostrophic wind. From this we would calculate the unbalanced vorticity

and divergence and form the two elliptic equations

$$\xi^{s\prime} = \nabla \times \mathbf{u}^{s\prime} = \nabla^2 \psi^{s\prime}, \tag{4.75}$$

$$\delta^{s\prime} = \nabla \cdot \mathbf{u}^{s\prime} = \nabla^2 \chi^{s\prime}, \tag{4.76}$$

to find an unbalanced streamfunction and velocity potential increments. The main difference here from the current T transform is we have separated the balanced divergent flow from the full divergence which the standard method using the full vorticity and divergence does not do.

We would be able to reconstruct the unbalanced wind increment through applying the Helmholtz decomposition, (4.73) with $\psi^{s\prime}$ and $\chi^{s\prime}$ in place of ψ' and χ', and then adding the balanced and unbalanced wind field together

$$\mathbf{u}' = \mathbf{u}^{c\prime} + \mathbf{u}^{s\prime}. \tag{4.77}$$

An alternative method of finding an unbalanced height or stream function is to consider equation (4.67) but substitute 0 for the left hand side. This comes from [57], where in Wlasak's thesis he considers unbalanced variables have zero PV.

4.5 Summary

We began this chapter with a summary of the different techniques for initialising the 2-D shallow water equations and the 3-D primitive equations

model. We also summarised the significant results from the work by Salmon and McIntyre and Roulstone and the definition of the balanced wind field, (3.61), the work in this thesis is based on.

After the summary we briefly derived the SWE for the sphere, (4.1), (4.2) and (4.3) in Section 4.1.1, where we also reviewed a derivation of a spherical non-linear balance equation, [22], which is (4.10).

In Section 4.2 we derived the spherical version of the balanced wind field, (4.12) and (4.13) based on (3.61). It is from these that we derived a spherical Monge-Ampère equation, (4.17), through taking $\mathbf{k} \cdot \nabla \times \mathbf{u}^c$ which gives us the constrained relative vorticity, ξ^c.

The aim of Sections 4.3 and 4.4 was to develop the balanced wind field in spherical coordinates to be used with an incremental 3-D or 4-D VAR scheme. As the scheme works with increments to the model variables we introduced a linearisation to the height, $h = \bar{h} + h'$, which enables us to derive a generalised form for the balanced wind field in vector form, (4.24), and in component form, (4.25) and (4.26).

In Section 4.3.2 we formed $\xi^{c\prime}$ through $\xi^{c\prime} = \mathbf{k} \cdot \nabla \times \mathbf{u}^{c\prime}$. The final result for a constant f is a variable coefficient Poisson equation, (4.55). We complete the implementation of the approximation by substituting the variable $\xi' = \xi - \bar{\xi}$ for $\xi^{c\prime}$. We briefly commented about the equation for the two values of α but we go into more detail in Chapter 5.

We then extended this idea to a PV approach in Section 4.3.3. We started from the PV equation, (4.57), and through the substitution of a linearisation to ξ^c as $\xi^c = \bar{\xi}^c + \xi^{c\prime}$ which arises from a linearisation to the height field, $h = \bar{h} + h'$. The final equation is (4.67).

In the last section, Section 4.4, we gave a brief description of the current control variable transform, (4.71) and (4.72) and briefly explained the 3D VAR scheme's cost functional.

In Section 4.4.2 we described an alternative to the T transform using (4.55) or (4.67) to calculate the balanced variable, where the two unbalanced variables could be calculated from (4.75) and (4.76). The alternative U transforms were (4.25), (4.26) and (4.73) (evaluated with $\psi^{s\prime}$ and $\chi^{s\prime}$).

In the next chapter we develop the numerical tools to solve (4.55) and (4.67) and to calculate (4.25) and (4.26), but also explain the underlying theory for elliptic partial differential equations for both the continuous and discrete problems. We also derive the ellipticity conditions for the four equations as well as giving a brief description of the numerical model that we use to generate the base states for three different test cases that are introduced in Chapter 5.

Chapter 5

Ellipticity Theory

In Chapter 4 we derived two new generalised balance equations whose solutions are a balanced height increment. The first equation, (4.55)

$$\xi' = \frac{g}{f}\nabla^2 h' - \frac{2\alpha g}{a^3 f^2 \cos^2\theta}\left(2u_{g\lambda}h_{\theta\lambda} + \cos\theta v_{g\lambda}h_{\theta\theta} - u_{g\theta}h_{\lambda\lambda}\right.$$
$$+2\tan\theta u_{g\lambda}h_\lambda - \cos\theta v_g h_\lambda - 2\tan\theta\sin\theta v_g h_\lambda - 2\sin\theta v_g h_{\theta\lambda} + \cos^2\theta u_g h_\theta$$
$$\left. + \sin\theta\cos\theta\left(u_{g\theta}h_\theta + u_g h_{\theta\theta}\right)\right). \qquad (5.1)$$

is for the relative vorticity method and (4.67)

$$\frac{\xi'}{\bar{h}} - \frac{f+\bar{\xi}}{\bar{h}^2}h'_f = \frac{\xi^{c\prime}}{\bar{h}} - \frac{\left(f+\bar{\xi}^c\right)}{\bar{h}^2}h', \qquad (5.2)$$

is for the potential vorticity method. If we consider (5.1) then we have two choices for α. If we take $\alpha = 0$ then we obtain a Poisson equation. If we allow $\alpha = 1$ then the equation is a variable coefficient Poisson equation. For

(5.2) then α is implicit in the $\xi^{c\prime}$ and $\bar{\xi}^{c\prime}$ terms. For either value of α, 0 or 1, the resulting equation is a variable coefficient Helmholtz equation. All four of these equations are boundary value problems and as such there is a large amount of theory associated with these types of equation, [8], [10], [11], [16], [23], [32], [46].

In Section 5.1 we briefly begin by explaining the spherical grid and the choices for the boundary conditions, we then go on to introduce the theory for the continuous problem by first defining what is meant by an elliptic differential operator and then state the theorem that allows for a solution to exist. This theorem is dependent on the ***ellipticity condition*** which we introduce in Section 5.1.2. We have seen this for the non-linear case (Section 3.3.3) but we now introduce the linear version in Section 5.1.2.

We then derive the ellipticity condition for the four new balance equations in Section 5.1.3. This condition has a significant effect on the equations and many meteorologists have looked for a link between certain flows in the atmosphere and this condition, [25], [26] and [33].

We start Section 5.2 with a brief description of the Met Office's shallow water model from which we generate the base state data. In Section 5.2.2 we describe the numerical approximation that we use to solve (5.1) and (5.2) and we also introduce the theory for discrete elliptic equations.

In the final section, 5.3, we start with a description of the experiments

for which we show results in Chapters 6 and 7. The first is to investigate the structure of the ellipticity condition and the coefficients of the discrete equations. The second is to see the difference between the solutions to the balanced equations. We also describe experiments associated with the assumption that under constant f then the geostrophic wind is non-divergent and the higher order balance, $\mathbf{u}^{c\prime}$ is not divergence free.

To start the shallow water equation model that is described in Section 5.2.1, we use a Rossby-Haurwitz wave and we introduce this in Section 5.3.2. In Section 5.3.3 we introduce three test cases that describe three different Burger regimes. We begin with a summary of the four new balance equations with which the remainder of the thesis is concerned.

5.1 Linearised Balance Equations

As we mention in the introduction to this chapter the four linearised equations are given by (5.1) with $\alpha = 0$ or 1 and by (5.2) again with either $\alpha = 0, 1$ but for (5.2), α is in $\xi^{c\prime}$ and $\bar{\xi}^{c}$.

The two methods arise from considering either the relative vorticity to capture the balanced flow, (Section 4.3.2), or the potential vorticity, (Section 4.3.3). In this section we look at the four equations and their classification as elliptic equations (Section 5.1.1), and the boundary conditions associated

with the equations. The theorem for the existence of the elliptic equation which introduces the ellipticity condition for linear pdes is given in Section 5.1.2, and we examine this condition for the four balance equations in Section 5.1.3.

5.1.1 Balance Equations and Boundary Conditions

As we mention in Chapter 4, the four balance relations are all boundary value problems but so far we have not mentioned the boundary conditions associated with the equations. If we consider the following two diagrams of the domains, (Figures 5.1 and 5.2), we see that the boundary condition for the λ axis is periodicity, but the θ directional boundary condition poses a problem.

The same condition that we use for the λ direction is a possible choice for the two θ boundaries. However, as we cross the poles we change direction. If we consider the direction that the $\mathbf{j}$ unit vector is pointing in as we enter the northern pole then the values of θ are increasing, but as we cross the pole the values of θ are now decreasing.

Another boundary condition is the information that there cannot be a λ derivative at either of the poles due to the singularity there, i.e. all the lines of latitude coincide there, but there is no change in the longitudinal direction

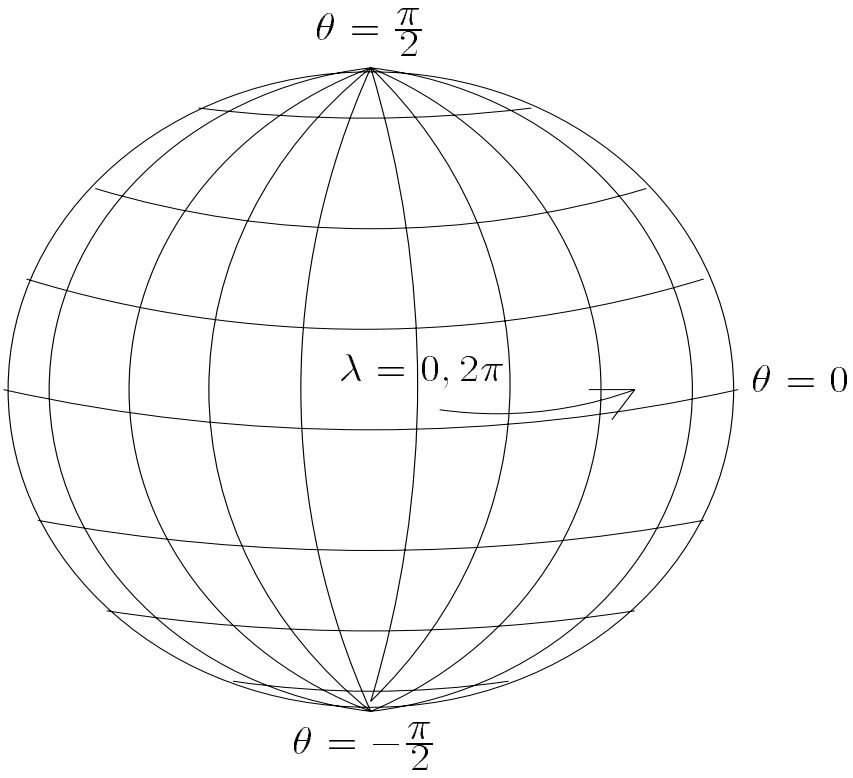

Figure 5.1: Diagram of the Spherical Domain.

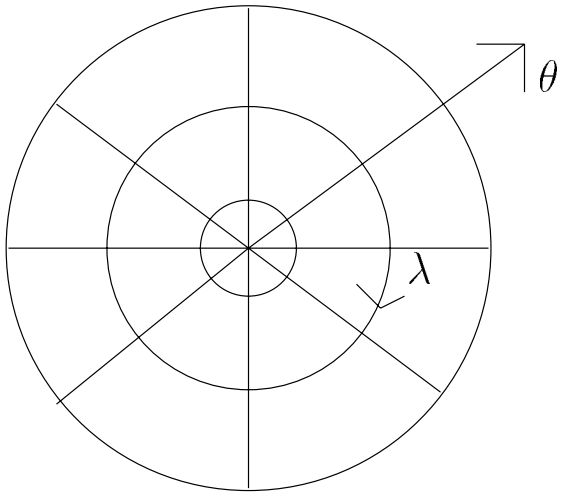

Figure 5.2: Diagram Showing the Spherical Coordinates at The Pole.

(see Figure 5.2).

A straightforward condition, for the two poles, is a Dirichlet condition. If we were considering a simple Poisson equation then there is a proof in [46] that shows by assigning a constant boundary condition then the solution is uniquely determined.

For our problems we shall use the periodicity condition for λ and a Dirichlet condition for the poles.

5.1.2 Elliptic Differential Equations

We start by considering the general form for a second order partial differential equation

$$\begin{aligned} &A(\theta,\lambda)\frac{\partial^2 S}{\partial\lambda^2}+B(\theta,\lambda)\frac{\partial^2 S}{\partial\theta\partial\lambda}+C(\theta,\lambda)\frac{\partial^2 S}{\partial\theta^2}\\ &+D(\theta,\lambda)\frac{\partial S}{\partial\theta}+E(\theta,\lambda)\frac{\partial S}{\partial\lambda}+F(\theta,\lambda)S=G(\theta,\lambda), \end{aligned} \tag{5.3}$$

where the coefficients, $A,\cdots,G$ are functions of θ and λ and S is the solution to the equation. This can be classified as either a *hyperbolic*, *parabolic* or *elliptic* equation, [8], [11] and [16].

Before we give the theorem for the existence of the unique solution for a general linear elliptic equation we give the following definitions for an elliptic operator.

Definition 1 *A pde of the form*

$$AS_{\lambda\lambda} + BS_{\lambda\theta} + CS_{\theta\theta} + DS_{\lambda} + ES_{\theta} + FS = G, \tag{5.4}$$

where the coefficients, $A, \ldots, G$ *are functions of* θ *and* λ*, is* ***hyperbolic*** *if* $B^2 - 4AC > 0$*,* ***parabolic*** *if* $B^2 - 4AC = 0$ *and* ***elliptic*** *if* $B^2 - 4AC < 0$*.*

This then enables the following definition for the operator to be elliptic.

Definition 2 *The differential operator*

$$L[S] \equiv AS_{\lambda\lambda} + BS_{\lambda\theta} + CS_{\theta\theta}, \tag{5.5}$$

is elliptic if and only if $B^2 - 4AC < 0$*.*

We now give a specific version of a theorem from [11], that defines the existence and uniqueness of the solution to a homogenous elliptic problem.

Theorem 2 *Given the elliptic operator,* $L[S]$*, then the differential equation*

$$L[S] + DS_{\lambda} + ES_{\theta} + FS = 0 \tag{5.6}$$

has one solution which has continuous derivatives up to second order in the interior of the domain and is continuous throughout the interior and the boundaries and assumes the prescribed boundary conditions values on the boundary.

The more specific theorem is given [11] for the inhomogenous case.

We can classify the equations further with the following definition.

Definition 3 *The pde, (5.3) is said to be* ***semi-linear*** *if A, B and C are only functions of the independent variables and* ***quasi-linear*** *if the same coefficients are functions of the independent variables and S, S_θ or S_λ.*

Therefore the three balance relations, (5.1) with $\alpha = 1$ and both values for α in (5.2), are semi-linear where the Poisson equation is linear.

The inequality, $B^2 - 4AC < 0$ in definition 1 is the ***ellipticity conditions*** as they are the conditions that ensures that the differential equation has complex characteristics, [11], [16]. This condition is an important property of elliptic equations. We examine the ellipticity condition for the new balance equations next in Section 5.1.3.

5.1.3 Ellipticity Conditions

We start with (5.1) where we multiply throughout by $a^2 f^2 \cos\theta$ to remove the singularity at the poles due to the terms $\frac{1}{\cos\theta}$ and also, from a numerical point of view, for the approximations in Section 5.2.2, to remove a large number from the denominator, a^2. The coefficients A, B and C are then given as

$$A(\theta,\lambda) = gf + 2g\alpha\frac{\partial \bar{u}_g}{\partial\theta}, \tag{5.7}$$

$$B(\theta,\lambda) = -4g\alpha\frac{\partial \bar{u}_g}{\partial\lambda} + \frac{4g\alpha\sin\theta}{a}\bar{v}_g, \tag{5.8}$$

$$C(\theta,\lambda) = gf\cos^2\theta - 2g\alpha\cos\theta\frac{\partial \bar{v}_g}{\partial\lambda} - \frac{2g\alpha\sin\theta\cos\theta}{a}\bar{u}_g. \tag{5.9}$$

The coefficents for the ellipticity condition, $B^2 - 4AC < 0$, are given by

$$B^2 = \alpha^2 \left(16g^2 \left(\frac{\partial \bar{u}_g}{\partial \lambda} \right)^2 - \frac{32g^2 \sin\theta}{a} \frac{\partial \bar{u}_g}{\partial \lambda} \bar{v}_g + \frac{16g^2 \sin^2\theta}{a^2} \bar{v}_g^2 \right), \tag{5.10}$$

$$\begin{aligned} 4AC &= 4g^2 f^2 \cos^2\theta - 8\alpha g^2 f \cos\theta \frac{\partial \bar{v}_g}{\partial \lambda} - \frac{\alpha 8 g^2 f \sin\theta \cos\theta}{a} \bar{u}_g \qquad (5.11) \\ &+ 8\alpha g^2 f \cos^2\theta \frac{\partial \bar{u}_g}{\partial \theta} - 16\alpha^2 g^2 \cos\theta \frac{\partial \bar{v}_g}{\partial \lambda} \frac{\partial \bar{u}_g}{\partial \theta} - \frac{\alpha^2 16 g^2 \sin\theta \cos\theta}{a} \frac{\partial \bar{u}_g}{\partial \theta} \bar{u}_g. \end{aligned}$$

Therefore for the ellipticity condition to hold and hence for there to be solutions we require (5.10) $-$ (5.11) < 0. If we recall (4.17), we may write

$$\begin{aligned} \xi^c &\equiv \frac{1}{\cos\theta} \left(\frac{\partial v_g}{\partial \lambda} - \frac{\partial u_g}{\partial \theta} + \frac{\sin\theta}{a} u_g \right) + \frac{2\alpha}{f \cos^2\theta} \left(\left(\frac{\partial u_g}{\partial \lambda} \right)^2 + \cos\theta \frac{\partial v_g}{\partial \lambda} \frac{\partial u_g}{\partial \theta} \right. \\ &- \left. 2 \frac{\sin\theta}{a} v_g \frac{\partial u_g}{\partial \lambda} + \frac{\sin^2\theta}{a^2} v_g^2 + \frac{\sin\theta \cos\theta}{a} u_g \frac{\partial u_g}{\partial \theta} + \frac{\cos^2\theta}{2a^2} \left(u_g^2 + v_g^2 \right) \right). \end{aligned} \tag{5.12}$$

Comparing (5.12) with (5.11) we see that we can now write the ellipticity condition for (5.1) as

$$\alpha \cos^2\theta f \xi^c \left(\bar{u}_g, \bar{v}_g \right) < \frac{\cos^2\theta}{2a^2} \left(f^2 a^2 + \alpha^2 f \left(\bar{u}_g^2 + \bar{v}_g^2 \right) \right), \tag{5.13}$$

where $\xi^c \left(\bar{u}_g, \bar{v}_g \right)$ represents (5.12) evaluated with $\bar{u}_g, \bar{v}_g$ instead of u_g, v_g. This is therefore a bound on the choice of base state, which we may use for the linearisation. If we set $\alpha = 0$ (5.13) we see that the condition for the interior of the domain, $\left(-\frac{\pi}{2}, \frac{\pi}{2} \right) \times [0, 2\pi)$, is

$$0 < f^2, \tag{5.14}$$

and is always satisfied, given the boundary condition, for a constant f.

For the PV equation, (5.2), then the coefficients for the ellipticity condition are given by

$$A(\theta,\lambda) = \frac{\left(gf + 2\alpha g\frac{\partial \bar{u}_g}{\partial \theta}\right)}{\bar{h}}, \tag{5.15}$$

$$B(\theta,\lambda) = \frac{\left(-4\alpha g\frac{\partial \bar{u}_g}{\partial \lambda} + \frac{4\alpha g\sin\theta}{a}\bar{v}_g\right)}{\bar{h}}, \tag{5.16}$$

$$C(\theta,\lambda) = \frac{\left(gf\cos^2\theta - 2\alpha g\cos\theta\frac{\partial \bar{v}_g}{\partial \lambda} - \frac{2\alpha g\sin\theta\cos\theta}{a}\bar{u}_g\right)}{\bar{h}}. \tag{5.17}$$

This then gives the ellipticity condition coefficients as

$$B^2 = \frac{\alpha^2 16g^2\left(\frac{\partial \bar{u}_g}{\partial \lambda}\right)^2}{\bar{h}^2} - \frac{\alpha^2 32g^2\sin\theta\frac{\partial \bar{u}_g}{\partial \lambda}\bar{v}_g}{a\bar{h}^2} + \frac{\alpha^2 16g^2\sin^2\theta\bar{v}_g^2}{a^2\bar{h}^2}, \tag{5.18}$$

$$\begin{aligned} 4AC = {} & \frac{4g^2f^2\cos^2\theta}{\bar{h}^2} - \frac{\alpha 8g^2 f\cos\theta\frac{\partial \bar{v}_g}{\partial \lambda}}{\bar{h}^2} + \frac{\alpha 8g^2 f\cos^2\theta\frac{\partial \bar{u}_g}{\partial \theta}}{\bar{h}^2} \\ & - \frac{\alpha^2 16g^2\cos\theta\frac{\partial \bar{u}_g}{\partial \theta}\frac{\partial \bar{v}_g}{\partial \lambda}}{\bar{h}^2} - \frac{\alpha^2 16g^2\sin\theta\cos\theta\frac{\partial \bar{u}_g}{\partial \theta}\bar{u}_g}{a\bar{h}^2} \\ & - \frac{8\alpha g^2 f\sin\theta\cos\theta\bar{u}_g}{a\bar{h}^2}. \end{aligned} \tag{5.19}$$

For (5.2) to be elliptic we require (5.18) $<$ (5.19). As with the RV ellipticity condition, (5.13), we are able to reduce the condition to be in terms of the base state relative constrained vorticity. If we multiply throughout by $\bar{h}^2$, then the resulting condition is (5.13) and for $\alpha = 0$ then the result is also the same as for the RV condition.

In the next section we describe the numerical approximations we use to solve (5.1) and (5.2) and introduce the condition for a solution to the

numerical approximation to exist.

5.2 Numerical Approximations

In the last section we derived the ellipticity conditions for the four balance equations, (5.1) and (5.2) with either $\alpha = 0, 1$. As we see from theorem 2, these are the conditions for the differential equations to have solutions.

In this section we summarise the numerical approximations to (5.1) and (5.2) along with the boundary conditions that we use to calculate the balanced wind field with. We also introduce, in Section 5.2.2, the condition for solutions to the discrete problem to exist.

We start with an introduction to the Met Office's shallow water model that we use to calculate the base states.

5.2.1 Met Office's Shallow Water Model

In this section we briefly introduce the numerical model that we use to calculate the base states. These base states are the three output variables, height, h, zonal wind, u and meridional wind, v.

The grid which the model uses is the Arakawa C-grid, (Figure 5.3). This grid staggers the points, where the height field discrete values are at the points $\left((j-1)\,\Delta\lambda, -\frac{\pi}{2} + (i-1)\,\Delta\theta\right)$, with $i = 1, 2, \ldots, N$, $j = 1, 2, \ldots, M$,

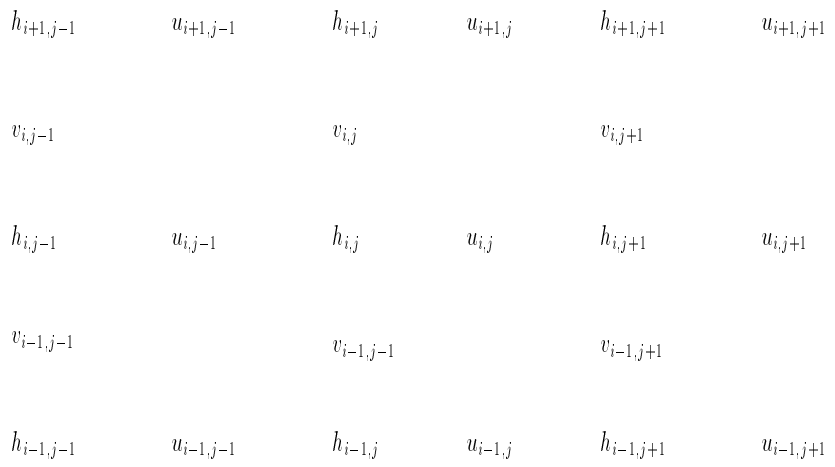

Figure 5.3: Diagram of the Arakawa C Grid.

and the constants N and M are the total number of points in the θ and λ directions respectively. The step sizes $\Delta\lambda$ and $\Delta\theta$ are given by

$$\Delta\lambda = \frac{2\pi}{M}, \qquad \Delta\theta = \frac{\pi}{(N-1)}. \tag{5.20}$$

The u points are $\left((j-1)\,\Delta\lambda + \frac{\Delta\lambda}{2}, -\frac{\pi}{2} + (i-1)\,\Delta\theta\right)$ and the v points are $\left((j-1)\,\Delta\lambda, -\frac{\pi}{2} + \frac{\Delta\theta}{2} + (i-1)\,\Delta\theta\right)$.

The code that solves the shallow water equations is the same as that used within the Met Office's numerical weather prediction model; this is referred to as the Unified Model, [28], [54]. The numerical approximation is a semi-Lagrangian, semi-implicit, predictor-corrector scheme. The wind field is predicted for the next time step and the difference between the present time step and the next is calculated and stored. From the continuity equation a variable coefficient Helmholtz equation is solved for the difference between

the two time levels. The solution to the Helmholtz problem is obtained through using a multigrid procedure. There is a more detailed description in [28].

5.2.2 Numerical Approximations to the New Balance Equations

In this section we describe the numerical approximations that we use to solve equations (5.1) and (5.2), we also give a description of the approximations to calculate $\mathbf{u}^{c\prime}$.

We shall also summarise the conditions for a solution to the discrete equation to exist; a more detailed description is given in [32] and [46]. We start with a description of the numerical approximations used for the coefficients in the differential equation.

The linearisation factors are the geostrophic winds and their derivatives. We calculate the geostrophic winds from the base height, $\bar{h}$, given in spherical coordinates by (4.22) and (4.23). We approximate these with the central differences

$$u_{g,i,j} \approx -\frac{g}{f_i a}\frac{\bar{h}_{i+1,j}-\bar{h}_{i-1,j}}{2\Delta\theta}, \qquad v_{g,i,j} \approx \frac{g}{a f_i \cos\theta_i}\frac{\bar{h}_{i,j+1}-\bar{h}_{i,j-1}}{2\Delta\lambda}, \qquad (5.21)$$

where $f_i = 2\Omega\sin\theta_i$ and $\theta_i = -\frac{\pi}{2} + (i-1)\,\Delta\theta$. These approximations are second order,[32], [46] and consistent with (4.22) and (4.23), [1] and [23].

To enforce the periodicity condition in the λ direction we use the conditions that for the points $j = M$ then $j + 1 = 1$ and for the points $j = 1$ then $j - 1 = M$. At the two θ boundaries, we use the periodicity condition to approximate $(i + 1, j)$ at the north pole with $\left(i - 1, j + \frac{M}{2}\right)$ for $j \leq \frac{M}{2}$ and $\left(i - 1, j - \frac{M}{2}\right)$ for $\frac{M}{2} < j \leq M$. For the south pole it is the $(i - 1, j)$ term that is approximated. Then for $(i - 1, j)$ this is $\left(i - 1, j + \frac{M}{2}\right)$ for $j \leq \frac{M}{2}$ and $(i - 1, j)$ is $\left(i + 1, j - \frac{M}{2}\right)$ for $\frac{M}{2} < j \leq M$.

For the numerical experiments we perform in Chapters 6 and 7 we have taken $M = 96$ and $N = 65$.

To calculate the first derivatives of the geostrophic winds we apply the central differences

$$\frac{\partial \bar{u}_g}{\partial \lambda} \approx \frac{\bar{u}_{g,i,j+1} - \bar{u}_{g,i,j-1}}{2\Delta\lambda}, \qquad \frac{\partial \bar{v}_g}{\partial \lambda} \approx \frac{\bar{v}_{g,i,j+1} - \bar{v}_{g,i,j-1}}{2\Delta\lambda}, \tag{5.22}$$

for the λ derivatives and

$$\frac{\partial \bar{u}_g}{\partial \theta} \approx \frac{\bar{u}_{g,i+1,j} - \bar{u}_{g,i-1,j}}{2\Delta\theta}, \tag{5.23}$$

for the θ derivative.

The stencil we use to approximate (5.1) and (5.2) is a nine-point stencil. This entails the nine points surrounding and including the central point shown in Figure 5.4. To approximate the second derivative of the height field we use the standard central differences for the λ and θ. These approximations

are given by

$$\frac{\partial^2 h'}{\partial \lambda^2} \approx \frac{h'_{i,j+1} - 2h'_{i,j} + h'_{i,j-1}}{a^2 \Delta \lambda^2}, \qquad \frac{\partial^2 h'}{\partial \theta^2} \approx \frac{h'_{i+1,j} - 2h'_{i,j} + h'_{i-1,j}}{a^2 \Delta \theta^2}. \quad (5.24)$$

where for the λ direction we use a periodicity condition and apply this the same way as for the geostrophic wind calculations. These can be shown to be a second order approximation, [46], [32], and also consistent, [1], [23].

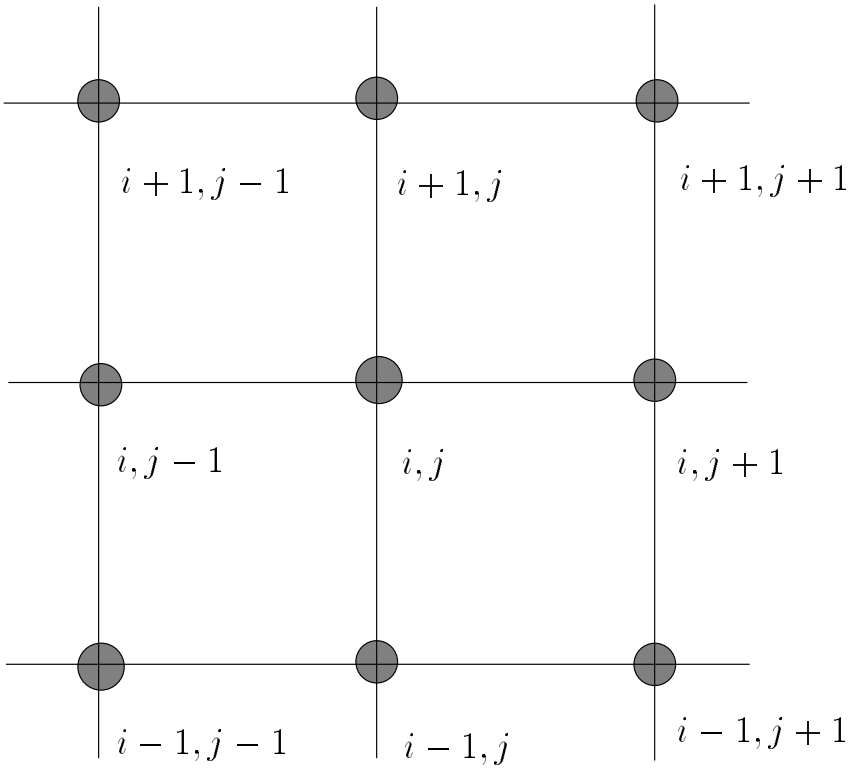

Figure 5.4: Diagram of the Nine-Point Stencil.

The cross derivative approximation is derived as follows

$$\begin{aligned} \frac{\partial^2 h'}{\partial \theta \partial \lambda} &\approx \frac{1}{2\Delta\theta}\left(\frac{h'_{i+1,j+1} - h'_{i+1,j-1}}{2\Delta\lambda} - \frac{h'_{i-1,j+1} - h'_{i-1.j-1}}{2\Delta\lambda}\right), \\ &\approx \frac{h'_{i+1,j+1} + h'_{i-1,j-1} - h'_{i+1,j-1} - h'_{i-1,j+1}}{4\Delta\theta\Delta\lambda}. \end{aligned} \quad (5.25)$$

It is this last approximation that makes the numerical approximate to the differential equation into a nine-point stencil, as we use the four corner points in Figure 5.4.

To complete the discrete approximation to equations (5.1) and (5.2) we require approximations for $\bar{\xi}^c$ and $\xi^{c\prime}$. We use the full relative vorticity, ξ, and calculate $\bar{\xi} = \mathbf{k} \cdot \nabla \times \bar{\mathbf{u}}$, with $\xi' = \xi - \bar{\xi}$, and $\bar{\mathbf{u}}$ is the base state wind field.

We require ξ' at the h points in the grid but this variable is dependent on the derivatives of the wind fields which are not evaluated at the h points. We overcome this by using the following approximation which is second order in the horizontal directions, [57].

$$\begin{aligned}
\xi'_{i,j} &\approx \left(\mathbf{k} \cdot \nabla \times \mathbf{u}'_{i,j}\right), \qquad (5.26)\\
&\approx \frac{1}{a\cos\theta}\left(\frac{\partial v'}{\partial \lambda} - \frac{\partial}{\partial \theta}\left(\cos\theta u'\right)\right)_{i,j},\\
&\approx \frac{1}{a\cos\theta_i}\left(\frac{v'_{i,j+1} - v'_{i,j-1} + v'_{i-1,j+1} - v'_{i-1,j-1}}{4\Delta\lambda}\right.\\
&\quad \left. -\frac{\cos\theta_{i+1}\left(u'_{i+1,j} + u'_{i+1,j-1}\right) - \cos\theta_{i-1}\left(u'_{i-1,j} + u'_{i-1,j-1}\right)}{4\Delta\theta}\right).
\end{aligned}$$

In some of the experiments that we perform on $\mathbf{u}^{c\prime}$ we require an approximation for the divergence. The expression for δ' is given by

$$\begin{aligned}
\delta'_{i,j} &\approx \nabla \cdot \mathbf{u}'_{i,j}, \qquad (5.27)\\
&\approx \frac{1}{a\cos\theta}\left(\frac{\partial u'}{\partial \lambda} + \frac{\partial}{\partial \theta}\left(\cos\theta v'\right)\right)_{i,j}
\end{aligned}$$

$$\approx \quad \frac{1}{a\cos\theta_i}\left(\frac{u'_{i+1,j}-u'_{i,j}}{\Delta\lambda}+\frac{\cos\theta_{i-1}v'_{i,j}-\cos\theta_{i-1}v'_{i-1,j}}{\Delta\theta}\right).$$

The result of using the nine-point stencil to approximate the elliptic equations is a large, sparse matrix to invert. We apply a direct method to invert the matrix by using the two NAG routines, F01BRF and F04AXF.

The program F01BRF performs a LU decomposition

$$WAV = LU, \tag{5.28}$$

where the matrices W and V are permutation matrices to enable pivoting of the matrix to make the decomposition stable, [1]. The matrix L is unit lower triangular and U is upper triangular. The factorisation uses a sparse variant of Gaussian elimination to maintain a balance between the sparseness property of the matrix and the accuracy through round off error. More details are available from *www.nag.co.uk*. The routine F04AXF takes the output from the first routine and solves the equation through a block forward or backward substitution.

We now briefly summarise the theory for the solution to the matrix equation. We start with a definition.

Definition 4 *The matrix A is called a M-matrix if the following are all true,*

1. $a_{ii} > 0$, $a_{i,j} \leq 0$ $(i \neq j)$,

2. *A is diagonally dominant and strictly diagonally dominant for at least one row,*

3. *A is irreducible.*

This then leads to the following theorem, [51].

Theorem 3 *If the matrix A is a M-Matrix, then it is invertible.*

Therefore if the matrix that arises from the discretisation of the elliptic pde satisfies these conditions then there exist a solution.

The final set of numerical approximations we derive concern $\mathbf{u}^{c\prime}$. Once we have solved the discrete elliptic equation we have a *balanced* height increment but to calculate the other two control variables, $\psi^{s\prime}$ and $\chi^{s\prime}$, (Section 4.4), we have to calculate the velocity split, (4.74), and so we have to calculate $\mathbf{u}^{c\prime}$ from the height, (4.24) i.e. we have to numerically approximate (4.25) and (4.26). To do this we have to calculate both the base state and incremental geostrophic wind, $\bar{u}_g, \bar{v}_g, u'_g$ and v'_g at the u, v points, along with their first derivatives.

To do this we follow a similar method that is used to calculate ξ'. We begin with u_g at the u points, where u_g is geostrophic wind. If we follow the approximation for ξ' we see that the fields have been averaged to be evaluated at the half points either side of the $h_{i,j}$ point. We extend this idea to have the height fields averaged either side of the u or v point.

To calculate the u_g component at the u points we evaluate the following expression

$$-\frac{1}{a}\frac{\partial h}{\partial \theta}\bigg|_{i,j+\frac{1}{2}} \approx \frac{1}{a}\left(\frac{h_{i-1,j}+h_{i-1,j+1}-(h_{i+1,j+1}+h_{i+1,j})}{4\Delta\theta}\right). \tag{5.29}$$

If we look at Figure 5.5 we see where the averages lie and how we can use these to calculate u_g at the u points. Here we have used a general height to illustrate that we can apply the same approximation to either $\bar{h}$ or h'.

$h_{i+1,j}$ $\quad$ $\hat{h}_{i+1}$ $\quad$ $h_{i+1,j+1}$

$h_{i,j}$ $\quad$ $u_{i,j}$ $\quad$ $h_{i,j+1}$

$h_{i-1,j}$ $\quad$ $\hat{h}_{i-1}$ $\quad$ $h_{i-1,j+1}$

Figure 5.5: Diagram for the weighting of the u component of the geostrophic wind at the u point, where $\hat{h}_{i+1} = \frac{h_{i+1,j+1}+h_{i+1,j}}{2}$ and $\hat{h}_{i-1} = \frac{h_{i-1,j+1}+h_{i-1,j}}{2}$.

To calculate the v_g component at the u point we use

$$\frac{1}{a\cos\theta}\frac{\partial h}{\partial \lambda}\bigg|_{i,j+\frac{1}{2}} \approx \frac{1}{a\cos\theta_i}\left(\frac{h_{i,j+1}+h_{i,j+2}-(h_{i,j}+h_{i,j-1})}{4\Delta\lambda}\right). \tag{5.30}$$

We have drawn a diagram to show where the averages lie for this approximation, Figure 5.6. For the two geostrophic winds to be evaluated at the v

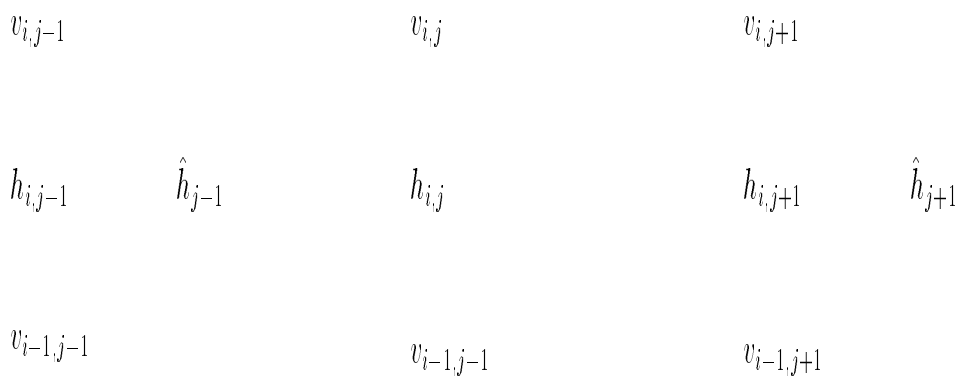

Figure 5.6: Diagram for the weighting of the v component of the geostrophic wind at the u point where $\hat{h}_{j+1} = \frac{h_{i,j+1} + h_{i,j+2}}{2}$ and $\hat{h}_{j-1} = \frac{h_{i,j-1} + h_{i,j}}{2}$.

points we use the following expression (see also the diagrams of the approximations in Figures 5.7 and 5.8)

$$-\frac{1}{a}\frac{\partial h}{\partial \theta}\bigg|_{i+\frac{1}{2},j} \approx -\frac{1}{a}\left(\frac{h_{i+1,j} + h_{i,j} - h_{i-1,j} - h_{i-2,j}}{4\Delta\theta}\right), \tag{5.31}$$

$$\frac{1}{a\cos\theta}\frac{\partial h}{\partial \lambda}\bigg|_{i+\frac{1}{2},j} \approx \frac{1}{a\cos\theta_{i+\frac{1}{2}}}\left(\frac{h_{i,j-1} + h_{i-1,j-1} - h_{i,j+1} - h_{i-1,j+1}}{4\Delta\lambda}\right). \tag{5.32}$$

This completes all the numerical approximations we use to calculate h', $u^{c\prime}$, $v^{c\prime}$, $u^{s\prime}$ and $v^{s\prime}$; we define these in Section 4.4. For $\psi^{s\prime}$ and $\chi^{s\prime}$, also derived in Section 4.4, we evaluate (5.26) and (5.27) with $\mathbf{u}^{s\prime}$ and use a five-point stencil, [32], to approximate (4.75) and (4.76) with Dirichlet boundary conditions.

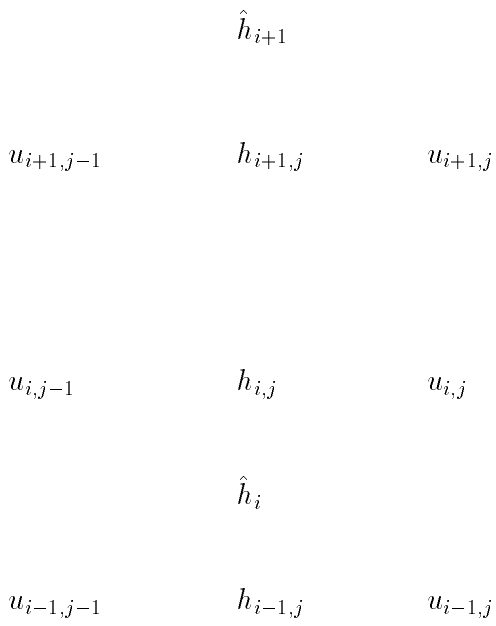

Figure 5.7: Diagram for the weighting of the u component of the geostrophic wind at the v point where $\hat{h}_{i+1} = \frac{h_{i+2,j} + h_{i+1,j}}{2}$ and $\hat{h}_i = \frac{h_{i,j} + h_{i-1,j}}{2}$.

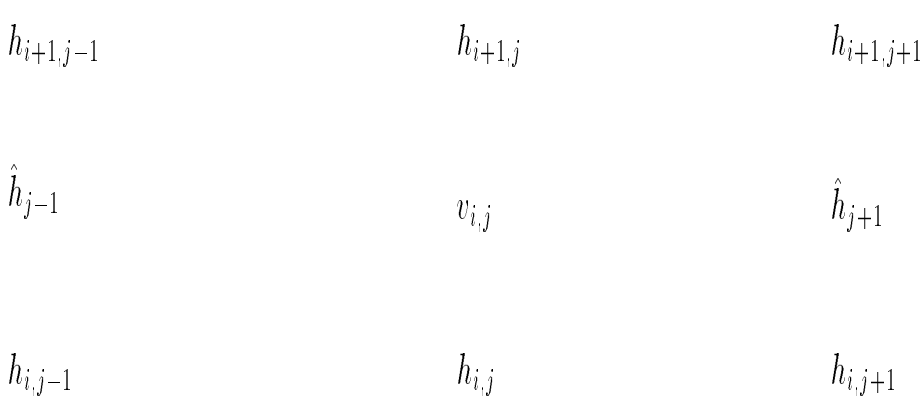

Figure 5.8: Diagram for the weighting of the v component of the geostrophic wind at the v point where $\hat{h}_{j+1} = \frac{h_{i,j+1} + h_{i+1,j+1}}{2}$ and $\hat{h}_{j-1} = \frac{h_{i+1,j-1} + h_{i,j-1}}{2}$.

5.3 Initial Conditions

In this section we describe briefly in 5.3.1 the experiments that we perform using the data generated from the shallow water model. Then in Section 5.3.2 we introduce the Rossby-Haurwitz wave. This wave is the initial condition that we use to generate different types of flow regimes in the SWE model. In Section 5.3.3 we introduce three test cases that arise from varying certain parameters in the Rossby-Haurwitz wave. This then generates different Burger number regimes, which we also introduce in this section.

5.3.1 Experiments

There are four sets of experiments that we perform involving the four balance equations. The first experiment involves evaluating the ellipticity condition for (5.1) and (5.2) with $\alpha = 1$, for three test cases both at the initial time and at 72 hrs into the model run. At both time levels we compare the condition to that of the equations when $\alpha = 0$.

The second set involves a scale analysis at $\theta = 45°N$ of the terms in the ellipticity conditions and the coefficients of the differential equation to see if there are any terms that could be removed to make the solution of the numerical equation more economical.

The other two experiments, the results of which are presented in Chapter

7, are concerned with the numerical solutions of the four balance relations on the sphere for the same three test cases. We look at $\|\boldsymbol{b}\|_2 = \sqrt{\sum_{i=1}^{N} b_i^2}$ where $\boldsymbol{b}$ is a general vector and b_i is a general entry in $\boldsymbol{b}$. For our experiment we form a vector for each latitudinal ring of the difference between the full height increment, h'_f, and the balanced height increment, h', in the mid-latitudes to see how each method differs in the different Burger regimes. The last experiment involves testing the hypothesis that for constant f the new balanced wind field is divergent.

5.3.2 Rossby Haurwitz Wave

The Rossby-Haurwitz wave was shown to be an analytical solution to the non-linear barotropic vorticity equation on the sphere by Haurwitz [18]. The equation for the barotropic vorticity model is

$$\frac{\partial \zeta}{\partial t} + (\mathbf{u} \cdot \nabla)\, \zeta = 0, \tag{5.33}$$

with

$$\boldsymbol{u} = \boldsymbol{k} \times \nabla \psi, \qquad \zeta = \boldsymbol{k}.\nabla \times \boldsymbol{u} = \nabla^2 \psi.$$

A solution to this differential equation is of the following form

$$\psi = -a^2 \omega \sin\theta + K \cos^R \theta \sin\theta \cos R\lambda, \tag{5.34}$$

where ω, K and R are constants. In Williamson *et al*, [55], the values of $\omega = K = 7.848 \times 10^{-6} s^{-1}$ and $R = 4$ are suggested as good conditions for the initial wave profile.

In Wlasak's thesis, [57], the value for ω of $7.848 \times 10^{-7} s^{-1}$ was also used in some experiments. The effect of using different values for ω, and hence K, is to change the height field from the pole to the equator. This affects the ellipticity condition.

The Rossby-Haurwitz waves do not have the non-dispersive property that it has in the non-linear barotropic vorticity model. Williamson et al reassures us that the use of both the SWE model and the initial condition are good approximations for numerical weather modelling.

In [55] expressions are given for the height, h, the horizontal wind components, u and v and also the absolute vorticity ζ that make up the Rossby-Haurwitz wave. These are given in terms of constants ω, K and R and are

$$h = \frac{1}{g}\left(gh_0 + a^2 A(\theta) + a^2 B(\theta)\cos R\lambda + a^2 C(\theta)\cos 2R\lambda\right), \quad (5.35)$$

$$u = a\omega\cos\theta + aK\cos^{R-1}\theta\left(R\sin^2\theta - \cos^2\theta\right)\cos R\lambda, \quad (5.36)$$

$$v = -aKR\cos^{R-1}\theta\sin\theta\sin R\lambda, \quad (5.37)$$

$$\zeta = 2\omega\sin\theta - K\sin\theta\cos^R\theta\left(R^2 + 3R + 2\right)\cos R\lambda, \quad (5.38)$$

where $A(\theta), B(\theta)$ and $C(\theta)$ are given by

$$\begin{aligned} A(\theta) &= \frac{\omega}{2}(2\Omega+\omega)\cos^2\theta + \frac{1}{4}K^2\cos^{2R}\theta\left[(R+1)\cos^2\theta\right. \\ &+ \left.\left(2R^2-R-2\right)-2R^2\cos^{-2}\theta\right], \end{aligned} \tag{5.39}$$

$$B(\theta) = \frac{2(\Omega+\omega)K}{(R+1)(R+2)}\cos^R\theta\left[\left(R^2+2R+2\right)-(R+1)^2\cos^2\theta\right], \tag{5.40}$$

$$C(\theta) = \frac{K^2}{4}\cos^{2R}\theta\left[(R+1)\cos^2\theta-(R+2)\right]. \tag{5.41}$$

The main feature of this wave in equation (5.33) is that it travels west to east in a non-divergent form. The direction in which the wave travels in the SWE model is in the same direction but the wave is diverging i.e. $\nabla\cdot\mathbf{u}\neq 0$.

5.3.3 Test Cases

As we mentioned earlier in this section, we perform numerical experiments in Chapters 6 and 7 using data from three different test cases. We now define these three test cases and the type of flows associated with them. We use the Rossby-Haurwitz wave described in Section 5.3.2 where we are able to generate three different test cases by varying the height at the poles, h_0, and the amplitude and speed through ω.

Before we explain the three test cases that we use with the balance equa-

tions we define the *Burger number*, [5], [6], B_u, given by

$$B_u \equiv \frac{\sqrt{gh}}{fL} = \frac{L_R}{L}, \tag{5.42}$$

where L_R is the Rossby radius of deformation. As we can see from (5.42), as we approach the equator, $\theta = 0$, then $f \to 0$ and so $B_u \to \infty$. The three test cases that we consider generate different values for B_u at different latitudinal levels.

As we mentioned in Section 2.1, it is often assumed that the atmospheric motions in the horizontal directions are larger than those in the vertical. A result of this is that the atmosphere can be considered as a number of layers of fluid. A fluid with this property is said to be stably stratisfied, [34]. The Burger number describes the relative importance between the effects of stratification and rotation. When the number is larger than one then the layers are stable with respect to changes in the interfaces between them. If the Burger number is less than one then the rotation dominates the flow.

Returning to the expression for the initial height profile of the Rossby-Haurwitz, (5.35), there are three parameters that can be chosen to affect the wave's profile, h_0, ω and K. We have chosen the wavenumber to be 4 as it is the largest stable wavenumber of the wave, [20], [55]. However there has been a paper recently that questions this, [50], in certain numerical models.

The first test case, (TC1), is defined to be $h_0 = 50m$, $\omega = K = 7.848 \times$

$10^{-7}s^{-1}$. The second test case, (TC2), is defined to be $h_0 = 8000m$, $\omega = K = 7.848 \times 10^{-6}s^{-1}$. The third test case, (TC3), is defined to be $h_0 = 8000m$, $\omega = K = 7.848 \times 10^{-7}s^{-1}$. For the initial height profiles see Figure 5.9.

A feature of TC1 and TC3 is that the increase in the height from the pole to the equator is around $300m$ whereas for TC2 the increase is nearer to $2500m$. This affects the Burger number as we enter the equatorial region.

In [57] there is a study of the Burger number for different initial heights for the Rossby-Haurwitz wave. The results show that if we consider flows where their height is similar to TC1 then $B_u < 1$ throughout the interior whereas for TC3 $B_u > 1$ throughout the whole interior. Also for TC2, we have $B_u > 1$ throughout the domain. The other values of h_0 considered in [57] show a mixture of both low and high Burger numbers.

Therefore TC1 is a low Burger number regime where TC2 and TC3 are high Burger number regimes. An extra feature of TC2 is the speed of the propagation of the Rossby wave. As pointed out in [57], the shallower waves in the larger latitudes are moving slower that the waves in the smaller latitudes.

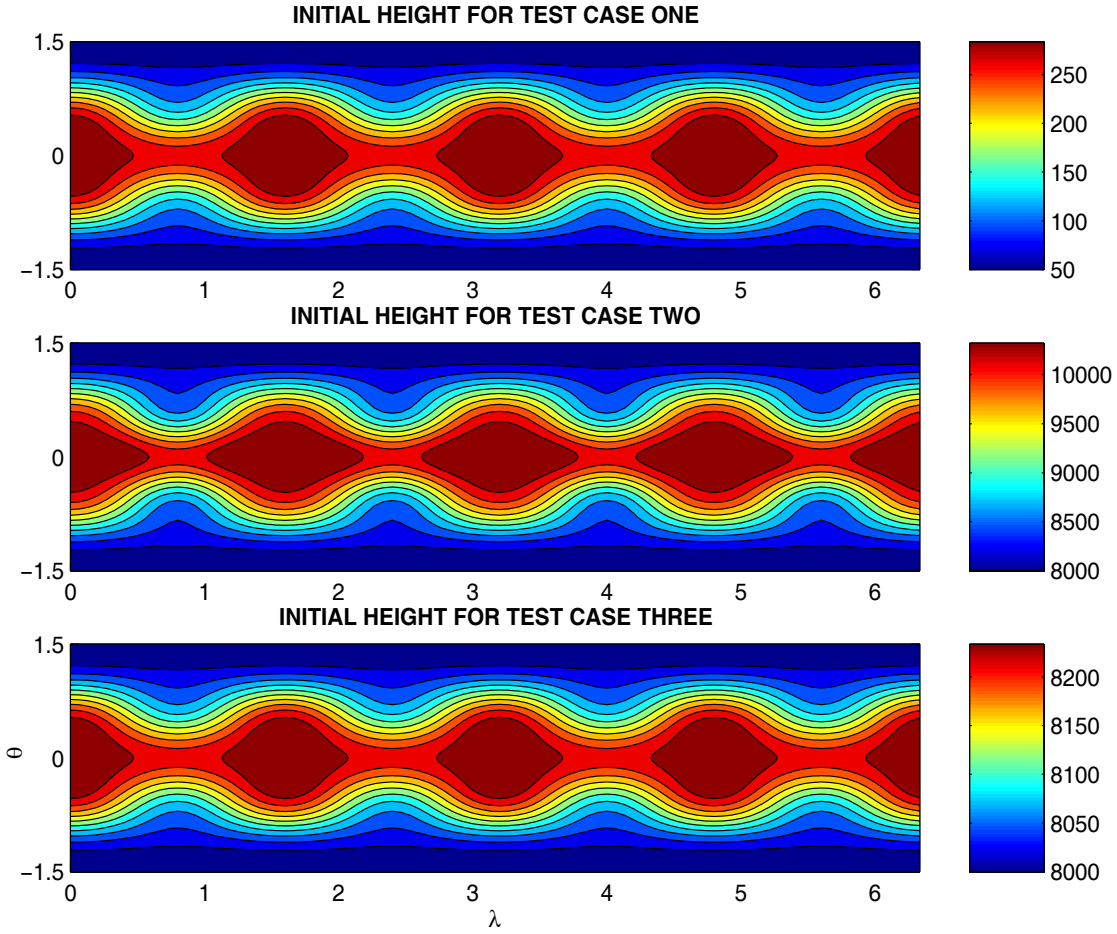

Figure 5.9: Contour Plots of the Initial Height Profiles for Test Cases 1,2 and 3. The unit for the scales on the right are metres.

5.4 Summary

In this chapter we have introduced the underlying theory that allows the solution to both continuous and discrete elliptic pdes to exist. We have defined the ellipticity condition that defines whether or not a differential operator is elliptic. We have derived this condition for the four balance

equations.

In Section 5.2 we gave a brief description of the shallow water equations model that we use to generate the base state data. Also in this section we gave a description of the numerical approximations that we use to solve the balance equations (5.1) and (5.2) and also a description of the approximations to calculate $\mathbf{u}^c$ from h' at the u, v points in the C grid. We use these approximations in the experiments in Chapter 7, which are briefly described in Section 5.3.1.

In the final section, 5.3 we gave a brief description of the Rossby-Haurwitz wave that we use as the initial condition for the SWE model.

In Section, 5.3.3, we introduced three test cases, TC1 - TC3, where we have changed different parameters to generate different Burger number regimes. In the next chapter we look at the effects that these different regimes have on the ellipticity condition.

Chapter 6

Ellipticity Experiments

In this chapter we explain and present results from experiments on the ellipticity conditions for the two equations (5.1) and (5.2).

We describe the experiments that we perform on the ellipticity condition in Section 6.1. The first set of experiments are concerned with the initial heights for the three test cases. As we require the geostrophic winds, calculated from the height fields, we have to calculate the derivatives of the height field. In Section 6.2 we describe how we calculate these derivatives for both the initial height profile and the height at 72hrs. At the initial time we use the continuous expression for the height and the derivatives are explained in Section 6.2.1. For the experiments at 72hrs we only have the numerical values for the height rather than the continuous expressions and as such we describe the procedure to approximate the derivatives in Section 6.2.2.

In Sections 6.3 and 6.4 we present the results for the experiments described in Section 6.1. Finally in Section 6.5 we present conclusions from the experiments.

6.1 Ellipticity Condition Experiments

The main aim of this research is to see if we gain any extra information from these new balance relations compared to geostrophic balance. The calculations involved in using these new balance equations are more complex than those with geostrophic balance.

If we were using geostrophic balance we would be solving a spherical Poisson equation. This would only involve a five-point stencil and the resulting matrix equation would have a more sparse structure and would be easier to store on size alone. Therefore, one of the objectives is to identify possible flow regimes where we would expect the higher order correction to the geostrophic balance to be of use. We tackle this objective by the following means.

The first experiment involves the Rossby-Haurwitz wave at $t = 0$. For this case we have the analytic height profile and as such we can calculate the coefficients of the ellipticity condition analytically. We show the derivation of the derivatives in Section 6.2.1.

For the second experiment we again form the same coefficients but now at

72hrs into the run of the SWE model with the three test cases. To calculate the coefficients for this experiment we use the numerical approximations explained in Section 5.2.2.

In both experiments we compare the ellipticity plots with the equivalent condition for the case where $\alpha = 0$, geostrophic balance. For the RV method this is simply a set of increasingly valued parallel lines as we enter the equatorial regions. This is not the case for the PV method and we present the condition for the PV method in separate plots for all three test cases.

We also introduce a fourth test case that fails the ellipticity condition, which shows that the ellipticity condition will not be satisfied by unphysical data.

We then repeat the plots for the three test cases at 72 hours into the 120 hour run of the shallow water model. Here we see how the condition is affected by the slanting in the waves and the movement of the height field.

Another objective of this research is to see whether or not we need to calculate all the terms in the equation. To do this we perform a scale analysis using values from each of the three test cases for the mid-latitudes. We apply this to both the coefficients in the ellipticity condition and the coefficients in the differential equations, (5.1) and (5.2). The reason for this is both equations contain many lower order differential terms that may be very small.

6.2 Calculations of the Ellipticity Condition's Coefficients

As we described in Section 6.1, we perform experiments on the coefficients of the ellipticity condition and the discrete and continuous elliptic differential equations that we derived in Chapters 4 and 5. In this section we briefly explain how we evaluate the coefficients. We start with the continuous coefficients in Section 6.2.1 and then briefly recall the expression for the derivatives from Section 5.2.2 in Section 6.2.2.

6.2.1 Continuous Coefficients Calculations

If we recall the expression that we gave in Section 5.3.2 for the initial height profile for a Rossby-Haurwitz wave, (5.35)

$$h = \frac{1}{g}\left\{gh_0 + a^2A(\theta) + a^2B(\theta)\cos R\lambda + a^2C(\theta)\cos 2R\lambda\right\},$$

where A, B and C are given by (5.39), (5.40) and (5.41) respectively, then to calculate the geostrophic winds we require the first derivatives of (5.35) with respect to both θ and λ. This is therefore

$$\frac{\partial h}{\partial \lambda} = \frac{1}{g}\left(-Ra^2B(\theta)\sin R\lambda - 2Ra^2C(\theta)\sin 2R\lambda\right), \quad (6.1)$$

$$\frac{\partial h}{\partial \theta} = \frac{1}{g}\left(a^2\frac{\partial A(\theta)}{\partial \theta} + a^2\cos R\lambda\frac{\partial B(\theta)}{\partial \theta} + a^2\cos 2R\lambda\frac{\partial C(\theta)}{\partial \theta}\right), \quad (6.2)$$

where the expressions for the θ derivatives of A, B, and C are in Appendix C. We also require the second derivatives of h and these are given by

$$\frac{\partial^2 h}{\partial \lambda^2} = \frac{1}{g}\left(-Ra^2 B(\theta)\cos R\lambda - 4R^2 a^2 C(\theta)\cos 2R\lambda\right), \tag{6.3}$$

$$\frac{\partial^2 h}{\partial \theta \partial \lambda} = \frac{1}{g}\left(-Ra^2 \sin R\lambda \frac{\partial B(\theta)}{\partial \theta} - 2Ra^2 \sin 2R\lambda \frac{\partial C(\theta)}{\partial \theta}\right), \tag{6.4}$$

$$\frac{\partial^2 h}{\partial \theta^2} = \frac{1}{g}\left(a^2 \frac{\partial^2 A(\theta)}{\partial \theta^2} + a^2 \cos R\lambda \frac{\partial^2 B(\theta)}{\partial \theta^2} + a^2 \cos 2R\lambda \frac{\partial^2 C(\theta)}{\partial \theta^2}\right), \tag{6.5}$$

where the expressions for the second derivatives for A, B and C are in Appendix C.

To calculate the geostrophic winds we use the expressions (4.16), assuming a constant f. Then the first derivatives of the geostrophic winds are

$$\frac{\partial u_g}{\partial \lambda} = -\frac{g}{af}\frac{\partial^2 h}{\partial \theta \partial \lambda}, \quad \frac{\partial v_g}{\partial \lambda} = \frac{g}{af\cos\theta}\frac{\partial^2 h}{\partial \lambda^2}, \quad \frac{\partial u_g}{\partial \theta} = -\frac{g}{af}\frac{\partial^2 h}{\partial \theta^2}. \tag{6.6}$$

To evaluate the initial ellipticity conditions we take the analytical expression derived above and in Appendix C, and evaluate these at the θ and λ values that make up the grid.

6.2.2 Discrete Coefficient Calculations

In the process of solving the matrix equation that arises in the discrete approximations to the balance equations we output from the FORTRAN90 program the coefficients of the second order finite difference terms. These are then the discrete equivalent values for the ellipticity condition.

We have used the central differences that were described in Section 5.2.2 to approximate the derivatives in the coefficients, (5.7) - (5.9) and (5.15) - (5.17). We therefore evaluate the coefficients of the ellipticity condition at the grid points.

6.3 Results I: Ellipticity Plots

In this section we present discussion for the initial ellipticity condition that has been calculated using the analytical expressions derived in Section 6.2.1.

We present the ellipticity conditions in a series of figures, Figures 6.2 to 6.7 and 6.11 to 6.16. Each figure contains four plots. These show, from top left to bottom right, B^2, $4AC$, $B^2 - 4AC$ and h. We compare the ellipticity plots with the equivalent condition for the Laplacian. For the PV method we present the ellipticity condition for $\alpha = 0$ in Figure 6.1 for $t = 0$ and Figure 6.10 for $t = 72$, and then compare the relevant plot for each test case.

We also give a fourth test case that fails the ellipticity condition. This problem is unphysical, but where the height is unphysical is near where the condition fails.

6.3.1 Initial Ellipticity Conditions

As we have mentioned in the introduction to this section we are to compare the ellipticity plots for each test case against the equivalent condition for the Laplacian. We take each test case in order but we present the figures for both the RV and PV method together with observations that we make about the structure that is visible in the plots. We start with Figure 6.1 which is displaying the initial ellipticity for the PV method with $\alpha = 0$.

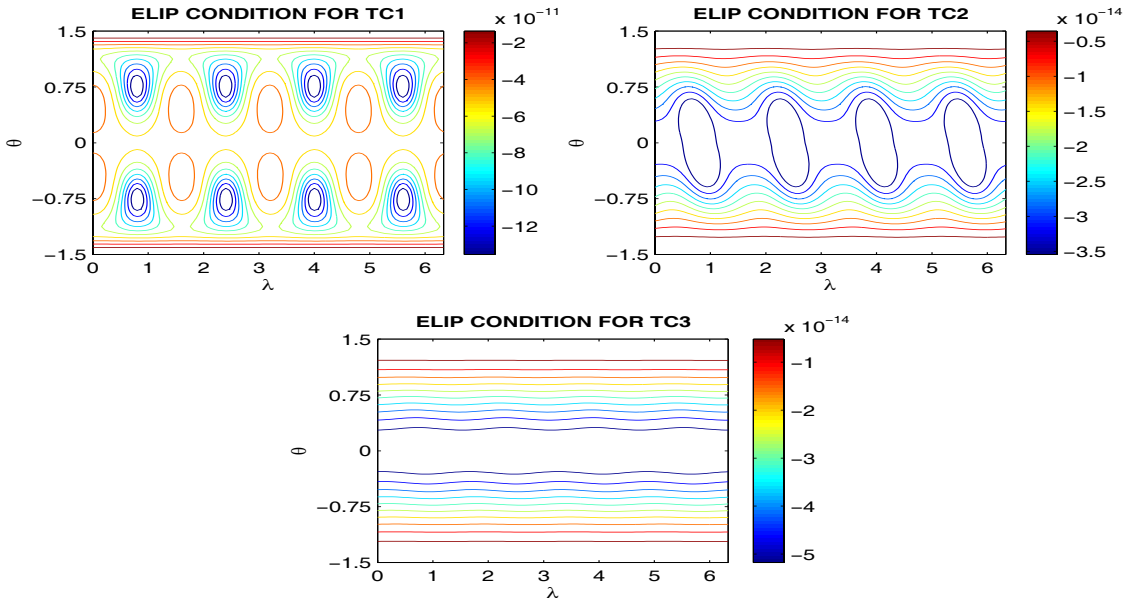

Figure 6.1: The Initial Ellipticity Conditions for the PV Method for $\alpha = 0$, where TC stands for test case

We start the observations with TC1, where Figure 6.2 shows the results for the RV method and Figure 6.3 shows results for the PV method.

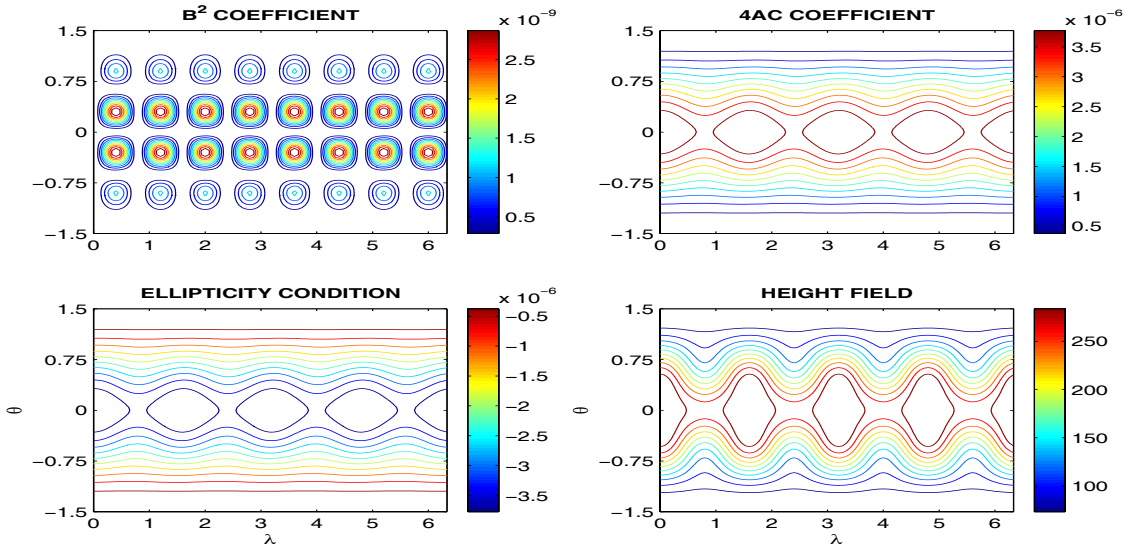

Figure 6.2: Plots Showing the Coefficients of the Ellipticity Condition and the Condition for the RV Method for TC1

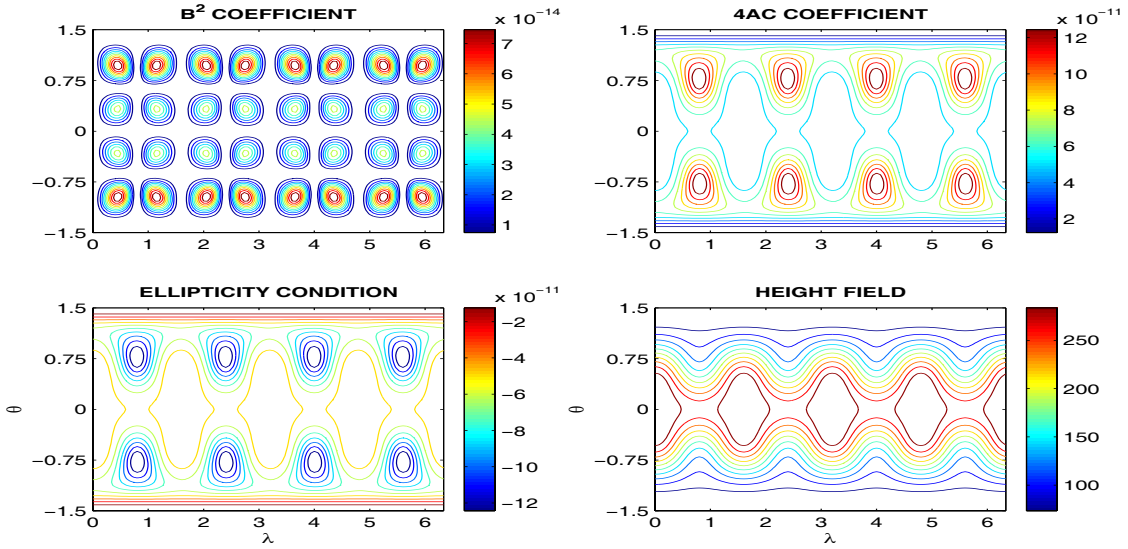

Figure 6.3: Plots Showing the Coefficients of the Ellipticity Condition and the Condition for the PV Method for TC1

As we can see from the two figures there is a significant difference in the structure in the two ellipticity conditions but both conditions are dominated by the $4AC$ term. We are not surprised by the difference between the two methods' conditions as this is consistent with the findings from [57]. We shall see the consequences of this in Chapter 7.

If we consider the results for the RV method (Figure 6.2) then comparing to a set of parallel lines there would appear a similar structure to this in the mid-latitudes but as we enter the equatorial regions this is not the case. The structure as we enter this region appears similar to that of the wave.

Another feature is the size of the dominance of the $4AC$ term over the B^2 term. For this test case this is 10^3 which is quite a substantial difference but as we can see, the changes in the wave's height profile with respect to the two directions is larger in TC2 than TC1.

A noticeable feature in the PV method's ellipticity condition is the vortitices that are formed in the troughs of the Rossby-Haurwitz wave. In these areas the ellipticity condition is at its most negative possible suggesting a more balanced area of the flow. Comparing the plot to the Laplacian equivalent for this test case, (top left in Figure 6.1), then there appears to be some similar structures between the two plots.

Figures 6.4 and 6.5 have the results for TC2. The first figure is the results for the RV method and the second for the PV method.

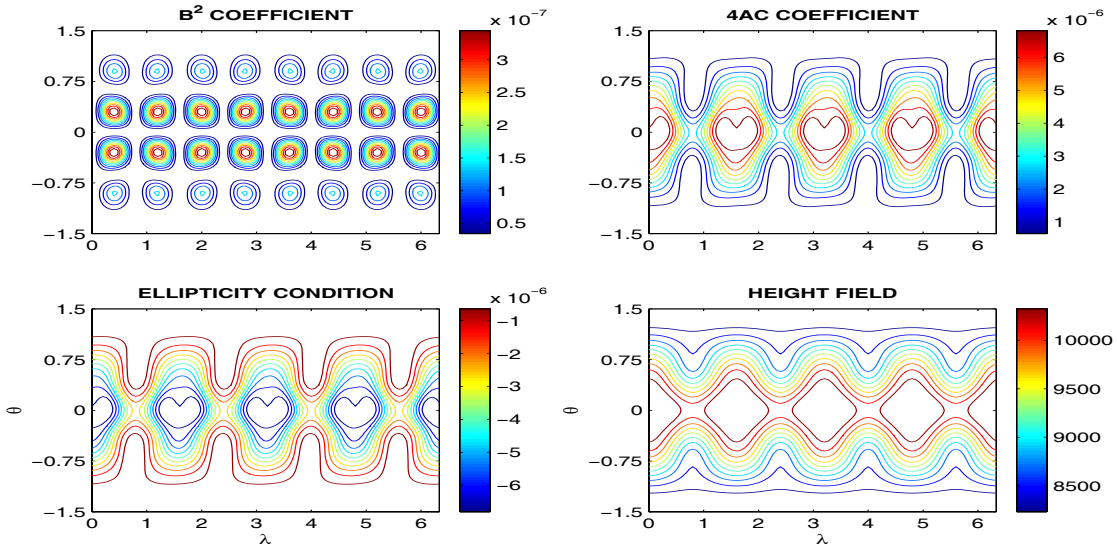

Figure 6.4: Plots Showing the Coefficients of the Ellipticity Condition and the Condition for the RV Method for TC2

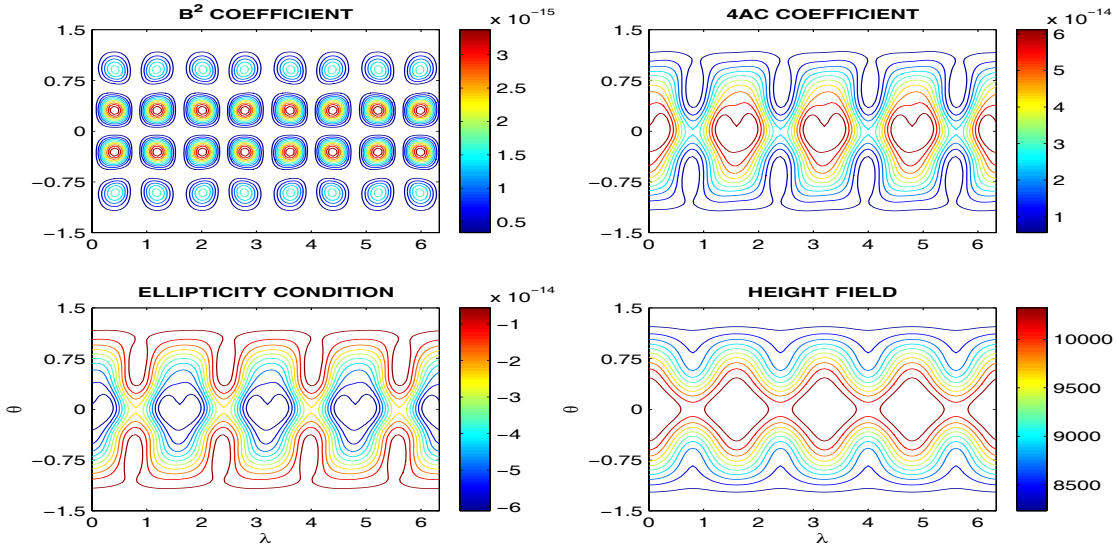

Figure 6.5: Plots Showing the Coefficients of the Ellipticity Condition and the Condition for the PV Method for TC2

The first feature that stands out from Figure 6.4 is that there is nothing resembling the structure of a set of parallel lines. Comparing the PV method's ellipticity condition to its Laplacian equivalent, (top right in Figure 6.1), then this is also suggesting that for this type of flow then the extra terms from taking the higher order balance are essential.

Another striking difference between the results for TC1 and TC2 is the size of the difference between B^2 and $4AC$ for this test case. This difference is only 10 compared to 10^3 for TC1. Therefore, flows similar to that of TC2 could violate the ellipticity condition. This is true for both the RV and PV results.

A final comment about these findings is that the structure between the two methods does not change substantially compared to the obvious difference between the two methods for TC1. We are not surprised by this as again this consistent with the findings in [57].

The final test case's results, TC3, are displayed in Figures 6.6 and 6.7. The condition for the RV method is the same as that for TC1. This is not surprising as the change in the wave's height across the domain is the same for both test cases.

Comparing the conditions against that for the Laplacian then the observations for TC1's RV results apply here also. The significant difference is in the ellipticity condition for the PV method results.

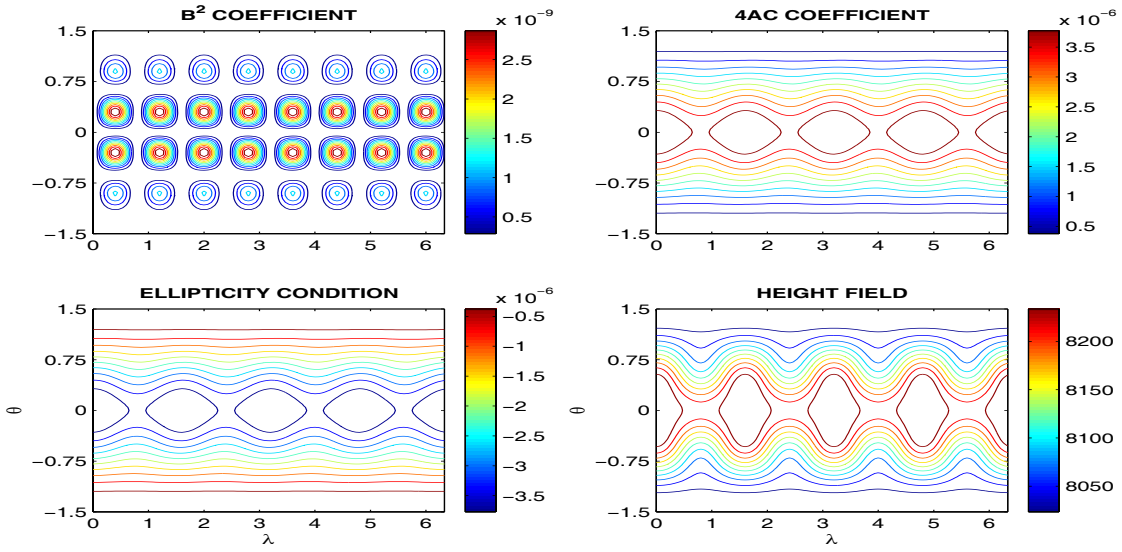

Figure 6.6: Plots Showing the Coefficients of the Ellipticity Condition and the Condition for the RV Method for TC3

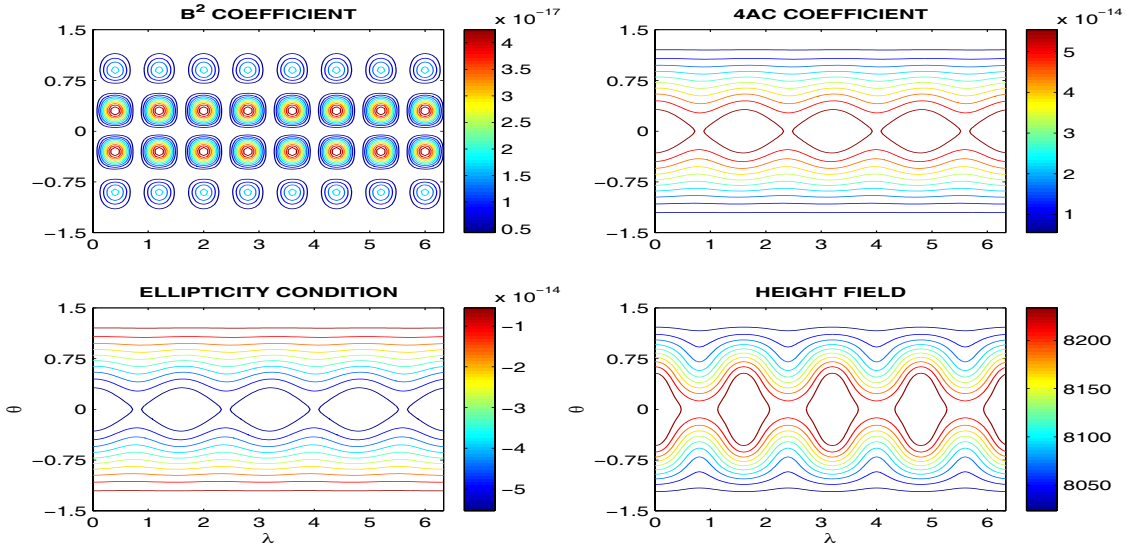

Figure 6.7: Plots Showing the Coefficients of the Ellipticity Condition and the Condition for the PV Method for TC3

We do not have a change in the structure of the conditions between the RV and PV methods as in TC1. This is again consistent with [57], we go into more details about these findings when we calculate the solutions to the equations in Chapter 7.

As we mentioned in the introduction to this section we have a fourth test case that has the ellipticity condition failing for both methods. For this fourth test case, TC4, is defined by $h_0 = 8000m$, $\omega = K = 7.848 \times 10^{-5} s^{-1}$, the height field is shown in Figure 6.8. The ellipticity plots are in Figure 6.9.

As we can see this is an unphysical example as we can not have negative values for the full height field. The effect this has on the coefficients in the ellipticity conditions is seen in Figure 6.9.

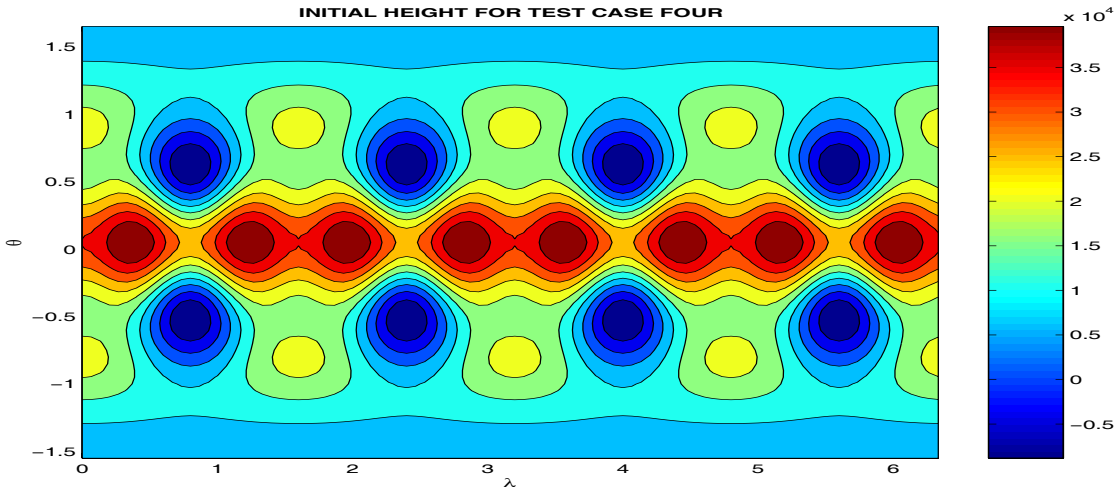

Figure 6.8: Contour Plot of the Initial Height Profiles for Test Case 4

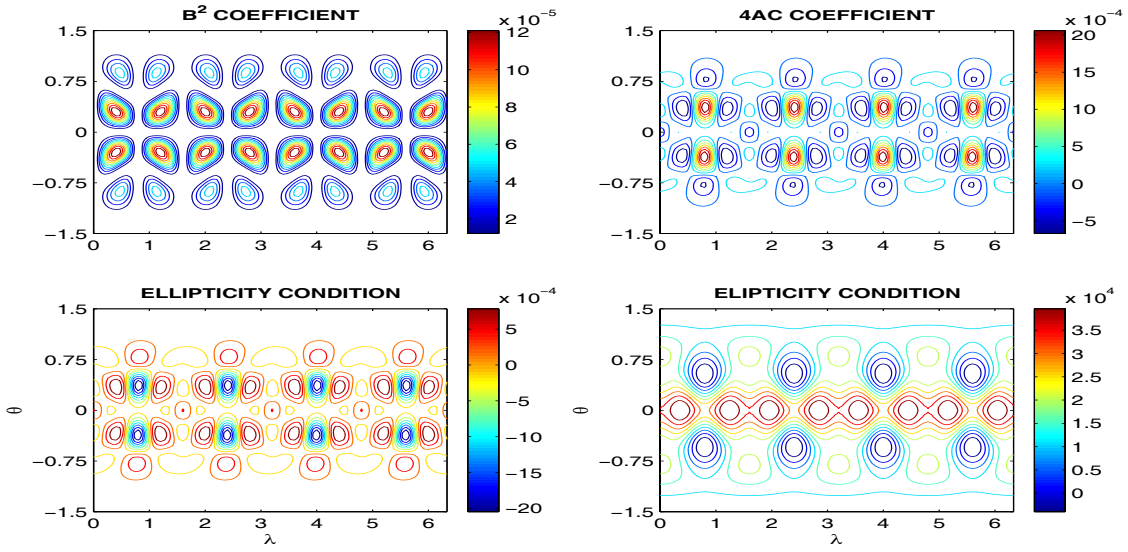

Figure 6.9: Plots Showing the Coefficients of the Ellipticity Condition and the Condition for the RV Method for TC4

6.3.2 72 Hours Ellipticity Conditions

In Section 6.3.1 we used the analytical derivatives of the height to evaluate the ellipticity condition at the grid points. In this section we investigate the effects on the ellipticity condition at 72 hours into the model run. The figures are in the same format to those in Section 6.3.1.

As with the analysis in Section 6.3.1, we require the Laplacian equivalent for the three test cases at 72 hours. This is shown in Figure 6.10. We shall use this to compare the structures in the ellipticity conditions to see if they are dependent on the Laplacian.

A clear difference between the initial ellipticity condition for TC1 using

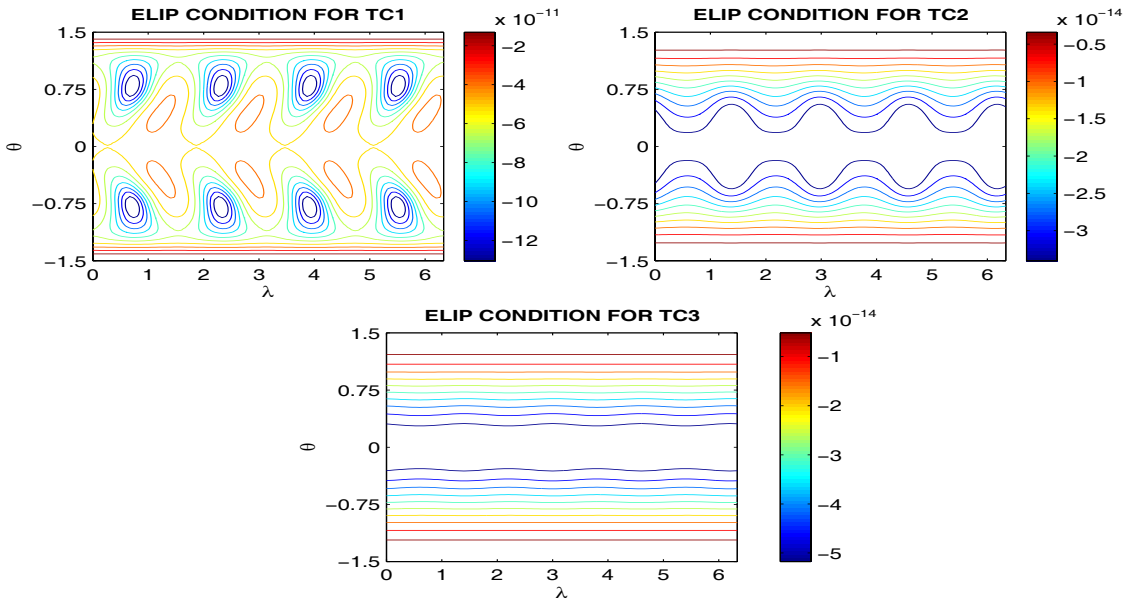

Figure 6.10: Ellipticity Condition for the Laplacian with the PV Method at 72hrs

the RV method and 72 hour condition (Figure 6.11) is that the wave formation that was present initially has been damped in some manner but the remaining form of the wave has started to be distorted in a similar manner to the full height field.

The figure does suggest that there is a dependence on the Laplacian with the RV method in the mid-latitudes but as we enter the equatorial regions we see that this is not the case.

For the PV method (Figure 6.12) we see that there is a similar structure to the Laplacian equivalent (top left in Figure 6.10) but there is a formation in the Laplacian condition that is not present in the full condition. There is

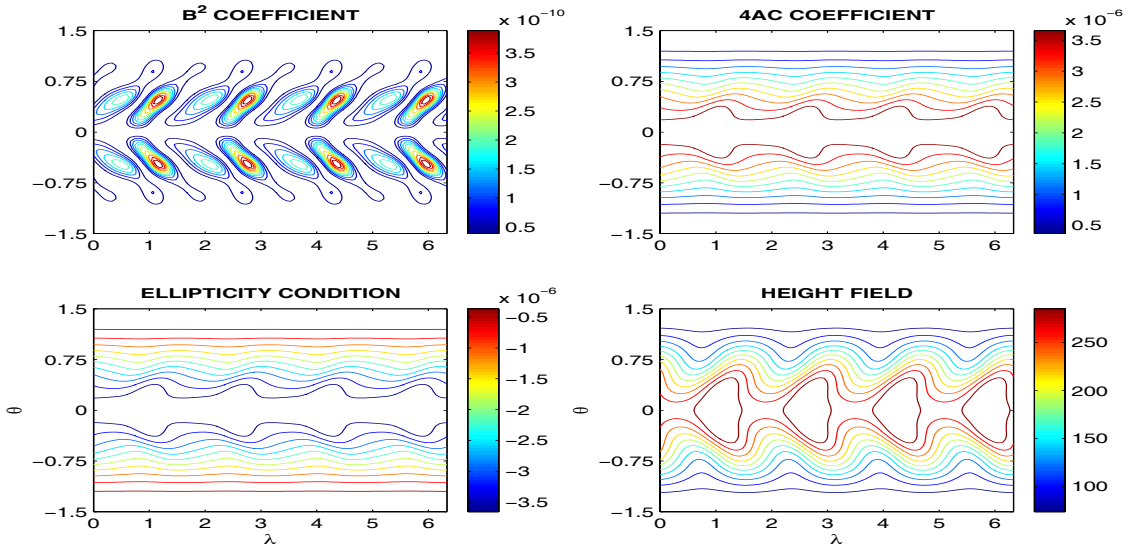

Figure 6.11: Plots Showing the Coefficients of the Ellipticity condition and the Condition for the RV method at $t = 72$ for TC1

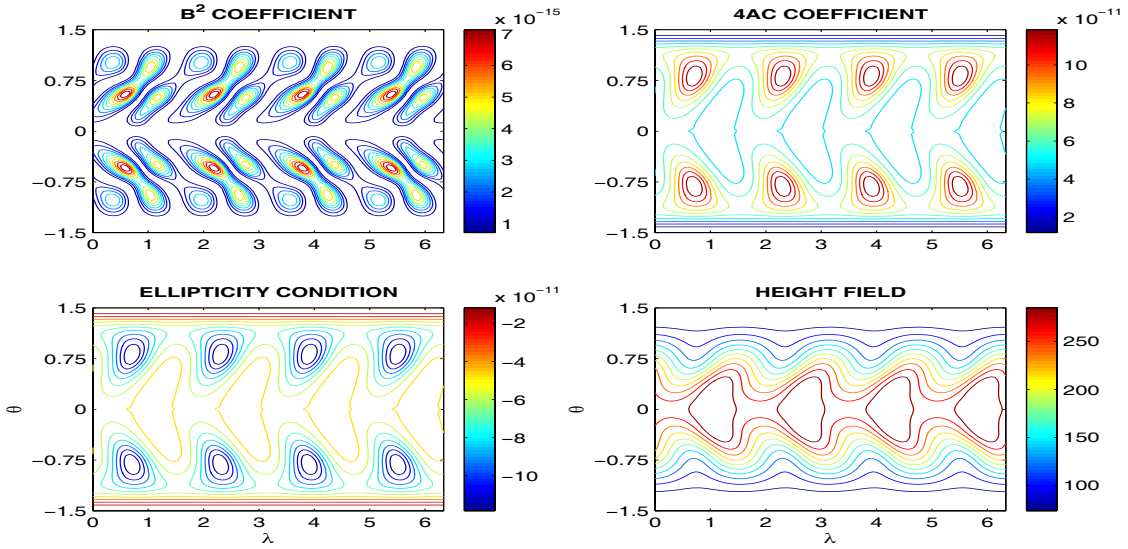

Figure 6.12: Plots Showing the Coefficients of the Ellipticity condition and the Condition for the PV method at $t = 72$ for TC1

also still a noticeable difference between the two methods.

An interesting feature in the plots is the distortion of the B^2 term for both methods for TC1. In the initial plots (Figures 6.2 and 6.3) then this coefficient has a circular structure to it which has been distorted by the time we arrive at 72hrs.

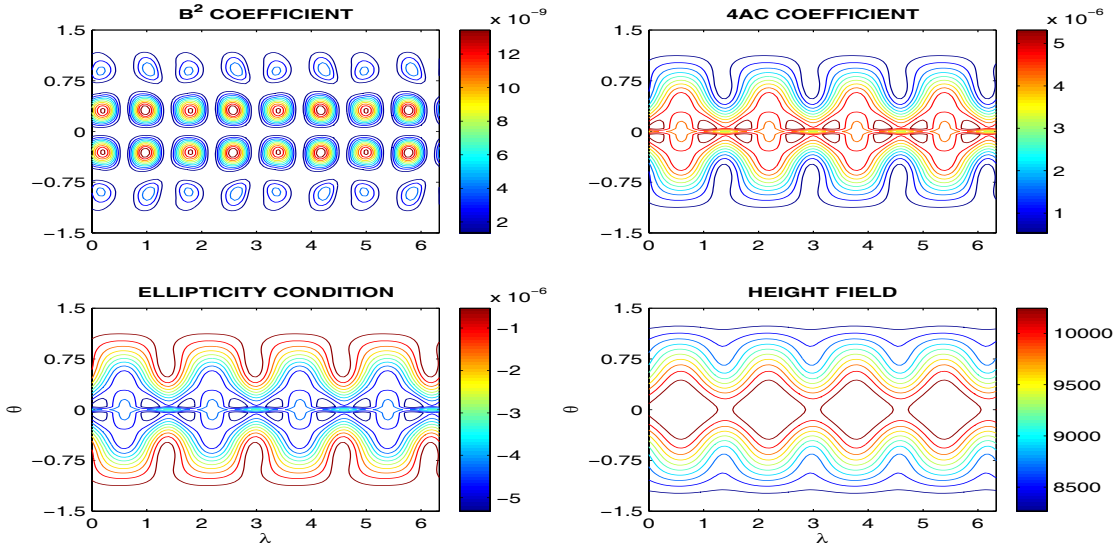

Figure 6.13: Plots Showing the Coefficients of the Ellipticity Condition and the Condition for the RV method at $t = 72$ for TC2

If we now consider TC2's results, Figures 6.13 and 6.14, then we see that there is still nothing representing a set of parallel lines to suggest that the Laplacian is the dominant term in the ellipticity condition for the RV method. For the PV method then there is again nothing at all similar to the equivalent condition in Figure 6.10, (top right). For this test case we can

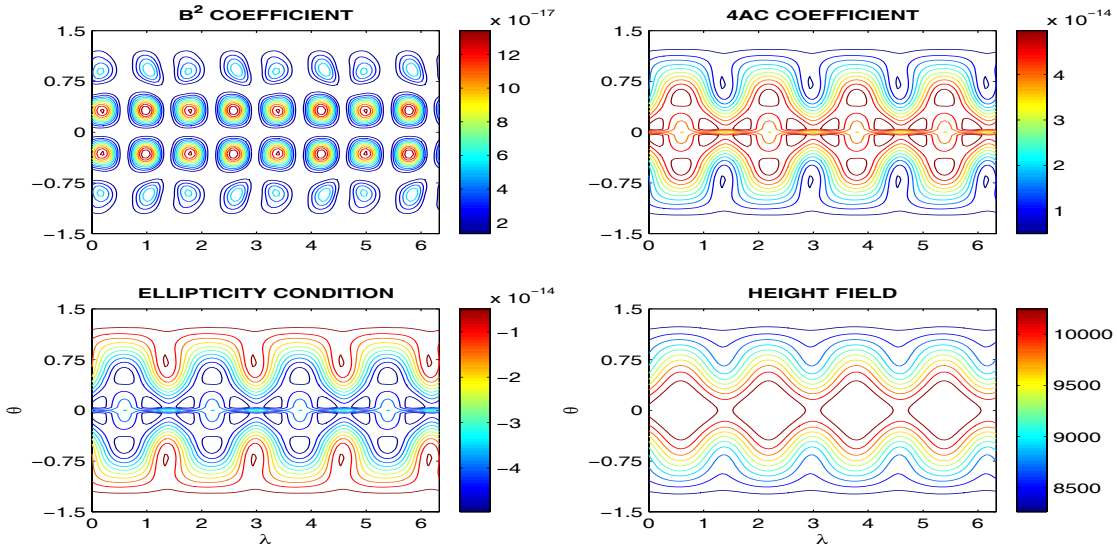

Figure 6.14: Plots Showing the Coefficients of the Ellipticity Condition and the Condition for the PV method at $t = 72$ for TC2

say that there is evidence to suggest that the inclusion of the extra terms is necessary.

There is also a noticeable feature in the conditions for this test case for the PV methods where we have a small vorticity forming in the trough of the position of the wave. This same structure is present in the absolute vorticity for this flow, [57].

However, for TC3, we see a structure similar to a set of parallel lines, Figure 6.15. This may not be throughout the whole of the domain but it is clearly noticeable in the mid-latitudes for the RV method. For the PV method, Figure 6.16, then there appears to be a similar structure to the

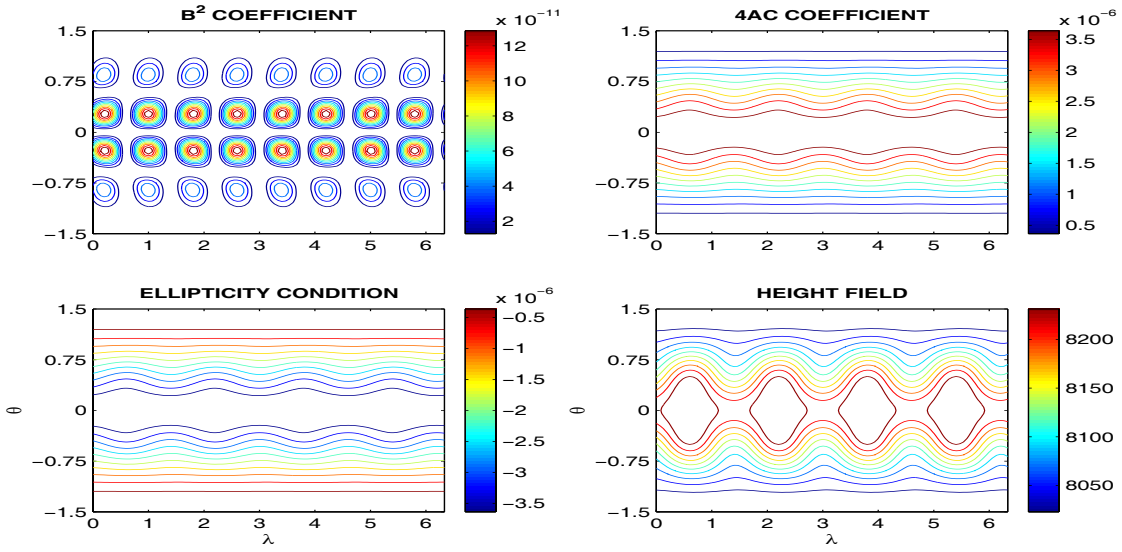

Figure 6.15: Plots Showing the Coefficients of the Ellipticity Condition and the Condition itself for the RV method at $t = 72$ for TC3

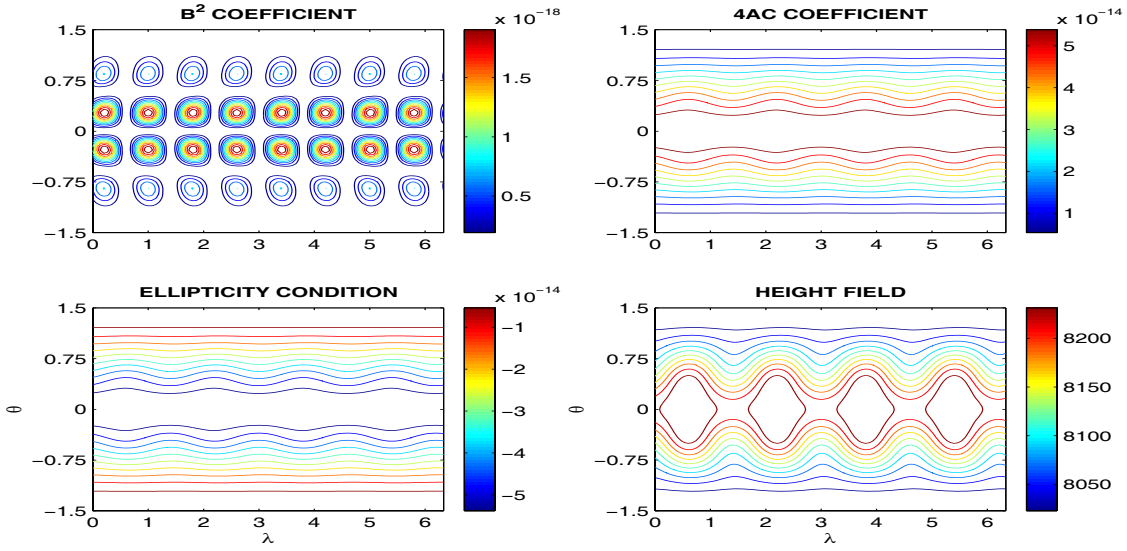

Figure 6.16: Plots Showing the Coefficients of the Ellipticity Condition and the Condition itself for the PV method at $t = 72$ for TC3

equivalent Laplacian condition.

An interesting difference between the B^2 coefficients for TC1 and TC3 is that there is no distorting of the circular forms for TC3. For TC3 we would be tempted to suggest that the Laplacian may be enough for these types of flows.

As we mentioned in Section 6.1, the new equations have many more terms than if we were simply calculating the balanced height as a solution to a Poisson equation. We have seen some evidence that for certain Burger regimes the extra terms may have an effect on the solution. These are only an indicator with the ellipticity condition as the condition is determined by the factors of the second order differential terms. As we can see from (5.1) and (5.2) we have many lower order terms. We now investigate the sizes of these extra terms in the next section.

6.4 Results II: Scale Analysis

We now perform an experiment to identify which are the larger coefficients in both the ellipticity conditions for (5.1) and (5.2) and the coefficients in the differential equation. The purpose of this is to see if any of the lower order terms could be dropped from the approximations.

We have taken averaged values for the following derivatives from the three

test cases at 72 hrs. These are in Table 6.1, where we have taken the value for f at 45°N of $1.0312 \times 10^{-4} s^{-1}$ and $a = 6371220m$

Test Case	$\bar{h}$	$\bar{u}_g$	$\bar{v}_g$	$\frac{\partial \bar{u}_g}{\partial \lambda}$	$\frac{\partial \bar{v}_g}{\partial \lambda}$	$\frac{\partial \bar{u}_g}{\partial \theta}$
1	165.79	3.48	2.73	6.72×10^{-7}	1.69×10^{-6}	1.14×10^{-6}
2	9.10×10^{3}	27.94	26.72	5.83×10^{-6}	1.66×10^{-6}	5.30×10^{-6}
3	8.10×10^{3}	3.65	2.22	6.45×10^{-7}	1.38×10^{-6}	2.78×10^{-7}

Table 6.1: Table of the Average Values for Scale Analysis, where h has units m, $\bar{u}_g$, $\bar{v}_g$ have ms^{-1} and their derivatives have s^{-1}

We firstly perform the scale analysis on the RV based method's ellipticity condition. The following tables, (6.2 and 6.3), contain approximations to the coefficients in B^2 and $4AC$ respectively for the three test cases.

Coefficient $(m^2 s^{-6})$	TC1	TC2	TC3
$16g^2 \left(\frac{\partial \bar{u}_g}{\partial \lambda}\right)^2$	6.95×10^{-10}	5.23×10^{-8}	6.41×10^{-10}
$-\frac{32g^2 \sin\theta}{a} \frac{\partial \bar{u}_g}{\partial \lambda} \bar{v}_g$	-6.27×10^{-10}	-5.32×10^{-8}	-4.89×10^{-10}
$\frac{16g^2 \sin^2\theta}{a^2} \bar{v}_g^2$	1.41×10^{-10}	1.35×10^{-8}	9.35×10^{-11}
B^2	1.82×10^{-10}	1.26×10^{-8}	2.46×10^{-10}

Table 6.2: Scale Analysis of the Coefficients in B^2 for the RV Method

Coefficient $(m^2 s^{-6})$	TC1	TC2	TC3
$4g^2 f^2 \cos^2\theta$	2.05×10^{-6}	2.05×10^{-6}	2.05×10^{-6}
$8g^2 f \cos^2\theta \frac{\partial \bar{u}_g}{\partial \theta}$	4.53×10^{-8}	2.10×10^{-7}	1.10×10^{-8}
$-8g^2 f \cos\theta \frac{\partial \bar{v}_g}{\partial \lambda}$	-9.48×10^{-8}	-9.32×10^{-7}	-7.76×10^{-8}
$-16g^2 \cos\theta \frac{\partial \bar{u}_g}{\partial \theta}\frac{\partial \bar{v}_g}{\partial \lambda}$,	-2.10×10^{-9}	-9.56×10^{-8}	-4.16×10^{-10}
$-\frac{16g^2 \sin\theta\cos\theta}{a}\frac{\partial \bar{u}_g}{\partial \theta}\bar{u}_g$	-4.80×10^{-10}	-1.79×10^{-8}	-1.23×10^{-10}
$-\frac{8g^2 f \sin\theta\cos\theta}{a}\bar{u}_g$	-2.17×10^{-8}	-1.74×10^{-7}	-8.83×10^{-8}
$4AC$,	1.97×10^{-6}	1.04×10^{-6}	1.89×10^{-6}

Table 6.3: Scale analysis of the Coefficients in $4AC$ for the RV Method

As we can see from the two tables the largest term in magnitude in the analysis is the coefficient associated with the Laplacian, first row in Table 6.3, which is consistent with the plots in Section 6.3.2 for TC1 and TC3. The interesting feature is also the closeness of the averaged value of B^2 to the average value of $4AC$ for TC2 compared to the other two test cases.

The scale analysis for TC2 also shows that the Laplacian, (first row of Table 6.3), is affected by the extra terms and that for this form of flow the extra terms is comparable to the Laplacian. If we consider the last line of Table 6.3 we see that the averaged value has only altered slightly from the Laplacian for TC1 and TC3; However, we see that the value for TC2 is

altered substantially.

If we were to consider whether or not to remove terms we would have to say that for TC2 we would have to consider not removing any of the terms that make up $4AC$ as these are comparable with the Laplacian term in the mid-latitudes. We would also have to consider leaving all the terms in B^2 as again these are comparable to $4AC$.

For the other two test cases the averaged value for B^2 is not comparable with $4AC$ and as such the removal of the cross derivative terms from the point of view of the ellipticity condition would not affect the condition too severely. For TC1 we could possibly remove the term involving the $\frac{\partial^2 h'}{\partial \lambda^2}$ as the coefficient that comes from this term in the ellipticity condition is involved with the two smallest, $O\left(10^{-4}\right)$ smaller.

For the third test case we would conclude that it would be possible to remove all of the extra terms in the balance relation and the ellipticity condition would not be affected to severely. We must remember here that this scale analysis is only for the mid-latitudes and we have used averaged values to perform the analysis with.

We now look at the magnitudes of the coefficients in the discrete approximation to (5.1) in Table 6.4, where we now have the coefficients of the first derivatives in the table for all three test cases.

The first three entries in Table 6.4 as the same for all three test cases.

Coefficient (ms^{-3})	Term	TC1	TC2	TC3
gf	$h_{\lambda\lambda}$	1.01×10^{-3}	1.01×10^{-3}	1.01×10^{-3}
$\sin\theta\cos\theta fg$	h_{θ}	5.06×10^{-4}	5.06×10^{-4}	5.06×10^{-4}
$\cos^2\theta fg$	$h_{\theta\theta}$	5.06×10^{-4}	5.06×10^{-4}	5.06×10^{-4}
$2g\frac{\partial \bar{u}_g}{\partial \lambda}$	$h_{\theta\lambda}$	2.62×10^{-5}	2.29×10^{-4}	2.53×10^{-5}
$2g\cos\theta\frac{\partial \bar{v}_g}{\partial \lambda}$	$h_{\theta\theta}$	2.34×10^{-5}	2.30×10^{-5}	1.94×10^{-5}
$2g\frac{\partial \bar{u}_g}{\partial \theta}$	$h_{\lambda\lambda}$	2.24×10^{-5}	1.04×10^{-4}	5.45×10^{-6}
$\frac{4g\sin\theta}{a}\bar{v}_g$	$h_{\theta\lambda}$	1.19×10^{-5}	1.16×10^{-4}	9.67×10^{-6}
$\frac{2g\sin\theta\cos\theta}{a}\bar{u}_g$	$h_{\theta\theta}$	5.36×10^{-6}	4.30×10^{-5}	5.62×10^{-6}
$\frac{(4g\tan\theta\sin\theta + 2g\cos\theta)}{a}\bar{v}_g$	h_{λ}	1.78×10^{-5}	1.75×10^{-4}	1.45×10^{-5}
$\frac{2g\cos^2\theta}{a}\bar{u}_g$	h_{θ}	5.36×10^{-6}	4.30×10^{-6}	5.62×10^{-6}
$4g\tan\theta\frac{\partial \bar{u}_g}{\partial \lambda}$	h_{λ}	2.64×10^{-5}	2.29×10^{-4}	2.53×10^{-5}
$2g\sin\theta\cos\theta\frac{\partial \bar{u}_g}{\partial \theta}$	h_{θ}	1.12×10^{-5}	5.20×10^{-5}	2.73×10^{-6}

Table 6.4: Scale Analysis of the Coefficients in the Differential Equation for the RV Method

These are the coefficients that make up the Laplacian operator. For TC1 we see that the extra terms are of a similar scale to the Laplacian, but $O\left(10^{-1}\right)$ smaller. The only terms that are 10^{-2} smaller are those that arise from T_6 in (4.34) and (4.45) and as such for this type of flow we may consider dropping

these terms. One of these coefficients does multiply a second derivative term and as such would affect the ellipticity condition but this is a term that would be removed if the $\frac{\partial^2 h'}{\partial \lambda^2}$ term was dropped as well. However, when we consider the size of this term in Table 6.4 we see that this is comparable with some of the terms in the Laplacian.

For TC2 the scale analysis of the differential equations follows that of the ellipticity condition and suggests that all the terms should be kept with the exception of the same term that we noticed was small for TC1.

The third test case's results would suggest that nearly all the extra terms could be considered to be removed as their magnitudes are almost all 10^{-2} smaller than the Laplacian term. This is consistent with the scale analysis for the ellipticity condition and the noticeable conclusions from Figure 6.15.

We now consider the same scale analysis for the PV method where we have used the same values from Table 6.1. We start again with the results for the ellipticity coefficients. These are in Tables 6.5 and 6.6. If we consider TC1 first from both tables we see that there are coefficients in Table 6.6 that are now comparable with coefficients for B^2 in Table 6.5. This is suggesting that although the Laplacian is a large factor there are some effects from the B^2 term in the mid-latitudes.

If we were to consider removing any terms from the point of view of the ellipticity condition then we would have to consider the same two terms as

Coefficient (s^{-6})	TC1	TC2	TC3
$\frac{16g^2\left(\frac{\partial \bar{u}_g}{\partial \lambda}\right)^2}{\bar{h}^2}$	2.53×10^{-14}	6.31×10^{-16}	9.73×10^{-18}
$-\frac{32g^2 \sin\theta \frac{\partial \bar{u}_g}{\partial \lambda}\bar{v}_g}{a\bar{h}^2}$	-2.28×10^{-14}	-6.42×10^{-16}	-7.42×10^{-18}
$\frac{16g^2 \sin^2\theta \bar{v}_g^2}{a^2\bar{h}^2}$	5.13×10^{-15}	1.63×10^{-16}	1.42×10^{-18}
B^2	7.63×10^{-15}	1.52×10^{-16}	3.73×10^{-18}

Table 6.5: Scale Analysis of the Coefficients in B^2 for the PV Method

Coefficient (s^{-6})	TC1	TC2	TC3
$\frac{4g^2 f^2 \cos^2\theta}{\bar{h}^2}$	7.45×10^{-11}	2.47×10^{-14}	3.11×10^{-14}
$\frac{8g^2 f \cos^2\theta \frac{\partial \bar{u}_g}{\partial \theta}}{\bar{h}^2}$	1.65×10^{-14}	2.53×10^{-15}	1.67×10^{-16}
$-\frac{8g^2 f \cos\theta \frac{\partial \bar{v}_g}{\partial \lambda}}{\bar{h}^2}$	-3.45×10^{-14}	-1.13×10^{-14}	-1.18×10^{-15}
$-\frac{16g^2 \cos\theta \frac{\partial \bar{u}_g}{\partial \theta}\frac{\partial \bar{v}_g}{\partial \lambda}}{\bar{h}^2}$	-7.65×10^{-16}	-1.15×10^{-15}	-6.37×10^{-18}
$-\frac{16g^2 \sin\theta \cos\theta \frac{\partial \bar{u}_g}{\partial \theta}\bar{u}_g}{a\bar{h}^2}$	-1.75×10^{-16}	-2.16×10^{-16}	-1.87×10^{-18}
$-\frac{8g^2 f \sin\theta \cos\theta \bar{u}_g}{a\bar{h}^2}$	-7.89×10^{-13}	-2.10×10^{-15}	-3.47×10^{-16}
$4AC$	7.36×10^{-11}	1.25×10^{-14}	2.97×10^{-14}

Table 6.6: Scale Analysis of the Coefficients in $4AC$ for the PV Method

for the RV method.

For TC2 we see that the Laplacian term is not dominating this condition but again we have factors in the B^2 term that could not be dropped as for the RV method. This is consistent with the results in Figure 6.14.

The final test case's results are consistent with the RV method's results with the Laplacian being the largest factor in the $4AC$ term. We now consider the whole differential equation to see what lower order terms could also possibly be removed due to their size. The values for the terms are displayed in Table 6.7.

The first feature of the results in Table 6.7 is that the values for the Laplacian are no longer the same for each of the three test cases. The first striking feature for TC1 is the scale of the factor of the Helmholtz part of (5.2). This is by far the largest component of the equation and is larger than the terms for the Laplacian. For TC2 and TC3 this factor is the same size in magnitude as the Laplacian.

For the remainder of the terms in the equations for TC1 we could consider dropping the extra terms with respect to the Helmholtz component but if this is done then there is the question of the calculation of $\bar{\xi}^c$ in the Helmholtz part of (5.2). To obtain the value that we have here we have evaluated $\bar{\xi}^c$ as (4.68) with $\alpha = 1$ we then have to question consistency if we are not calculating $\xi^{c\prime}$ the same way as $\bar{\xi}^c$.

Coefficient, s^{-3}	Term	TC1	TC2	TC3
$\frac{gf}{\bar{h}}$	$h_{\lambda\lambda}$	6.09×10^{-6}	1.11×10^{-7}	1.25×10^{-7}
$\frac{\sin\theta\cos\theta fg}{\bar{h}}$	h_{θ}	3.05×10^{-6}	5.56×10^{-8}	6.24×10^{-8}
$\frac{\cos^2\theta fg}{\bar{h}}$	$h_{\theta\theta}$	3.05×10^{-6}	5.55×10^{-8}	6.23×10^{-8}
$\frac{2g\frac{\partial\bar{u}_g}{\partial\lambda}}{\bar{h}}$	$h_{\lambda\theta}$	1.59×10^{-7}	2.51×10^{-8}	3.12×10^{-9}
$\frac{2g\cos\theta\frac{\partial\bar{v}_g}{\partial\lambda}}{\bar{h}}$	$h_{\theta\theta}$	1.44×10^{-7}	2.53×10^{-9}	2.36×10^{-9}
$\frac{2g\frac{\partial\bar{u}_g}{\partial\theta}}{\bar{h}}$	$h_{\lambda\lambda}$	1.35×10^{-7}	1.14×10^{-8}	6.73×10^{-10}
$\frac{4g\sin\theta\bar{v}_g}{a\bar{h}}$	$h_{\lambda\theta}$	7.17×10^{-8}	1.28×10^{-8}	1.19×10^{-9}
$\frac{2g\sin\theta\cos\theta\bar{u}_g}{a\bar{h}}$	$h_{\theta\theta}$	3.23×10^{-8}	4.73×10^{-9}	6.94×10^{-10}
$\frac{(4g\tan\theta\sin\theta + 2g\cos\theta)\,\bar{v}_g}{a\bar{h}}$	h_{λ}	1.08×10^{-7}	1.92×10^{-8}	1.79×10^{-9}
$\frac{2g\cos^2\theta\bar{u}_g}{a\bar{h}}$	h_{θ}	3.23×10^{-8}	4.73×10^{-9}	6.94×10^{-10}
$\frac{4g\tan\theta\frac{\partial\bar{u}_g}{\partial\lambda}}{\bar{h}}$	h_{λ}	1.59×10^{-7}	2.50×10^{-8}	3.12×10^{-9}
$\frac{2g\sin\theta\cos\theta\frac{\partial\bar{u}_g}{\partial\theta}}{\bar{h}}$	h_{θ}	6.76×10^{-8}	5.71×10^{-9}	3.37×10^{-10}
$a^2f^2\cos^2\theta\left(\frac{f + \mathbf{k}\cdot\nabla\times\bar{\mathbf{u}}_g^c}{\bar{h}^2}\right)$	h	8.68×10^{-4}	2.58×10^{-7}	3.10×10^{-7}

Table 6.7: Scale Analysis of the Coefficients in the Differential Equation for the PV Method

For TC2 we see that the scale of most of the terms in Table 6.7 are comparable with both the Helmholtz and the Laplacian part of the equations. The exception is again the terms arising from T_6 in (4.45). We would then have the same question of the effect that this has if the same term is removed from $\bar{\xi}^c$.

The final test case would appear again to be dominated by the Laplacian but there is an effect from the Helmholtz part. We would have to consider the removal of all the extra terms arising from the higher order terms in the balance relation in $\bar{\xi}^c$. For this flow we have seen that there is a more geostrophic structure to it than the other two and so the same approximation in $\bar{\xi}^c$ should not have too much of an affect.

6.5 Conclusions

The main aim of these experiments that we have shown in this chapter was to try and identify types of flows where we would gain extra information from the new balance equations. We undertook this by considering the initial ellipticity conditions for the three test cases and looked to see if this condition was dominated by the ellipticity condition for the Laplace operator.

The results for the RV method would suggest that for flows similar to TC1, (low Burger number), then the extra terms in the balance equation are

having some effect as the plots did not look similar to a latitudinal dependent condition. For the PV method then there was some similarity between the full condition and the Laplacian equivalent for TC1.

With the PV method the ellipticity condition changes quite drastically, (Figure 6.4), suggesting that there may be some benefit from using the extra terms in the calculation of $\xi^{c\prime}$ in the PV method. The same structure was still present at 72 hours but had moved with the wave, (Figure 6.12).

For TC2 we saw no structure resembling the ellipticity condition for the Laplacian, (Figure 6.2), which was still true at 72 hours (Figure 6.13) for the RV method. This suggests that the extra terms are needed here to model flows of this type. This was also true for the PV method.

In the plots of the initial ellipticity condition for both the RV and PV methods for TC3 (Figures 6.6 and 6.7) then there was a structure similar to the condition for the Laplacians in the mid-latitudes but not so in the lower latitudes. The same conclusions are still true at 72 hours for both methods (Figures 6.15 and 6.16). Therefore for these types of flows, slow high Burger number regimes then we would have to conclude that the extra terms may not be worth the extra information given the extra work to calculate the extra terms.

The other set of experiments that we performed in this chapter involved a scale analysis of the terms in the ellipticity conditions and the differential

equations. The main conclusion for the RV method was that for TC1 types of flows then the effects coming from T_6 in (4.34) could possibly be removed and the ellipticity condition would only be affected slightly. The same was true for the scale analysis for the coefficients in the differential equation.

For TC2 we saw that for the ellipticity condition the extra terms were comparable with the Laplacian operator and should be kept in but also that the B^2 coefficients were the same magnitude as some of the coefficients in $4AC$. This would suggest that the higher order correction is needed here but there was a question of the possibility that the ellipticity condition could be violated for flows that are much faster that the speed of the wave in TC2 but also for heights much higher than those in TC2.

TC3 analysis showed that for flows of this type we should only consider the Laplacian and that the extra terms are small in comparison.

In the PV method's scale analysis for TC1 we see that the Helmholtz term was the dominant term even over the Laplacian and that the remaining terms were nearly all of the same order as the Laplacian.

The second test case now had nearly all the terms of the same magnitude and would suggest that we would need all the terms in the approximation to the balance equation.

For TC3 the Laplacian and the Helmholtz term were comparable in magnitude but most of the extra terms were considerably smaller in the mid-

latitudes suggesting that the geostrophic approximation could be enough in the mid-latitudes.

Chapter 7

Balanced Variables Experiments

In this chapter we present results from two sets of experiments involving the numerical solutions to (5.1) and (5.2). The first set of experiments involve the solution to (5.1) and (5.2) with $\alpha = 0$ and 1. In these experiments we calculate the solutions to the diagnostic equations considering both a constant and a variable Coriolis parameter. The value that we use for the constant f case is 10^{-4} as an approximation to the value of f in the mid-latitudes. The shallow water equation model that we are using to propagate the Rossby-Haurwitz wave uses a variable f for all time. In the diagnostic calculation we do we do not include the extra terms arising from the variability of the Coriolis parameter, (4.56), as we are using this experiment as a first stage of

testing the variable.

The second set of experiments involve the calculation of $\mathbf{u}^{c\prime}$ to test the hypothesis that this balanced wind field is divergent. However, we test this statement with a constant Coriolis parameter to compare with the geostrophic wind with a constant f, as this is divergence free.

In Section 7.1 we outline the objectives for the experiments to calculate the balanced height field increment and the divergent wind components. In Section 7.2.2 we describe briefly the base state that we have chosen as a first test of the numerics and also how we introduce the increment.

We present results for the first experiment in Section 7.3 in the form of plots of the height field but also norm plots in the mid-latitude to compare the eight different solutions that we produce depending on whether or not we have used a constant or variable f.

The results from the second experiment, involving calculating the divergence of the balanced wind field for a constant f, are presented in the form of plots of the divergence of $\mathbf{u}^{c\prime}$ for (5.1), $\alpha = 0, 1$ and 5.2) with $\alpha = 0, 1$ in Section 7.4. We display these for the three test cases. We give conclusions for the experiments in Section 7.5.

7.1 Description of Experiments

As we mention in the introduction to this chapter we perform experiments to calculate the balanced height increment. We use the numerical approximations described in Section 5.2.2 where the result is a sparse square matrix that has to be inverted to find h'.

For the RV method the left hand side of the discrete version of (5.1) is approximated by (5.26), given $\mathbf{u}'$. This is defined in Section 7.2.2. For the PV method we use the central difference approximations to all the terms in the discrete version of (5.1) as this is the numerator of the first term on the right hand side of (5.2). To calculate the numerical approximation to $\bar{\xi}^c$ we use the central differences described in Section 5.2.2 for all the derivatives of $\bar{u}_g$ and $\bar{v}_g$ in (4.68).

For the constant f experiments we multiply throughout by $a^2 f^2 \cos^2\theta$. This is to remove the errors involved with working with small numbers. The term $\frac{1}{a^3} \approx 10^{-18}$ which is small but also the derivatives of the geostrophic winds are around 10^{-6}. For variable f we multiply throughout by $a^2 f^3 \cos^2\theta$. This is to avoid the singularity at the equator due to $f = 0$ there. We are not including the extra terms that arise from the variable f derivatives for these experiments as this is only a first test. This is also to model more physically the underlying flow. This is a Rossby wave and its propagation is dependent

on the Coriolis parameter, [14], [34].

The objective of the first set of experiments is to see whether or not we gain anything by using the extra terms in the balance relation. Therefore we are seeing if the conclusions from Chapter 6 follow through to the calculations. Although the elliptic conditions are for a constant f we also compute the global solutions with a variable f and compare these to the solution with a constant f.

We display the results in the following way: the first set of plots are the solutions for a constant f and variable f with $\alpha = 0$ and 1 for the RV method. The second plots have the same format as for the RV method but now this is for the PV method. The third plot contains $\|h'_f - h'\|_2$ (defined in Section 7.2.2) for each latitudinal ring between $40°N - 60°N$.

The reason for this is to identify whether or not there is any reduction in the norm, $\|h'_f - h'\|_2$, as defined in Chapter 5, between the geostrophic balance and the higher order balances as the underlying assumption about the manifold ($R_0 \ll 1$), is most valid here. We also compare to see if using the PV captures the balance any better. This is due to much discussion about whether or not to use PV as a balance variable, [57].

According to [57], for the low Burger number regimes, TC1, then we should consider the PV, and so we shall also see if this is the case for our test cases. We have seen a change in the ellipticity condition for TC1 with

the PV method compared to the RV method, which is more noticeable than in the other two test cases.

In the second experiment we only consider the constant f case as we are testing the hypothesis that the balanced wind field, which also defines the subspace in the phase space of the shallow water equations, is divergent for constant f.

We calculate $\mathbf{u}^{c\prime}$ through evaluating (4.25) and (4.26) where we calculate the coefficients through the expression that we derive in section 5.2.2. We then calculate the divergence by evaluating (5.27) with $\mathbf{u}^{c\prime}$.

7.2 Incremental Fields

In this section we introduce the choice of base state and increment of h, u and v fields that are used in the experiments described in Section 7.1.

7.2.1 Base State

To calculate our base states we run the shallow water model described in Section 5.2.1 with the three choices for the Rossby-Haurwitz wave, TC1 - TC3, out to 120 hours and use the output of the height, h and the two wind components, u and v at 72 hours into the run.

As a first test we have chosen to use zonal averages as our base state.

This has the affect of removing certain terms in the equations, specifically $\bar{v}_g, \frac{\partial \bar{u}_g}{\partial \lambda}$ and $\frac{\partial \bar{v}_g}{\partial \lambda}$. This does simplify the problem by eliminating the cross derivative terms in the equation but if we have problems with this simple test case then there may be problems with more complicated base states. We calculate the zonal averages by

$$\bar{h}_i = \frac{1}{M} \sum_{j=1}^{M} h_{i,j}, \tag{7.1}$$

$$\bar{u}_i = \frac{1}{M} \sum_{j=1}^{M} u_{i,j}, \tag{7.2}$$

$$\bar{v}_i = \frac{1}{M} \sum_{j=1}^{M} v_{i,j}, \tag{7.3}$$

where the i index represents the latitudinal ring and j the longitude.

Therefore to calculate these base states we have used the numerical values outputted from the three different runs of the shallow water model at 72 hours at the grid points and calculated their averages along each latitudinal ring using (7.1) - (7.3).

From these values we can calculate the geostrophic winds and their derivatives for the linearisation factors in (5.1) and (5.2) as well as the approximation to the left hand sides of the two equations.

With this type of base state we have chosen to use a Dirichlet boundary condition at the two poles for all of the experiments. This condition is $h' = 0$. The reason for this is that although we have a row of points for the pole in the rectangular grid these are representing the same point. We are saying

that at these two points there is no balanced part to the height above the zonal average here.

The other reason for this choice is when we try to implement the condition $\frac{\partial h'}{\partial \lambda} = 0$ the resulting matrix for the discrete problem is singular. The problem of modelling the pole in spherical coordinates is a tricky one. There are many mathematical ideas to cope with the pole, [2] and [49], but we shall use the simple Dirichlet condition as the theory for elliptic equations holds, [8], [11] and[16]. When we use the periodicity condition in the θ direction to calculate $\mathbf{u}^{c\prime}$ at the poles, we use the approximation $\frac{\Delta\theta}{4}$ to $\cos\theta$ as described in [29].

7.2.2 Increments

Given the base state described in Section 7.2 we have the following increments associated with (7.1) - (7.3)

$$h'_f = h - \bar{h}, \tag{7.4}$$

$$u' = u - \bar{u}, \tag{7.5}$$

$$v' = v - \bar{v}. \tag{7.6}$$

We create the increment to the base state left hand side for (5.1) through

$$\xi' \equiv \mathbf{k} \cdot \nabla \times \mathbf{u}' = \mathbf{k} \cdot \nabla \times (\mathbf{u} - \bar{\mathbf{u}}) = \xi - \bar{\xi}, \tag{7.7}$$

where $\mathbf{u}' = (u', v')^T$ and ξ is the full relative vorticity.

For equation (5.2) we calculate the PV left hand side using the full height increment (7.4) and evaluate (4.68) through using the central differences approximations described in Section 5.2.2 to the right hand side of (5.1), which equals the first term in (5.2). We use (7.1) for the denominators in (5.2).

7.3 Results I: Balanced Height Increments

We consider the results for each test case separately but we look at the results for both the RV and PV methods with constant and variable f.

The first figure, 7.1, displays the full height increments, h'_f, for the three test cases. The initial condition of the Rossby-Haurwitz wave is a balanced flow as the time scale associated with this wave is not that of the inertia mode. Therefore we would expect most of the flow to be balanced still. As a result of this the balanced height increment, h', should be similar to h'_f.

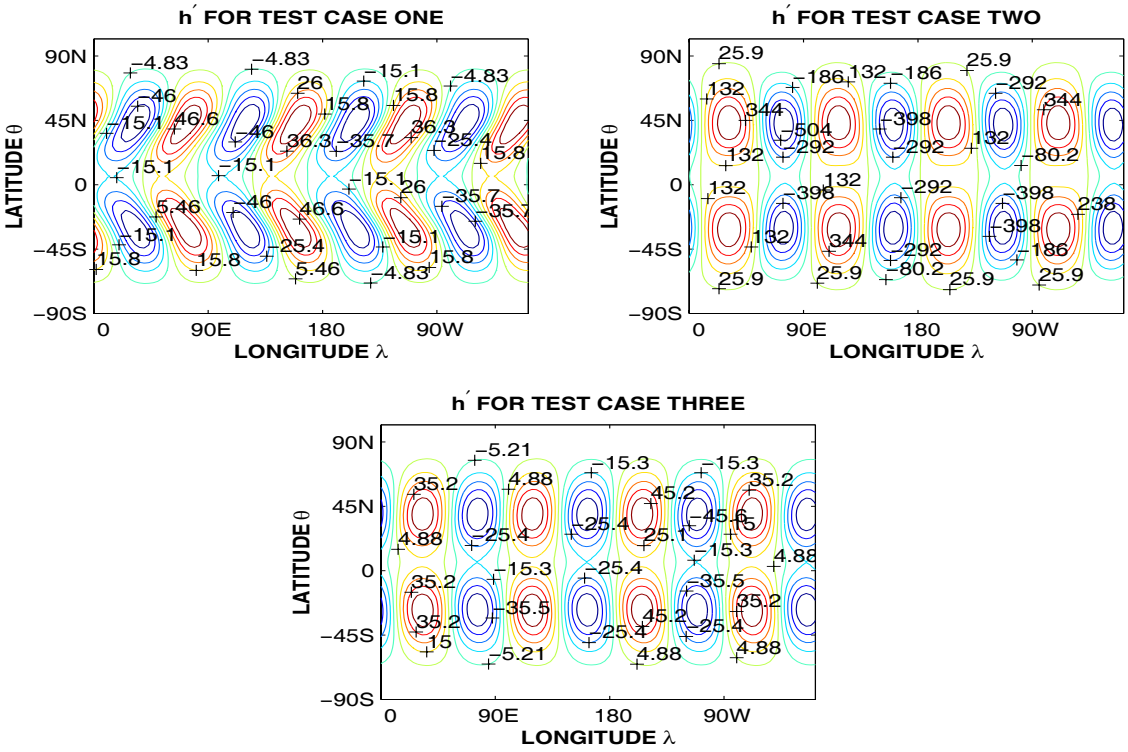

Figure 7.1: Contour Plots of the Three Full Height Increments, h'_f

Figure 7.2 shows the balanced height increment, h', for TC1 using constant f for the left hand plots and variable f for the right. We use the notation of LB to represent linear balance, $\alpha = 0$ and CB for the Charney balance, $\alpha = 1$. We use the RV and PV notation as introduced in Sections 4.3.2 and 4.3.3.

One clear feature is the effect the variable f has for (5.1) on $\alpha = 0$ and 1. We are now able to pick up the structure in the mid-latitudes that is present in the full height increment, (Top left plot in Figure 7.1).

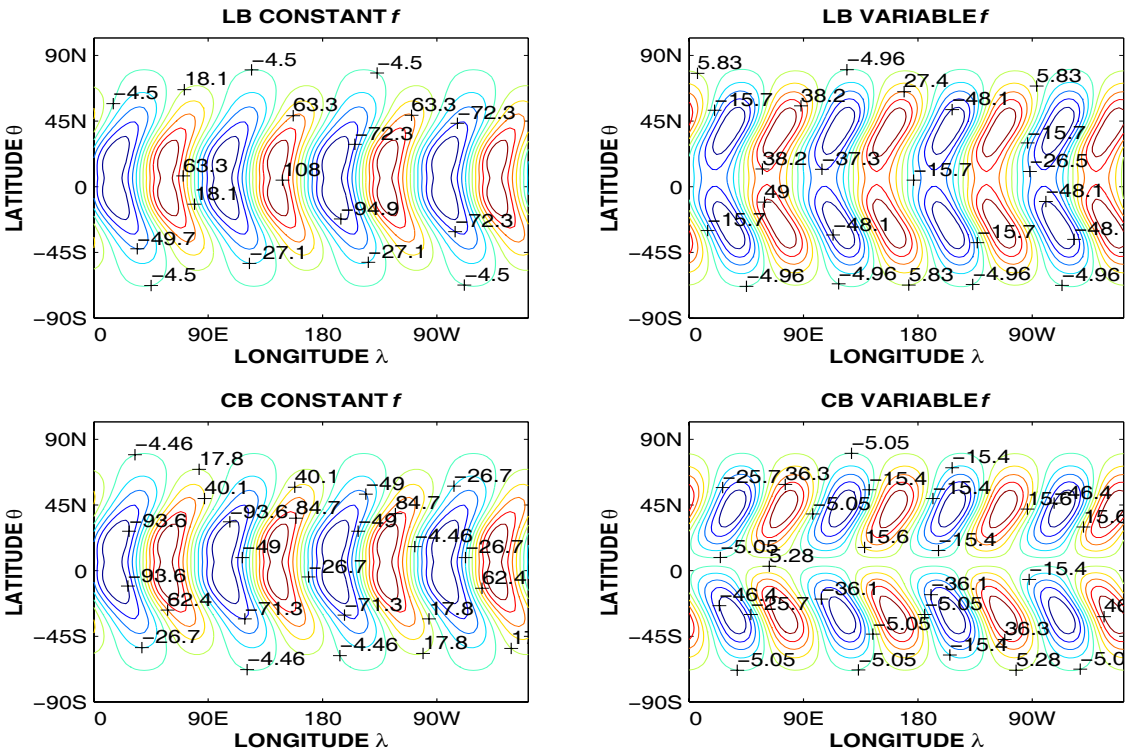

Figure 7.2: Contour Plots of the Numerical Solutions for h' found by the ξ method with $\alpha = 0, 1$ also Constant and Variable f for TC1

What we have to remember is that the numerical problem that we are solving is an elliptic pde and therefore the matrix equation associated with the discretisation has the strongly connected property, [51], [23], [32], [46]. This means that each point in the grid feeds information through the matrix back to all the other points, especially as we have Dirichlet conditions on the poles, [16]. Therefore if we are not correctly scaling the terms by the Coriolis parameter in the equatorial region then the errors are fed throughout the whole discretisation.

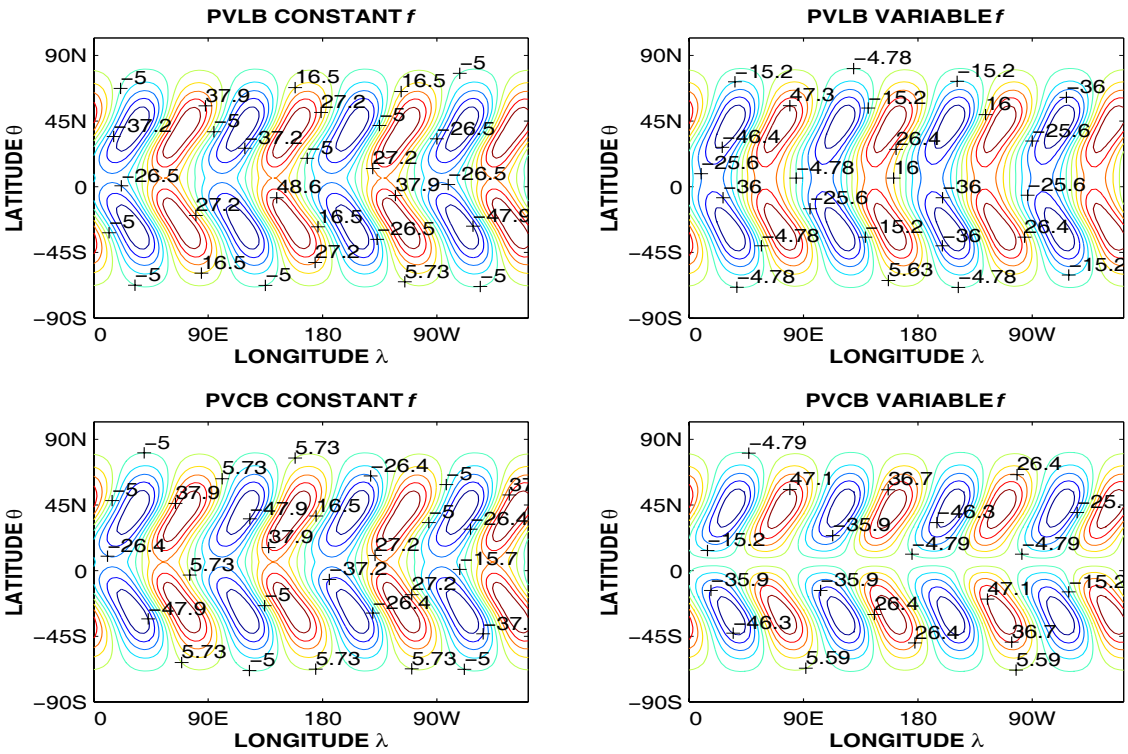

Figure 7.3: Contour Plots of the Numerical Solutions for h' found by the PV method with $\alpha = 0, 1$ also Constant and Variable f for TC1

There is also a meteorological explanation for this feature. As we are modelling a Rossby wave there is a dependence on the Coriolis parameter for the propagation, [19] and as such if we are not correctly using this parameter we would expect discrepancies.

However, if we consider the plots for the PV method, (Figure 7.3), we see that with a constant f we do capture a large part of the wave, for both $\alpha = 0$ and 1. A reason for this, as pointed out in [57], is that for this type of flow, low Burger number, we see that the potential vorticity, for the full field, is

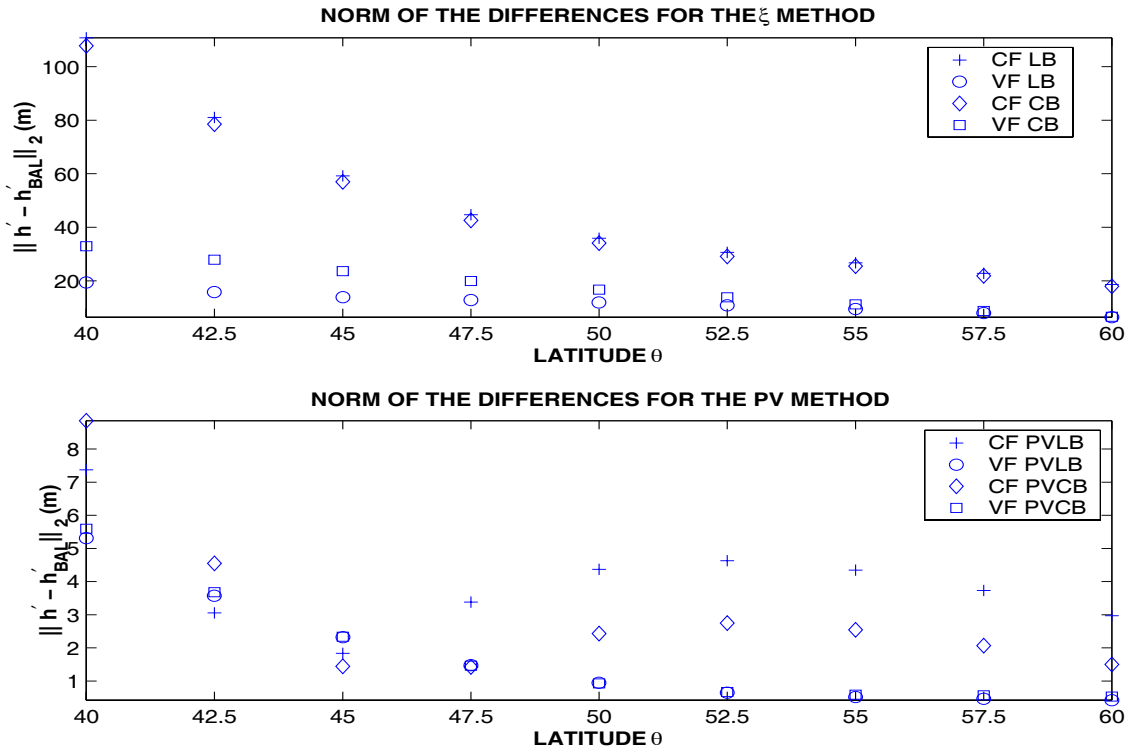

Figure 7.4: Plots of $\|h'_f - h'\|_2$ for TC1 in the Mid-Latitudes, CF represents constant f, VF represents variable f, LB stands for linear balance, $\alpha = 0$, and CB stands for Charney balance, $\alpha = 1$

dominated by the height and not the absolute vorticity. In other words, for this type of flow we would expect the balance to be in the PV and as such if trying to capture this balance flow, then Q is better that ξ as we see here.

The introduction of the variable f does not appear to improve the approximation when considering the PV method but when we look at Figure 7.4 we see that $\|h'_f - h'\|_2$ is reduced for both methods, with the introduction of the correct parameter in the equatorial regions. However, if we compare the

norm of the results for constant f from the PV method we see that the norm for this approximation is smaller than the variable f from the RV method.

For TC2 (see Figure 7.5), we do not have a tilt in the increment that is present in TC1, but the wave from test case two is travelling faster than the wave from test case one also the full height field from test case two grows substantially as we enter the lower latitudes. Although we have removed the $\bar{v}_g$ component from (5.2) and (4.55) along with $\bar{u}_{g\lambda}$ and $\bar{v}_{g\lambda}$ there are still large increases in the height field in the θ direction which could cause an effect on the ellipticity conditions. We do not see that here, as we have a solution that appears to be sensible, but we do again see that with a constant f there does appear to be an effect on the solutions with the under modelling near the equator feeding back into the mid-latitudes. We can see this with the left hand plots in Figure 7.5 where we have the circular formation in the mid-latitudes, (Upper right plot in Figure 7.1), drawn into the equatorial region.

An interesting feature of the constant f plots for the RV method with $\alpha = 1$ is that the circular formation for the full height increment, (top right plot in Figure 7.1), appears to be being dragged further into the equatorial region. When we allow f to vary we see that the motions become quite different. The feature of the mid-latitudes is in the correct place but we have a significant cut off in the balanced height increment near to the equator

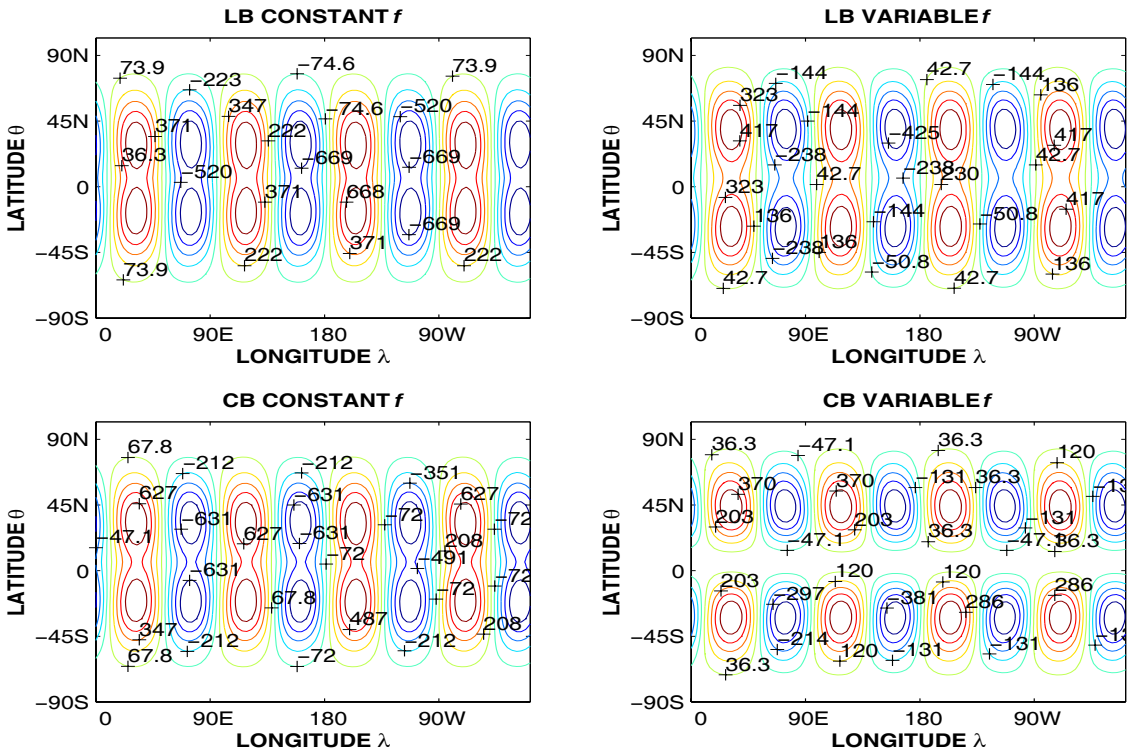

Figure 7.5: Contour Plots of the Numerical Solutions for h' found by ξ method with $\alpha = 0, 1$ also Constant and Variable f for TC2

when $\alpha = 1$.

This balanced wind field, (3.52), can also be understood from a Rossby number asymptotic expansion, [53]. As we enter the equatorial region in TC2 the Rossby numbers are quite large and so we would expect the approximation to break down. For this method the break down appears at higher latitudes than for TC3, (Figure 7.8), where we have the same type of full increment, but the flow is not as fast and also the height is not growing as much. The Rossby number does grow, however, as we approach the equator.

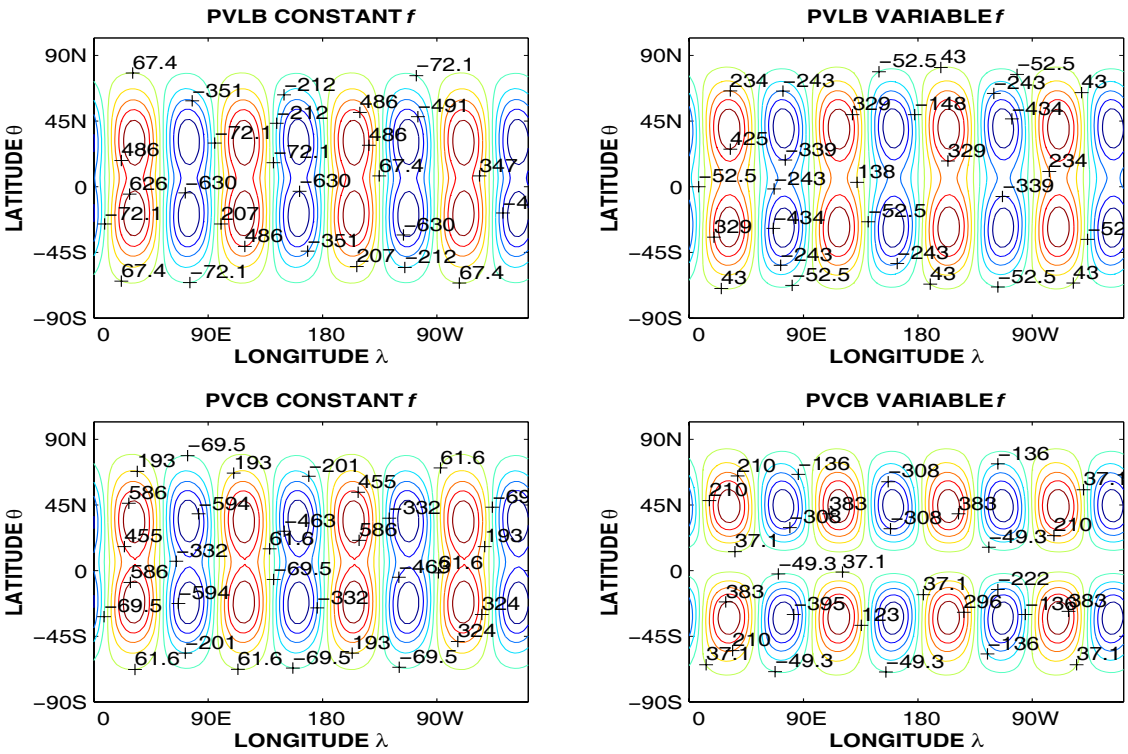

Figure 7.6: Contour Plots of the Numerical Solutions for h' found by PV method, with $\alpha = 0, 1$ also Constant and Variable f for TC2

When we consider the plots for the PV method we see that there is a difference in the position of the heights but there is also a reduction in the heights for the same contours. The balanced increment does appear to be nearer to the full increment using a constant f with the PV methods but the feature of the pulling to the equator is more pronounced in the PVCB plot (Bottom left in Figure 7.6).

When we introduce the variable f we see that the circular formation does return to the mid-latitudes, but for the PV method with $\alpha = 0$ plot,

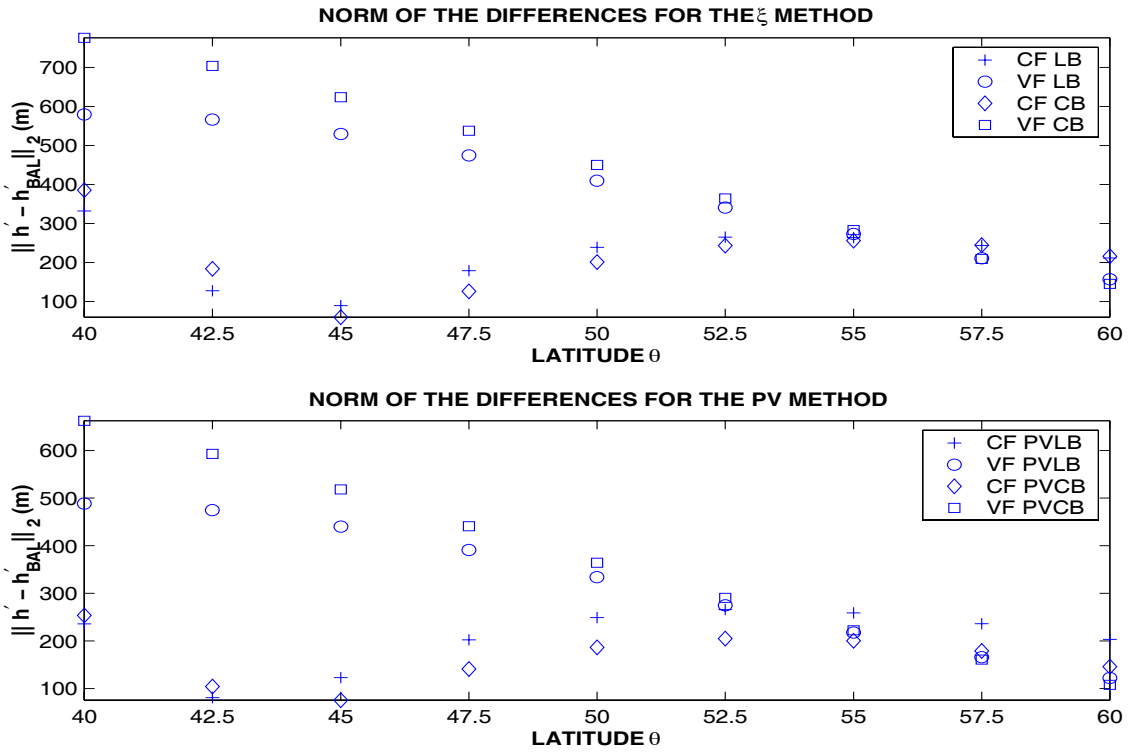

Figure 7.7: Plots of $\|h'_f - h'\|_2$ for TC2 in the Mid-Latitudes, where CF stands for constant f, VF stands for variable f, LB stands for linear balance, $\alpha = 0$ and CB stands for Charney balance, $\alpha = 1$

top right, we see that the curvature of the feature is not picked up by this method. However, for the PVCB method we do get this motion but we have the breakdown again as we come towards the equator.

If we now consider the norm plot for this test case, Figure 7.7, then we see that there is a slight reduction in the difference, although the values on the y axis may appear quite large compared to the values for TC1, Figure 7.4, we recall that the overall height increment is larger to start with than

for TC1 and as such the differences are on a different scale due to the speed and growth in the wave's height.

For the RV method we see that Figure 7.7 would indicate differently the closeness of the solutions with a variable f in the mid-latitudes. With the CB methods there is a smaller difference in the mid-latitude region for both the RV and PV methods. This does also show quite a difference for the PV method.

We now review the results for TC3. This flow is not as fast as that of TC2 but we start from the same mean height, h_0, at the pole of $8000m$. We see that the structure of the full height increment is quite similar to that of TC2 but with a more uniform shape to the circular formation, (Middle plot in Figure 7.1).

As we saw in the scale analysis in Section 6.4 the coefficients are not that large. We also saw from the ellipticity condition (Figure 6.15) there did not appear to be much variation of the condition from that of the Laplacian. Therefore we would not expect much difference in the solutions between $\alpha = 0$ or 1 for constant f for both the RV and PV methods.

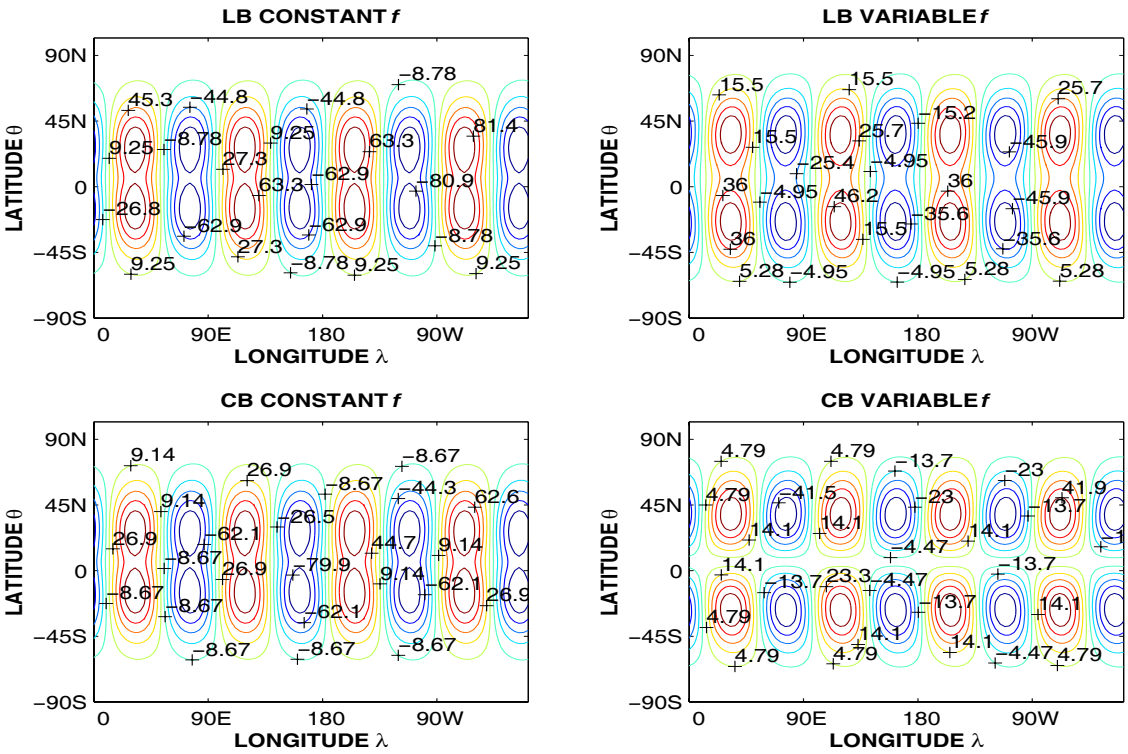

Figure 7.8: Contour Plots of the Numerical Solutions for h' found by the ξ method with $\alpha = 0, 1$, for Constant and Variable f for TC3

We do see this feature in the four plots concerned, left hand side in Figures 7.8 and 7.9, where, as we expect, there is only a slight difference.

Recalling the ellipticity plots for this test case with the initial condition, (Figure 6.6), showed variations in the ellipticity condition as we tend towards the equator. Although for that plot we were using the full fields, the zonal average would reduce the condition more to suggest a use of the Laplacian for this test case.

We do see this for the mid-latitudes when we look at the plot of $\|h'_f - h'\|_2$

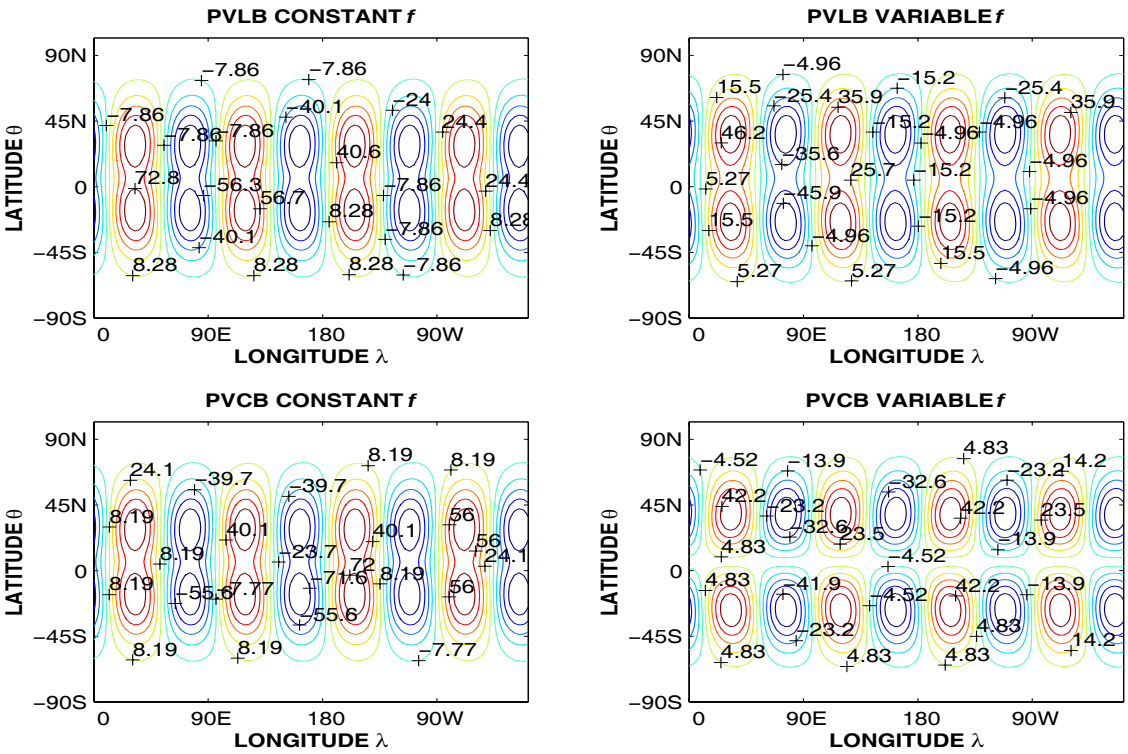

Figure 7.9: Contour Plots of the Numerical Solutions for h' found by the PV method with $\alpha = 0, 1$ for Constant and Variable f for TC3

for this test case, (Figure 7.10), where in the two plots if we consider the four constant cases, $+$ and $\diamond$, we see that through most of the domain the two shapes are on top of each other.

When we allow f to vary then the mid-latitude feature does appear to be in the correct place but we have the cut off again when $\alpha = 1$ for both the RV and PV. With the norm plot we see that the difference here is reduced by the $\alpha = 0$ based methods as we enter the equatorial region but as we reach the higher latitudes we see that the two methods are becoming similar.

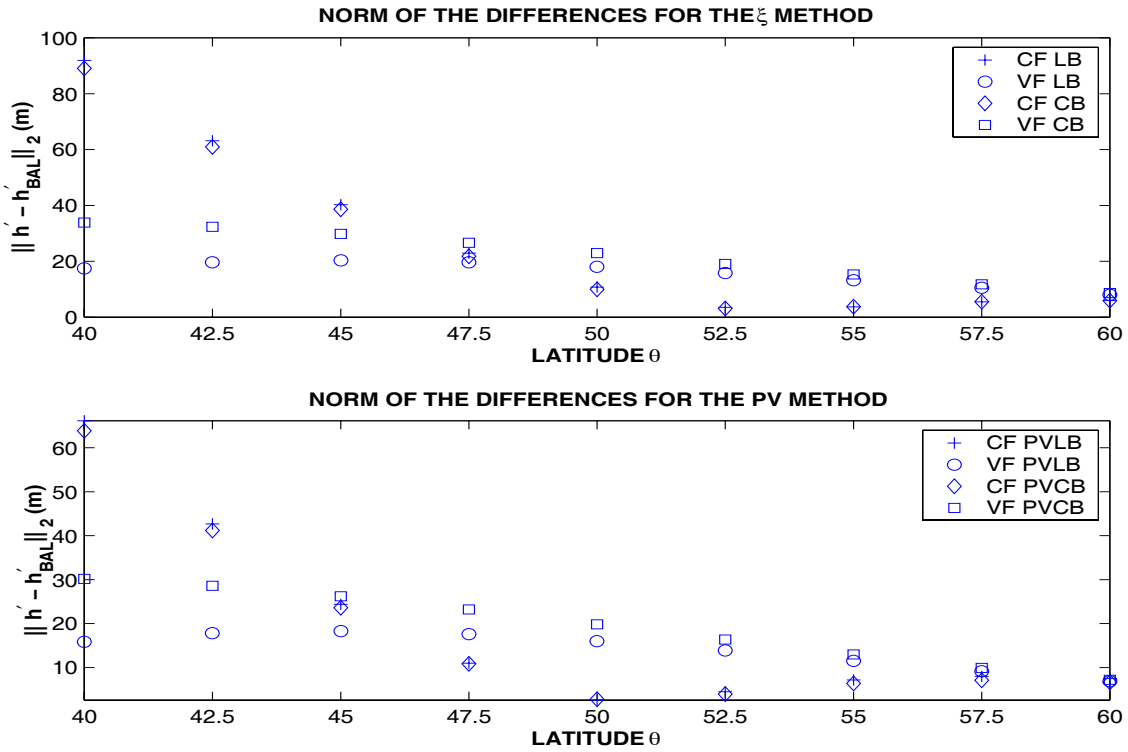

Figure 7.10: Plots of $\|h'_f - h'\|_2$ for TC3 in the Mid-Latitudes, where CF stands for constant f, VF for variable f, LB stands for linear balance, $\alpha = 0$ and CB for Charney balance, $\alpha = 1$

7.4 Results II: Divergent Balanced Wind

In this section we present results that show the linearised balanced wind field, (4.24), is divergent for constant Coriolis parameter, f. We have evaluated the components of $\mathbf{u}^{c\prime}$ through (4.25) and (4.26) using the numerical approximations to evaluate the geostrophic winds at the relevant grid point given in Section 5.2.2.

We consider each test case in turn. As we have seen from the results in Section 7.3, when we use a constant f then the consequences are quite severe for certain test cases. This has an effect on the calculations of $\mathbf{u}^{c\prime}$ due to $\mathbf{u}'_g$ being dependent on the derivatives of h', (4.22).

Before we show the results for the divergences of the wind field we make some comments about the consequences of some of the choices that we make in the numerical modelling. Where we have used a constant f we have changed the sign of this at the equator. Therefore there is an effect on the derivatives of the geostrophic winds with respect to θ. As a result the following plots are shown only between $90°S$ - $10°S$ and $10°N$ - $90°N$, as the effect of the equator over-shadows the results in the mid-latitudes using the contour command in MATLAB.

The consequence of using a zonal average for the base state removes some of the coefficients in (4.25) and (4.26). The new form is

$$u^{c\prime} \equiv u'_g - \frac{\alpha}{f}\left(\frac{\bar{u}_g}{a\cos\theta}\frac{\partial v'_g}{\partial\lambda} + \frac{2\tan\theta}{a}u'_g\bar{u}_g\right), \tag{7.8}$$

$$v^{c\prime} \equiv v'_g + \frac{\alpha}{f}\left(\frac{\bar{u}_g}{a\cos\theta}\frac{\partial u'_g}{\partial\lambda} + \frac{v'_g}{a}\frac{\partial u'_g}{\partial\theta} - \frac{\tan\theta}{a}\bar{u}_g v'_g\right). \tag{7.9}$$

To calculate the divergences we use the expression given in Section 5.2.2, (5.27), using $\mathbf{u}^{c\prime}$ in place of $\mathbf{u}$.

We firstly show the plots of the divergences of the full height increment, $\mathbf{u}'$, defined in Section 7.2.2 (Figure 7.11), as an indicator of how the divergence

of the full increment looks. We have separated the plots in Figures 7.12 -

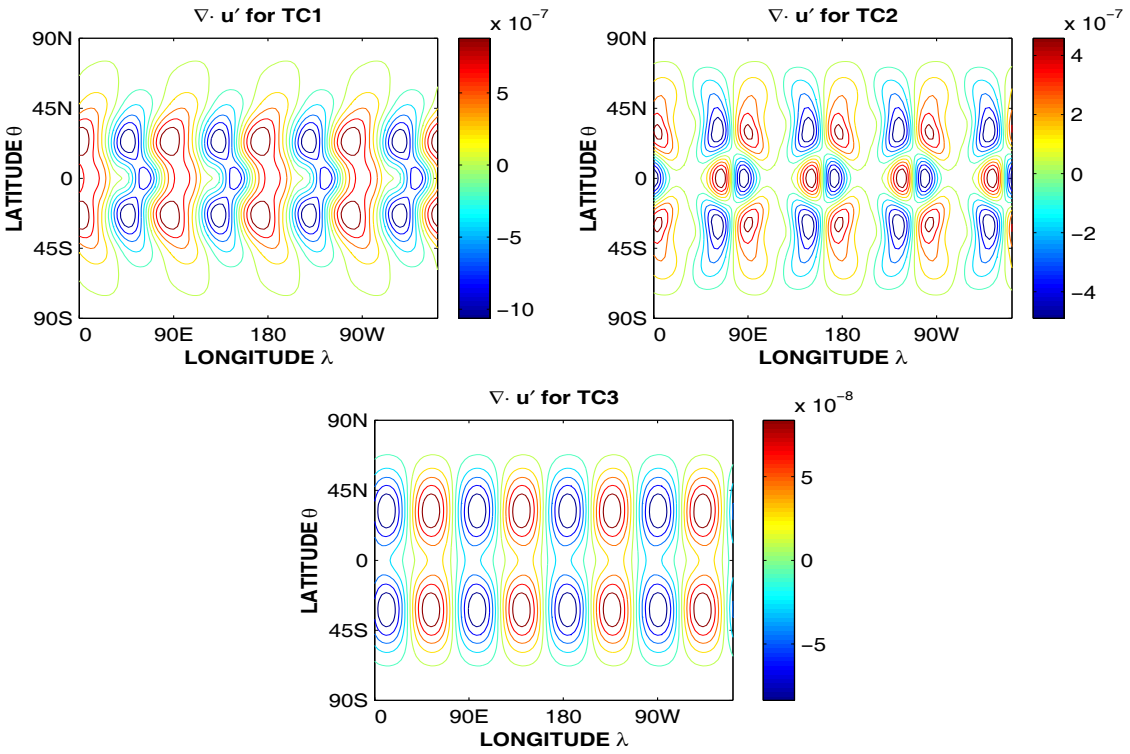

Figure 7.11: Plots of the divergence of the full wind field increment for the Three Test Cases at 72 Hours

7.17 into the Northern and Southern Hemispheres alternately for each test case into RV and PV. The RV results for TC1 are shown in Figure 7.12 and for the PV method in Figure 7.13.

The first feature to notice is that the divergence for the geostrophic wind, $\alpha = 0$ in (4.24), is simply machine random noise, i.e. the scale on the scale bar. This is same for both the RV method and PV method when (5.1) and (5.2) have been solved with $\alpha = 0$ and then h' is used to evaluate the first

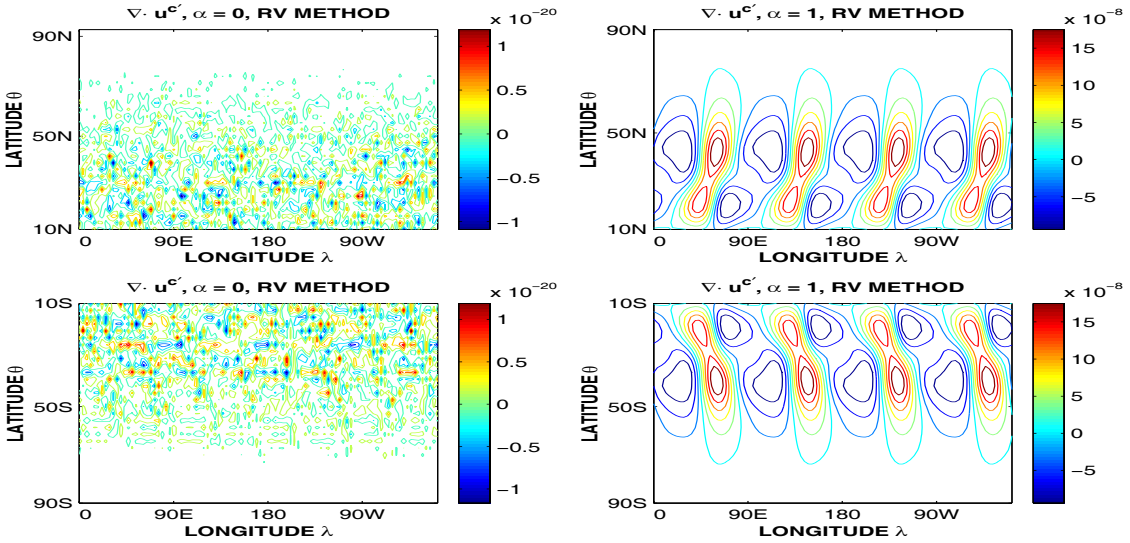

Figure 7.12: Plots of $\nabla \cdot \mathbf{u}^{c\prime}$ with $\alpha = 0, 1$ from RV Method for TC1 at 72hrs

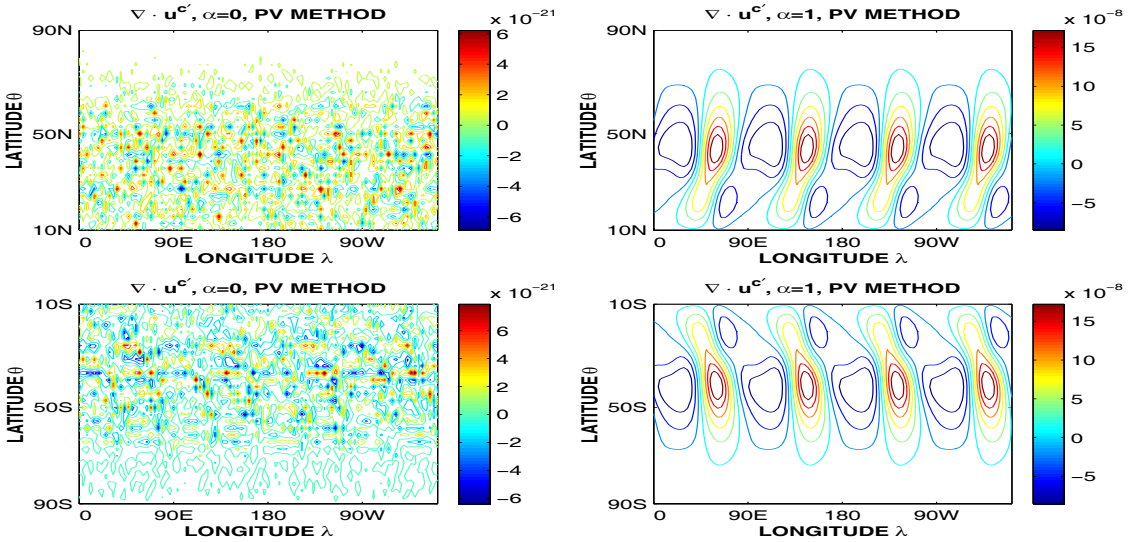

Figure 7.13: Plots of $\nabla \cdot \mathbf{u}^{c\prime}$ with $\alpha = 0, 1$ from PV Method for TC1 at 72hrs

components in (4.25) and (4.26).

Another feature is the difference in the divergences for the $\alpha = 1$ solutions

for the RV and PV method. However, another feature is the fact that the divergence of the balanced wind field is out of phase with the full divergence. We would not expect the whole divergence to be balanced but we have to recall that the heights for this test case when we use a constant f were severely different from the full height field even in the mid-latitudes. This would affect the calculations of $\mathbf{u}^{c\prime}$ as we mentioned earlier in this section. This would cause some of the displacement of the divergence due to the maximum heights being a lot larger than those of the full height increment.

If we now consider TC2 results, (Figures 7.14 and 7.15) then the plots corresponding to the divergence of the geostrophic winds for TC2 are again only showing random machine noise and are 10^{-14} smaller than the results for the higher order balanced wind and have no structure.

Unlike for TC1 the divergence is in phase with the full divergence but for this test case we have the balanced increments divergence larger than that of the full increments. If we recall the size of the height increment for this test case when we use a constant f then we see that there were large differences between the full height increment and the balanced increment even in the mid-latitudes (Figure 7.7).

Therefore, as we have mentioned in the summary of the results for the divergence for TC1, the height field is used to calculate $\mathbf{u}^{c\prime}$ and if this is incorrect then the divergence will be affected as well.

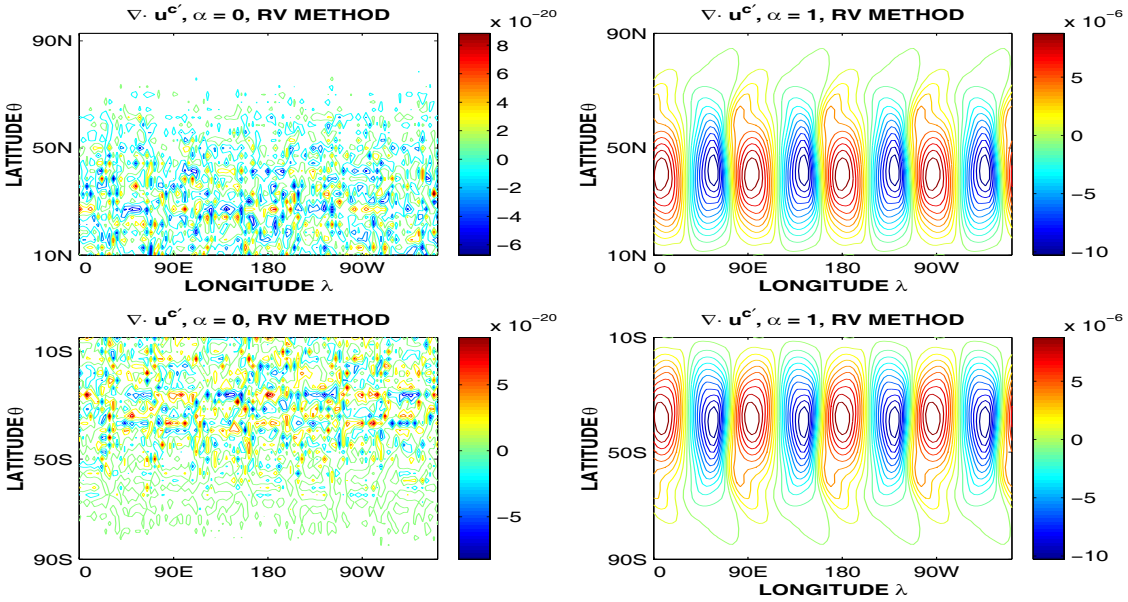

Figure 7.14: Plots of $\nabla \cdot \mathbf{u}^{c\prime}$ with $\alpha = 0, 1$ from RV Method for TC2 at 72hrs

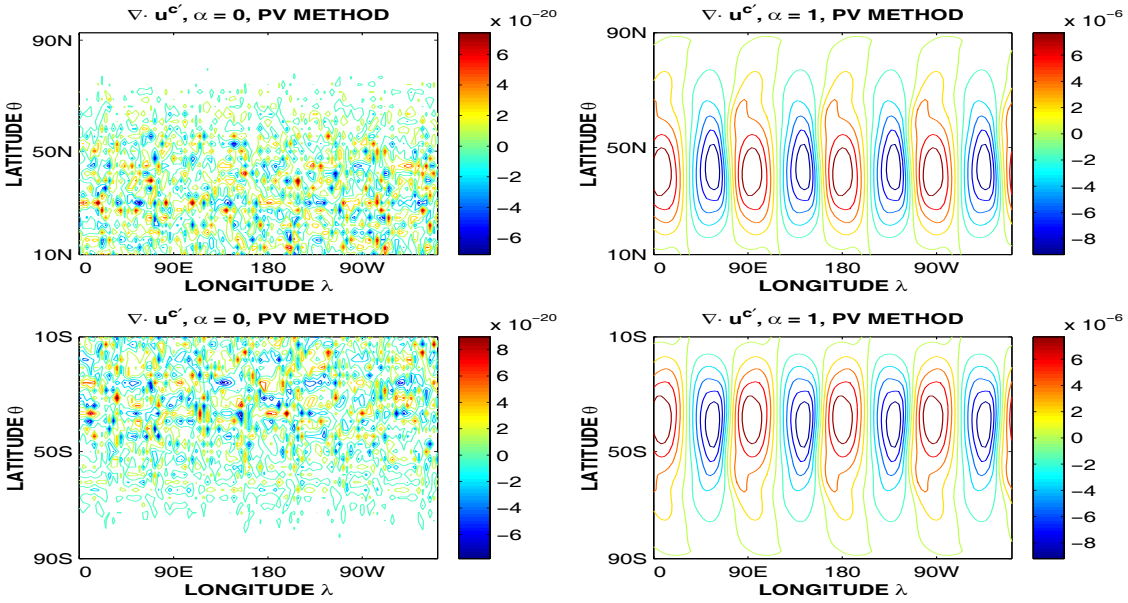

Figure 7.15: Plots of $\nabla \cdot \mathbf{u}^{c\prime}$ with $\alpha = 0, 1$ from PV Method for TC2 at 72hrs

Another feature is the difference between the divergence when $\alpha = 1$ for the RV and PV method. There appears to be a slanting of the divergence in the result for the RV method compared to the result for the equivalent in the PV method. This slanting effect is in the higher latitudes in both the Northern and Southern hemisphere.

If we now consider the final test case, TC3, then we again have the geostrophic winds being divergence free for constant f.

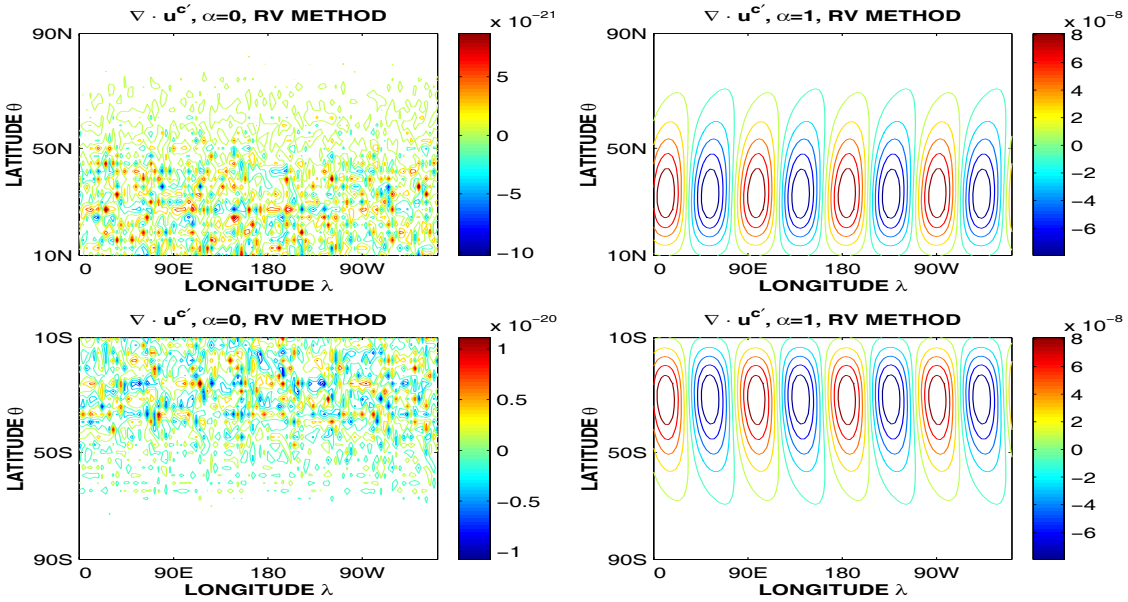

Figure 7.16: Plots of $\nabla \cdot \mathbf{u}^{c\prime}$ with $\alpha = 0, 1$ from RV Method for TC3 at 72hrs

As with TC1 the divergences are out of phase to the full divergence. This test case has the least divergent flow out of the three if we consider the scales in Figure 7.11. This would be consistent with the analysis from the ellipticity condition in Chapter 6. In Chapter 6 we saw that the Laplacian

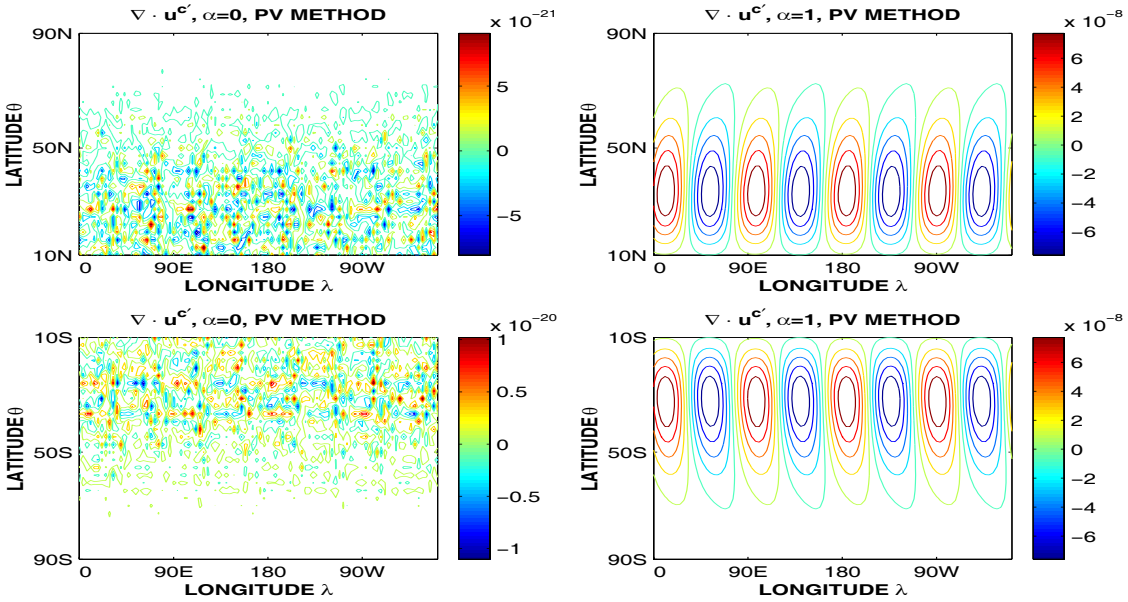

Figure 7.17: Plots of $\nabla \cdot \mathbf{u}^{c\prime}$ with $\alpha = 0, 1$ from PV Method for TC3 at 72hrs

was the dominant term in the equation, which would imply that this flow is quite close to geostrophic balance.

A final comment about the divergence plots is that for TC3 we see that the results from the two equations that have $\alpha = 1$ are the most similar amongst all of the results for the test cases.

7.5 Conclusions

The first conclusion that can be made from these results is that there are serious consequences if we use a constant f in a global solution. The problem arises due to the pde being elliptic and hence all the points in the numerical

approximation are connected. Hence the incorrect modelling in the equatorial regions is fed back to the mid-latitudes through the matrix inversion.

This then raises the problem of dealing with the $\frac{1}{f}$ term at the equator. We must remember that the underlying theory for this balanced subspace of the full phase space assumes that the Rossby number is small, [31], [41].

When we did introduce a variable f there was a noticeable improvement in the approximations. If we consider the results for TC1 in the mid-latitudes (Figure 7.4), then we see that the introduction of the PV instead of RV reduces $\|h'_f - h'\|$, consistent with [57].

The surprising result for TC1 is the test case's divergence for the balanced increment is the only one to be smaller than the full increment. This test case also had the smallest norm of the difference between the full height increment and the balanced increment.

For TC2 we had the variable f not improving the solution very much and for the most part, in the mid-latitudes (Figure 7.7) the RV and PV methods performed better with $\alpha = 0$ than with $\alpha = 1$. TC2 is the most extreme of the three and in the scale analysis we saw that the B^2 terms were of similar magnitude to $4AC$. The choice of base state that we use for these experiments makes the B^2 term zero, which may have affected the solution more for this test case.

However, for TC3 we saw in Section 6.3.2 that the removal of the extra

terms would not affect the solution too much, especially in the mid-latitudes. We also see this in Figure 7.10 where we have for most of the mid-latitudes, the symbols representing the $\alpha = 0$ and $\alpha = 1$ almost always together.

In summary: We have to say that the PV method does improve the approximations to the balanced flow for low Burger number regimes, (TC1). We also see that the effect of constant and variable f is the most severe for this type of flow. For flows similar to TC2 the use of a zonal average does not appear an appropriate choice for the base state as this removes the B^2 term from the ellipticity condition. This does not appear to be the case for TC1. Finally for flows similar to TC3 we would have to say that the inclusion of the extra terms does not gain much extra information for this type of flow when using a zonal average base state.

Chapter 8

Conclusions and Further Work

In this chapter we expand on the conclusion in Chapters 6 and 7 and then suggest some extension to this work in Section 8.2.

8.1 Conclusions

The main aim of this thesis is to see whether or not we could use the balanced wind field derived by Salmon, [41], and extended by McIntyre and Roulstone in [30] and [31] to define a new control variable that defined a balanced wind field that is not divergence free.

We linearised the non-linear version of the balanced wind field, (3.61), around a base state height field resulting in (4.24). From this expression we derive the elliptic partial differential equations to solve for a balanced height,

given either an increment to the relative vorticity or the linearised potential vorticity. If this new method is to be considered as a replacement for the current balanced control variable then we have to see if there is any benefit in the calculation of the extra terms and the extra storage required to calculate the numerical solutions to the elliptic equations (5.1) or (5.2) with $\alpha = 1$.

In Section 6.3 we compare the ellipticity condition for the three test cases at both the initial time and at 72 hrs for both the RV and PV method when $\alpha = 1$ to see if the Laplacian's ellipticity condition was the dominant feature.

For TC1 with the RV method then there appears to be some similarity to the ellipticity condition for the Laplacian in the mid-latitudes, (Figure 6.2).

The scale analysis in Section 6.4 for this method and test case suggested that there were certain terms that could be removed from the ellipticity condition, (Tables 6.2 and 6.3, first column) and also in the analysis of the coefficients in the differential equation, (Table 6.4, first column).

For the PV method with this test case we saw that comparing the initial Laplacian for the PV (Top left in Figure 6.1) with the condition for $\alpha = 1$, (Figure 6.3) then the structure of the condition for $\alpha = 1$ does appear to be similar to that of the condition for $\alpha = 0$, (Figure 6.3) and the same appears to be true for the results at 72 hrs although there is the extra ellipsoid structure that is not present in the results for $\alpha = 1$ initially and at 72 hrs (Figure 6.12).

The scale analysis for the ellipticity condition for this method would conclude that the extra terms are a small factor compared to the Laplacian, (Tables 6.5 and 6.6), in the mid-latitudes with a global constant f. When considering the terms in the differential equation, (Table 6.7), then we saw that the Helmholtz part of the equation dominated the remaining terms and therefore must be included. This would suggest that the PV method should be used for this type of flow. This is consistent with the findings in [57] but with the PV defined in a different manner.

From the numerical results to (5.1) and (5.2) for TC1, (Figures 7.2 and 7.3) then for a constant f the results were not too good with the RV method with either $\alpha = 0$ or 1 but with the PV method we saw major improvements especially in the mid-latitudes, (Figure 7.4) even for constant f.

We saw a cut off when we use a variable f with $\alpha = 1$ in both the RV and PV methods where the asymptotic expansion is no longer valid as the Rossby number is tending to infinity in the equatorial regions. The choice of a zonal average with this test case does not seem to affect the results too severely but the scale analysis suggested that the extra terms may only be a small consequence at 72 hrs.

The balanced wind increment associated with this height increment was divergent but out of phase with the full divergence. (Figures 7.12 and 7.13).

TC2 appears to be the type of flow that requires the extra terms. This

is seen visually in Figures 6.4 and 6.5 at the initial time where there is no structure resembling the ellipticity condition for the Laplacian operator even in the mid-latitudes. This is still true at 72 hours, (Figures 6.13 and 6.14).

The scale analysis in Section 6.4 also suggests that all the terms need to be used in the modelling, although unlike the TC1 case, the Helmholtz part is not dominating the other terms in the mid-latitudes but is comparable with most of the remaining terms.

The use of a zonal average with this type of flow would be not be recommended as the results appeared to be the most affected by this choice, (Figure 7.7). There does also appear not to be any gain by using the PV over the RV, which requires fewer calculations.

The balanced wind field is not divergence free but the increment itself is too large and is consistent with the size of the full height increment for constant f. This is possibly being caused by the choice of zonal average removing all of the cross derivative terms which the scale analysis in Section 6.4 suggested we should not do.

The final test case, representing a high Burger number regime, is the type of flow that would not benefit from the extra terms. At 72 hours, (Figures 6.15 and 6.16) there was a clear similarity between the Laplacian for both methods and the full equations. This was also shown in the scale analysis.

The height increment associated with both the RV and PV method would

suggest that with a constant f there are still problems with the bad modelling of the flow but also the removal of the zonal averaged relative vorticity could be too severe for this flow as well.

The balanced wind field with this test case using a constant f was divergent but too big again, which is consistent with the height increment being too large.

Therefore the final conclusions are that for flows similar to TC1, at low Burger number, the flow should be modelled with the PV method rather than with the RV and that a variable f should be used. There may be some benefit by using the extra terms in this model but more research is needed to see the effects of the zonal average.

For flows similar to TC2 then the extra terms should be included with a variable f, but the linearisation base state should not be the zonal average as this removes the B^2 terms from the ellipticity condition which defies the whole purpose for this flow. It is difficult to say whether or not to use the RV or PV method as there was not much difference between the two, but the choice of base state could be affecting this.

For flows similar to TC3, at high Burger number, it may probably not be worth the extra storage costs and matrix inversion to obtain quite similar results to using $\alpha = 0$. There is not much difference between the results using either the RV or PV method, and as such computationally it may be

economical to use the RV method.

Although these conclusions are for the Burger number we recall the definition given for the number

$$B_u \equiv \frac{\sqrt{gh}}{fL}, \tag{8.1}$$

we see that this is a ratio between the height and the horizontal length scale. There are other factors that have to also be considered. The expansion for the balance wind field is dependent on the Rossby number

$$R_0 \equiv \frac{V_H}{2\Omega L_H}, \tag{8.2}$$

being small. This number is dependent on the ratio of the horizontal wind speed scale and the length scale. Therefore we also have to consider the scale of the winds associated with the flow regime.

We also have to be aware of large changes in the height profile over short distances. This affect the geostrophic winds which are the gradients of the height field with respect to the two horizontal coordinate directions (4.16). These are some of the coefficients in the ellipticity condition but also their gradients as well.

Therefore the Burger number is a good first stage test to see if the flow requires the extra terms but we must also consider the speed of the winds associated with the flow to confirm that the Rossby number is small but also the change in the height over short distances to ensure that the geostrophic

component is small enough to not violate the ellipticity condition.

8.2 Further Work

The choice of base state was a simple first choice to test the numerics that we use to calculate the numerical solutions to the elliptic pde that arose from the balanced subspace in the shallow water equation's full phase space.

Therefore there are many other choices of base states that could be used in the linearisation. One possible choice is to perturb the parameters that define TC1 - TC3 so that the flow has a slightly different Burger number. We would then be linearising about a Burger number regime rather than a zonal average.

This choice would have all the terms that we looked at in Sections 6.3 and 6.4. However, the size of the increments, ξ' and h'_f, could be small. We do not want to perturb the model too much or the theory for the linearisation will not hold.

One way to generate these perturbations would be to increase h_0 at the poles by 10%. That would make $h_0 = 55m$ for TC1 and $h_0 = 8800m$ for TC2 and TC3. There would be more of an effect on TC2 with the new height than for TC3 as we have seen for the original data sets that we use for the experiments in this thesis.

When we were deciding on the base state we considered perturbing the ω parameter by 10% for the two choices used. Due to the properties of the Met Office's shallow water code, [28], when we implemented this to generate a perturbed field there was no difference in the results.

Another choice for the base state is to take the initial conditions for the three test cases and use the differences away from these at different times as the increments. This has the advantage of being a balanced field, which we could linearise about. A twist on this could be to take the fields at 24 hours and linearise about these. There would now be some form of imbalance in the base state, which is a more sensible approximation to how the method could be used operationally. To see the effects of this may require us to take the differences between the initial or 24 hour profiles from the fields at 96 or 120 hours.

Another test would be to use real global data. This could be possible with the data sets available from the National Center of Atmospheric Research (NCAR), [55].

We chose to discretise the equation by a finite difference scheme but we could have used a finite element approach and this could be developed to see what effects the choice of the discrete approximation has on the solutions to equations (5.1) and (5.2). Other choices of boundary conditions could also be investigated to observe if the choice we use is the most robust.

The main area of development for this work would be to introduce the balanced wind field into a limited area model, (LAM). There are plans to introduce a LAM at the Met Office for the North Atlantic this autumn. Constraining the balanced wind field to the mid-latitudes would be a logical step as we assume that the Rossby number is small, [31], [41].

We would then be able to calculate $\mathbf{u}^{c\prime}$ from (4.25) and (4.26), where we have f on the denominator and allow this to vary through the latitudes in the model without becoming zero. The only real concern with this would be boundary conditions for the balanced wind to enter the information from the full model. The matrix inversion would still be that of the numerical approximation to an elliptic boundary value problem and would be sensitive to the boundary conditions imposed on it.

A possible way to overcome the global problem could be to use a streamfunction instead of a height. The first formulation of (5.1) that we consider, not shown here in the thesis, was with a streamfunction. This then removed explicitly the dependence on the Coriolis parameter in the geostrophic winds. Numerical solutions to this problem showed errors as we entered the polar regions. It was also commented whilst attending the 5^{th} Adjoint Workshop in Pennslyvania in 2002 that if this new control variable was to be considered globally then the modelling of the Coriolis parameter should be explicit in the equation. We have seen the consequences effectively when we considered

the constant Coriolis case where we possibly had errors from the equator feeding back to the mid-latitudes, (Section 7.3).

A further suggestion for more work would be to develop a diagnostic test for the balanced height and the control variables described in Section 4.4. A possible means to do this would be to calculate the divergence tendencies for the variables using the technique described in [57].

The benefit of this test would be to see if the balanced and unbalanced control variables are capturing the correct parts of the flow. A balanced control variable should have a divergence tendency that is small.

One final comment is about a technique that was used in a simple form by Sasaki in his two papers in 1958 and 1970, [43] and [44], where he derives a variational approach to a simple cost functional between the observations of the meteorological elements at the grid points and the modified model variables.

He defines a sum of squares with arbitrary weights, α_i^2, to be decided, given by

$$\sum_i \alpha_i^2 \left(f_{0t} - f_i\right)^2 , \tag{8.3}$$

where f_{0t} represents the observations and f_i the state variables. He then defines a functional that has to be minimised over some domain with arbitrary

boundary conditions. This functional is given by

$$I \equiv \int_v \sum_i \alpha_i^2 \left(f_{0t} - f_i\right)^2 \mathrm{d}V. \tag{8.4}$$

Sasaki requires this functional to be minimised and so applies a variation to obtain

$$\delta I \equiv \delta \int_v \sum_i \alpha_i^2 \left(f_{0t} - f_i\right)^2 \mathrm{d}V. \tag{8.5}$$

Sasaki then applies standard calculus of variation techniques, [9], to find the minimum of the functional, (8.4). He introduces the following as the model variables, u, v ϕ and T, where ϕ is the geopotential and T is the absolute temperature.

Next Sasaki substitutes the geostrophic winds in place of the full wind fields and then forms the difference between the full fields and the observations. This then gives the sum of squares as

$$\varepsilon^2 \equiv \alpha_1^2 u'^2 + \alpha_2^1 v'^2 + \alpha_2^2 \phi'^2 + \alpha_3^2 T'^2, \tag{8.6}$$

where the increments are given by

$$u' = -\frac{1}{f}\frac{\partial \phi'}{\partial y} - u_o - \frac{1}{f}\frac{\partial \phi_o}{\partial y}, \tag{8.7}$$

$$v' = \frac{1}{f}\frac{\partial \phi'}{\partial x} - v_o + \frac{1}{f}\frac{\partial \phi_o}{\partial x}, \tag{8.8}$$

$$\phi' = \phi - \phi_0, \tag{8.9}$$

$$T' = \frac{\partial \phi'}{\partial p^*} - T_o + \frac{\partial \phi_o}{\partial p^*}, \tag{8.10}$$

where p^* represents the vertical coordinate system

The resulting Euler equation that minimises (8.4) given (8.6) is

$$\nabla^2\phi' - \left(\frac{\alpha_2}{\alpha_1}f\right)^2 = f\xi_0 - \nabla^2\phi_0, \tag{8.11}$$

where

$$\xi_0 \equiv \frac{\partial v_0}{\partial x} - \frac{\partial u_0}{\partial y}.$$

Sasaki interprets the results of (8.11) as follows: if the right hand side is zero then the modified values are equal to the observed quantities. These observed quantities could be used in numerical prediction routines that are based on a quasi-geostrophic assumption. When the right hand side is not zero solutions to (8.11) gives the deviation of the geopotential. The modified values may be obtained through evaluating (8.9). This again could be used in a numerical weather model using the quasi-geostrophic assumption.

We could modify this procedure by using the equations for either the non-linear version of $\mathbf{u}^c$, (3.61) or the linearised version (4.24). The result should be some form of an equation to ensure that the observations that we use with this new balance would be consistent with the flow being modelled.

There have been signs in this thesis that the new balanced wind field that we have researched could be a viable alternative to the current version of the balanced wind field. As a passing remark we were not able to test

these variables with a data assimilation scheme yet but do see this as an important part of the development of these variables.

Bibliography

[1] K. E. Atkinson. *An Introduction to Numerical Analysis.* Wileys, 1989.

[2] S. R. M. Barros. Multigrid Methods for Two- and Three-Dimensional Poisson-Type Equations on the Sphere. *Journal of Computational Physics*, **92**:313–348, 1991.

[3] G. K. Batchelor. *An Introduction to Fluid Dynamics.* Cambridge University Press, 1967.

[4] G. Browning, A. Kasahara, and H. Kreiss. Initialization of the Primitive equations by the Bounded Derivative Method. *Journal of Atmospheric Science*, **37**:1424–36, 1979.

[5] A. P. Burger. Scale Consideration of Planetary Motions of the Atmosphere. *A Quarterly Journal of Geophysics*, **10**:195–205, 1958.

[6] A. P. Burger. On the Non-Existence of Critical Wavelength in a Continuous Baroclinic Stability Problem. *Journal of Atmospheric Science*, **19**:30–38, 1962.

[7] J. Charney. The use of the Primitive Equations of Motion of the Atmosphere. *Tellus*, **7**:22–26, 1955.

[8] C. R. Chester. *Techniques in Partial Differential Equations.* McGraw-Hill Book Company, 1971.

[9] J. C. Clegg. *Calculus of Variation.* Oliver and Boyd Ltd, 1968.

[10] R. Courant and D. Hilbert. *Methods of Mathematical Physics, Volume One.* Interscience Publishers, Inc, 1953.

[11] R. Courant and D. Hilbert. *Methods of Mathematical Physics, Volume Two: Partial Differential Equations.* Interscience Publishers, Inc, 1962.

[12] W. Cox. *Vector Calculus.* Arnold, 1998.

[13] M. J. P. Cullen and R. J. Purser. An extended Lagrangian Theory of Semi-geostrophic Frontogenesis. *Journal of Atmospheric Sciences*, **41**:1477–1497, 1984.

[14] R. Daley. *Atmospheric Data Analysis.* Cambridge University Press, 1991.

[15] G. Desroziers and J. P. Lafore. A Co-ordinate Transformation for Objective Frontal Analysis. *Monthly Weather Review*, **121**:1531–1553, 1993.

[16] P. R. Garabedian. *Partial Differential Equations.* John Wiley and Sons, 1967.

[17] G. J. Haltiner and R. T. Williams. *Numerical Prediction and Dynamic Metrorology.* John Wiley and Sons, 1980.

[18] B. Haurwitz. The Motion of Atmospheric Disturbances on the Spherical Earth. *Journal of Marine Research*, **3**:254–267, 1940.

[19] J. R. Holton. *An Introduction to Dynamic Meteorology.* Academic Press, 1992.

[20] B. J. Hoskins. Stability of the Rossby-Haurwitz Wave. *Quarterly Journal of the Royal Meteorological Society*, **99**:723–745, 1973.

[21] B. J. Hoskins. The Geostrophic Momentum Approximation and the Semigeostrophic Equations. *Journal of Atmospheric Sciences*, **32**:233–242, 1975.

[22] D. D. Houghton. Derivation of the Elliptic Condition for the Balance Equation in Spherical Coordinates. *Journal of Atmospheric Sciences*, **25**:927–928, 1968.

[23] A. Iserles. *A First Course in the Numerical Analysis of Differential Equations*. Cambridge University Press, 1998.

[24] A. Kasahara. Nonlinear Normal Mode Initialisation and the Bounded Derivative Method. *Monthly Weather Review*, **20**:385–397, 1982.

[25] A. Kasahara. Significance of Non-Elliptic Regions in Balanced Flows of the Tropical Atmosphere. *Reviews of Geophysics and Space Physics*, **110**:1956–1967, 1982.

[26] J. A. Knox. Generalized Nonlinear Balance Criteria and Inertial Stability. *Journal of Atmospheric Sciences*, **54**:967–985, 1997.

[27] A. C. Lorenc. Analysis Methods for Numerical Weather Prediction. *Quarterly Journal of the Royal Meteorological Society*, **112**:1177–1194, 1986.

[28] A. J. Malcolm. Evaluation of the proposed new unified model scheme vs the current unified model scheme on the shallow water equations. Numerical Analysis Report, **1/96**, Department of Mathematics, University of Reading, U.K.

[29] M. H. Mawson. *The Shallow-Water Semi-Geostrophic Equations on the Sphere*. PhD thesis, The University of Reading, 1993.

[30] M. E. McIntyre and I. Roulstone. Hamiltonian balanced models: Constrained, slow manifolds and velocity-splitting. Technical report, Met. Office, U.K., 1996. Forecasting Research Scientific Paper **41**.

[31] M. E. McIntyre and I. Roulstone. Are there higher-accuracy analogues of semi-geostrophic theory? *Newton Institute: Large-Scale Atmosphere-Ocean Dynamics*, **2**: Geometric Methods and Models:301–364, 2002.

[32] K. W. Morton and D. F. Mayers. *Numerical Solution of Partial Differential Equations*. Cambridge University Press, 1996.

[33] J. Paegle and J. N. Paegle. An Efficient and Accurate Approximation to the Balance Wind with Application to Non-Elliptic Data. *Monthly Weather Review*, **102**:838–846, 1974.

[34] J. Pedlosky. *Geophysical Fluid Dynamics*. Springer-Valger, 1979.

[35] N. Phillips. On the Problem of the Initial Data for the Primitive Equations. *Tellus*, **12**:121–126, 1960.

[36] C. G. Rossby. Planetary Flow Patterns in the Atmosphere. *Quarterly Journal of the Royal Meteorological Society*, **66**:68–87, 1940. Supplement.

[37] I. Roulstone and M. J. Sewell. Potential Vorticities in Semi-geostrophic Theory. *Quarterly Journal of the Royal Meteorological Society*, **122**:983–992, 1996.

[38] R. Salmon. Practical use of the Hamilton's principle. *Journal of Fluid Mechanics*, **132**:431–444, 1983.

[39] R. Salmon. New Equations for the Nearly Geostrophic Flow. *Journal of Fluid Mechanics*, **153**:461–477, 1985.

[40] R. Salmon. Hamiltonian Fluid Dynamics. *Annual Review of Fluid Dynamics*, **20**:225–256, 1988.

[41] R. Salmon. Semi-Geostrophic Theory as a Dirac-Bracket Projection. *Journal of Fluid Mechanics*, **196**:345–358, 1988.

[42] R. Salmon. *Lectures on Geophysical Fluid Dynamics*. Oxford University Press, 1998.

[43] Y. Sasaki. An Objective Analysis Based on the Variational Method. *Journal of the Meteorological Society Japan*, **36**:77–88, 1958.

[44] Y. Sasaki. Some Basic Formalisms in Numerical Variational Analysis. *Monthly Weather Review*, **36**:875–883, 1970.

[45] G. J. Shutts. Planetary Semigeostrophic Equations Derived from Hamilton's Principle. *Journal of Fluid Mechanics*, **208**:545–573, 1989.

[46] G. D. Smith. *Numerical Solution of Partial Differential Equations.* Oxford University Press, 3rd Edition, 1999.

[47] C. Snyder, W. C. Skamarock, and R. Rotunno. A Comparison of Primitive-Equation and Semigeostrophic Simulations of Baroclinic Waves. *Journal of Atmospheric Sciences*, **48**:2179–2194, 1991.

[48] M. R. Spiegel. *Vector Analysis, Schaum's Outline.* McGraw Hill, 1959.

[49] P. N. Swarztrauber. The Direct Solution of the Discrete Poisson Equation on the Surface of the Sphere. *Journal of Computational Physics,*, **15**:46–54, 1974.

[50] J. Thurburn and Y Li. Numerical Simulations of the Rossby-Haurwitz Waves. *Tellus*, **52A**:181–189, 2000.

[51] R. S. Varga. *Matrix Iterative Analysis.* Prentice Hill Inc, 1962.

[52] G. Veitch and M. H. Mawson. A Comparison of Inertial Stability Conditions in the Planetary Semi-Geostrophic and Quasi-Equilibrium Models. Technical report, **60**, 2001. Forecasting Research Division, Met. Office, U.K.

[53] T. Warn, O. Bokhove, T. G. Shepherd, and G. K. Vallis. Rossby Number Expansions, Slaving Principles, and Balance Dynamics. *Quarterly Journal of the Royal Meteorological Society,*, :723–739, 1995.

[54] A. A. White. A view of the equations of meteorological dynamics and various approximations. *Newton Institute: Large-Scale Atmosphere-Ocean Dynamics*, **1**: Analytical Methods and Numerical Models, 2002.

[55] D. L. Williamson, J. B. Drake, J. J. Hack, R. Jakob, and P. N. Swartrauber. A Standard Test Set for Numerical Approximations to the Shallow Water Equations in Spherical Geometry. *Journal of Computational Physics.*, **102**:211–224, 1992.

[56] D. L. Williamson and C. Temperton. Normal Mode Initialisation for a Multilevel Grid-Point Model. Part II: Nonlinear Aspects. *Monthly Weather Review*, **109**:744–757, 1981.

[57] M. A. Wlasak. *The Examination of Balanced and Unbalanced Flow Using Potential Vorticity in Atmospheric Modelling.* PhD thesis, University of Reading, 2002.

Appendix A: Spherical Vector Operator

Spherical Unit Vectors

When transforming from Cartesian coordinates to spherical coordinates the direction in which the unit vectors are pointing changes. In spherical coordinates there is a local approximation through a tangential plane relative to the spherical surface, (see figure 8.1).

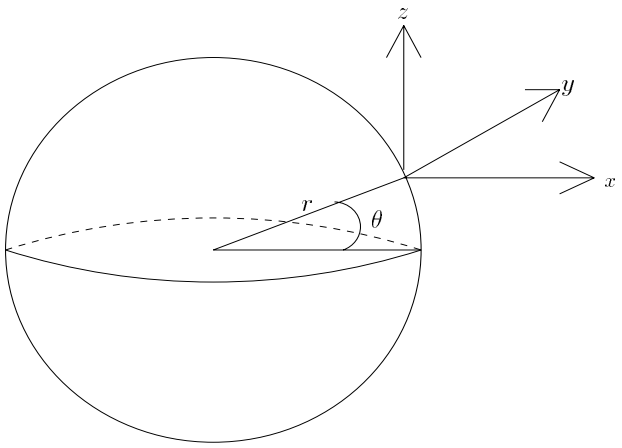

Figure 8.1: Diagram of the tangential coordinates on a spherical surface where r is the radius of the sphere, and the distance laid out from the radius is θ.

It is from this tangential plane approximation that the following nine derivatives for the unit vectors in a 3-D framework arise, [3],

$$\frac{\partial \mathbf{i}}{\partial r} = 0, \quad \frac{\partial \mathbf{i}}{\partial \theta} = 0, \qquad \frac{\partial \mathbf{i}}{\partial \lambda} = -\cos\theta \mathbf{k} + \sin\theta \mathbf{j},$$

$$\begin{aligned}\frac{\partial \mathbf{j}}{\partial r} &= 0, \quad \frac{\partial \mathbf{j}}{\partial \theta} = -\mathbf{k}, \quad \frac{\partial \mathbf{j}}{\partial \lambda} = -\sin\theta \mathbf{i}, \\ \frac{\partial \mathbf{k}}{\partial r} &= 0, \quad \frac{\partial \mathbf{k}}{\partial \theta} = \mathbf{j}, \quad \frac{\partial \mathbf{k}}{\partial \lambda} = \cos\theta \mathbf{i}.\end{aligned}$$

The full derivation of these expression is found in [3]. As we are using a 2-D framework for the SWE then we have a constant radial distance and hence no change along $\mathbf{k}$. This then makes all the terms in the derivtives that contain $\mathbf{k}$ zero. The remaining terms are

$$\frac{\partial \mathbf{i}}{\partial \lambda} = \sin\theta \mathbf{j}, \qquad \frac{\partial \mathbf{j}}{\partial \lambda} = -\sin\theta \mathbf{i}.$$

Spherical Vector Derivative Operators

Here we will list the Cartesian definitions of the vector operators and next to them their spherical co-ordinate counterpart. Let $\boldsymbol{G} = (G_x, G_y, G_z)^T$ for Cartesian coordinates where the subscripts represent their component position in the vector. For spherical coordinates $\boldsymbol{G} = (G_\lambda, G_\theta, G_r)^T$.

The definition of the gradient operator of a scalar function F is given by

$$\nabla F = \mathbf{i}\frac{\partial F}{\partial x} + \mathbf{j}\frac{\partial F}{\partial y} + \mathbf{k}\frac{\partial F}{\partial z},$$

which in spherical coordinates is

$$\nabla F = \frac{\mathbf{i}}{r\cos\theta}\frac{\partial F}{\partial \lambda} + \frac{\mathbf{j}}{r}\frac{\partial F}{\partial \theta} + \mathbf{k}\frac{\partial F}{\partial r}.$$

The next operator is the divergence. This is given for the vector field $\boldsymbol{G}$ by

$$\nabla \cdot \boldsymbol{G} = \frac{\partial G_x}{\partial x} + \frac{\partial G_y}{\partial y} + \frac{\partial G_z}{\partial z},$$

and in spherical coordinates is given by

$$\nabla \cdot \boldsymbol{G} = \frac{1}{r^2 \cos\theta} \left\{ \frac{\partial r G_\lambda}{\partial \lambda} + \frac{\partial r \cos\theta G_\phi}{\partial \theta} + \frac{\partial r^2 \cos\theta G_r}{\partial r} \right\}.$$

The curl is defined as

$$\begin{aligned} \nabla \times \boldsymbol{G} = \left(\frac{\partial G_z}{\partial y} - \frac{\partial G_y}{\partial z} \right) \mathbf{i} - \left(\frac{\partial G_z}{\partial x} - \frac{\partial G_x}{\partial z} \right) \mathbf{j} \\ + \left(\frac{\partial G_y}{\partial x} - \frac{\partial G_x}{\partial y} \right) \mathbf{k}, \end{aligned}$$

which in spherical coordinates is given by

$$\begin{aligned} \nabla \times \boldsymbol{G} = \frac{\mathbf{i}}{r} \left(\frac{\partial G_r}{\partial \theta} - \frac{\partial r G_\theta}{\partial r} \right) + \frac{\mathbf{j}}{r \cos\theta} \left(\cos\theta \frac{\partial r G_\lambda}{\partial r} - \frac{\partial G_r}{\partial \lambda} \right) \\ + \frac{\mathbf{k}}{r \cos\theta} \left(\frac{\partial G_\theta}{\partial \lambda} - \frac{\partial \cos\theta G_\lambda}{\partial \theta} \right). \end{aligned}$$

Finally the Laplacian of the scalar field F is given by

$$\nabla^2 F = \frac{\partial^2 F}{\partial x^2} + \frac{\partial^2 F}{\partial y^2} + \frac{\partial^2 F}{\partial z^2},$$

which is

$$\nabla^2 F = \frac{1}{r^2 \cos^2\theta} \frac{\partial^2 F}{\partial \lambda^2} + \frac{1}{r^2} \frac{\partial^2 F}{\partial \theta^2} + \frac{\partial^2 F}{\partial r^2} - \frac{\tan\theta}{r^2} \frac{\partial F}{\partial \theta} + \frac{2}{r} \frac{\partial F}{\partial r},$$

in spherical coordinates. The spherical Jacobian is given by

$$\frac{\partial (G_\lambda, G_\theta)}{\partial (\lambda, \theta)} = \frac{1}{a \cos\theta} \frac{\partial G_\lambda}{\partial \lambda} \left(\frac{1}{a} \frac{\partial G_\theta}{\partial \theta} \right) - \frac{1}{a} \frac{\partial G_\theta}{\partial \lambda} \left(\frac{1}{a \cos\theta} \frac{\partial G_\lambda}{\partial \lambda} \right)$$

A full explanation for all the operators can be found in [48].

Appendix B: Geostrophic Wind Identities

In Chapter 4 we use three different identities involving the θ derivatives of vg and here in this appendix we will show the derivation to these results. We begin with $\frac{\partial v_g}{\partial \theta}$

$$\frac{\partial v_g}{\partial \theta} = \frac{\partial}{\partial \theta}\left(\frac{g}{af\cos\theta}\frac{\partial h}{\partial \lambda}\right) = \overbrace{\frac{g\tan\theta}{af\cos\theta}\frac{\partial h}{\partial \lambda}}^{T_1} + \overbrace{\frac{g}{af\cos\theta}\frac{\partial^2 h}{\partial\theta\partial\lambda}}^{T_2} + \overbrace{\frac{g}{a\cos\theta}\frac{\partial h}{\partial\lambda}\frac{\partial}{\partial\theta}\left(\frac{1}{f}\right)}^{T_3}.$$

We can see that T_1 is simply $\tan\theta v_g$, T_2 is $-\frac{1}{\cos\theta}\frac{\partial u_g}{\partial\lambda}$, the third term, T_3 is almost v_g but we are missing the f^{-1} term so then this term is $fv_g\Gamma_1$, where Γ_1 is as defined in Chapter 4. We now consider the second order derivatives. We start with

$$\frac{\partial^2 v_g}{\partial\theta\partial\lambda} = \frac{\partial}{\partial\theta}\left(\frac{g}{af\cos\theta}\frac{\partial^2 h}{\partial\lambda^2}\right) = \overbrace{\frac{g\tan\theta}{af\cos\theta}\frac{\partial^2 h}{\partial\lambda^2}}^{T_1} + \overbrace{\frac{g}{af\cos\theta}\frac{\partial^3 h}{\partial\theta\partial\lambda^2}}^{T_2} + \overbrace{\frac{g}{a\cos\theta}\frac{\partial^2 h}{\partial\lambda^2}\frac{\partial}{\partial\theta}\left(\frac{1}{f}\right)}^{T_3}.$$

This now gives for T_1 here $\tan\theta\frac{\partial v_g}{\partial\lambda}$, T_2 is $-\frac{1}{\cos\theta}\frac{\partial^2 u_g}{\partial\lambda^2}$ and T_3 is $f\frac{\partial v_g}{\partial\lambda}$. The final identitiy is a little harder to derive but it starts from

$$\begin{aligned}\frac{\partial^2 v_g}{\partial\theta^2} &= \frac{\partial}{\partial\theta}\left(\frac{\partial}{\partial\theta}\left(\frac{g}{af\cos\theta}\frac{\partial h}{\partial\lambda}\right)\right)\\ &= \frac{\partial}{\partial\theta}\left(\frac{g\tan\theta}{af\cos\theta}\frac{\partial h}{\partial\lambda} + \frac{g}{af\cos\theta}\frac{\partial^2 h}{\partial\theta\partial\lambda} + \frac{g}{a\cos\theta}\frac{\partial h}{\partial\lambda}\frac{\partial}{\partial\theta}\left(\frac{1}{f}\right)\right)\end{aligned}$$

which gives

$$\frac{\partial^2 v_g}{\partial\theta^2} = \overbrace{\left(\frac{g}{af\cos^3\theta} + \frac{g\tan^2\theta}{af\cos\theta}\right)\frac{\partial h}{\partial\lambda}}^{T_1} + \overbrace{\frac{2g\tan\theta}{af\cos\theta}\frac{\partial^2 h}{\partial\theta\partial\lambda}}^{T_2} + \overbrace{\frac{g}{fa\cos\theta}\frac{\partial^3 h}{\partial\theta^2\partial\lambda}}^{T_3}$$

$$+ \underbrace{\frac{2g\tan\theta}{a\cos\theta}\frac{\partial h}{\partial\lambda}\frac{\partial}{\partial\theta}\left(\frac{1}{f}\right)}_{T_4} + \underbrace{\frac{2g}{a\cos\theta}\frac{\partial^2 h}{\partial\theta\partial\lambda}\frac{\partial}{\partial\theta}\left(\frac{1}{f}\right)}_{T_5} + \underbrace{\frac{g}{a\cos\theta}\frac{\partial^2}{\partial\theta^2}\left(\frac{1}{f}\right)}_{T_6}.$$

Therefore T_1 becomes $(2\tan^2\theta + 1)\, v_g$ where we have used the trig identity, $\sec^2\theta = \tan^2\theta + 1$. The second term, T_2 is $-\frac{\tan\theta}{\cos\theta}\frac{\partial u_g}{\partial\lambda}$, where T_3 is $-\frac{1}{\cos\theta}\frac{\partial^2 u_g}{\partial\lambda\partial\theta}$. The fourth term, T_4 is $2f\tan\theta v_g\Gamma_1$ and the fifth term, T_5, is $-\frac{2}{\cos\theta}\frac{\partial u_g}{\partial\lambda}\Gamma_1$. The final term, T_6 is $f v_g\Gamma_2$.

Appendix C: Rossby-Haurwitz Wave's Derivatives

In this appendix we list the derivatives for the A, B and C terms in the definition of the Rossby-Haurwitz wave with respect to θ.

We begin with the A term. This derivative is

$$\begin{aligned}
\frac{\partial A}{\partial \theta} &= -\omega\left(2\Omega+\omega\right)\sin\theta\cos\theta - \frac{RK^2}{2}\sin\theta\cos^{2R-1}\theta\left[\left(R+1\right)\cos^2\theta\right. \\
&+ \left.\left(2R^2-R-2\right)-2R^2\cos^{-2}\theta\right] \\
&- \frac{K^2}{4}\cos^{2R}\theta\left[2\left(R+1\right)\sin\theta\cos\theta+4R^2\frac{\tan\theta}{\cos^2\theta}\right], \\
\frac{\partial B}{\partial \theta} &= -\frac{2R\left(\Omega+\omega\right)K}{\left(R+1\right)\left(R+2\right)}\sin\theta\cos^{R-1}\theta\left[\left(R^2+2R+2\right)-\left(R+1\right)^2\cos^2\theta\right] \\
&+ \frac{4\left(\Omega+\omega\right)K}{\left(R+1\right)\left(R+2\right)}\left(R+1\right)^2\sin\theta\cos^{R+1}\theta, \\
\frac{\partial C}{\partial \theta} &= -\frac{RK^2}{2}\sin\theta\cos^{2R-1}\theta\left[\left(R+1\right)\cos^2\theta-\left(R+2\right)\right] \\
&- \frac{\left(R+1\right)K^2}{2}\cos^{2R+1}\theta\sin\theta.
\end{aligned}$$

For the second derivatives of the A term we shall break this down into smaller parts to make things easier. We denote the parts as

$$\begin{aligned}
A_1 &= -\omega\left(2\Omega+\omega\right)\sin\theta\cos\theta, \\
A_2 &= -\frac{RK^2}{2}\sin\theta\cos^{2R-1}\theta\left[\left(R+1\right)\cos^2\theta+\left(2R^2-R-2\right)-2R^2\cos^{-2}\theta\right], \\
A_3 &= -\frac{K^2}{4}\cos^{2R}\theta\left[2\left(R+1\right)\sin\theta\cos\theta+4R^2\frac{\tan\theta}{\cos^2\theta}\right].
\end{aligned}$$

Therefore we have

$$\begin{aligned}
\frac{\partial A_1}{\partial\theta} &= -\omega\left(2\Omega+\omega\right)\left(\cos^2\theta-\sin^2\theta\right),\\
\frac{\partial A_2}{\partial\theta} &= \frac{RK^2}{2}\left(\left(2R-1\right)\sin^2\theta\cos^{2R-2}\theta-\cos^{2R}\theta\right)\left[\left(R+1\right)\cos^2\theta\right.\\
&+ \left.\left(2R^2-R-2\right)-2R^2\cos^{-2}\theta\right]-\frac{RK^2}{2}\sin\theta\cos^{2R-1}\theta\left[-2\left(R+1\right)\sin\theta\cos\theta\right.\\
&- \left.\frac{4R^2\tan\theta}{\cos^2\theta}\right],\\
\frac{\partial A_3}{\partial\theta} &= \frac{RK^2}{2}\sin\theta\cos^{2R-1}\theta\left[2\left(R+1\right)\sin\theta\cos\theta+4R^2\frac{\tan\theta}{\cos^2\theta}\right]-\frac{K^2}{4}\cos^{2R}\theta\\
&\left[2\left(R+1\right)\left(\cos^2\theta-\sin^2\theta\right)+\frac{4R^2}{\cos^4\theta}+\frac{4R^2\tan^2\theta}{\cos^2\theta}\right]
\end{aligned}$$

We also break the B term into smaller parts as follows

$$\begin{aligned}
B_1 &= -\frac{2R\left(\Omega+\omega\right)K}{\left(R+1\right)\left(R+2\right)}\sin\theta\cos^{R-1}\theta\left[\left(R^2+2R+2\right)-\left(R+1\right)^2\cos^2\theta\right],\\
B_2 &= \frac{4\left(\Omega+\omega\right)K}{\left(R+1\right)\left(R+2\right)}\left(R+1\right)^2\sin\theta\cos\theta.
\end{aligned}$$

This then gives the derivatives as

$$\begin{aligned}
\frac{\partial B_1}{\partial\theta} &= -\frac{2R\left(\Omega+\omega\right)K}{\left(R+1\right)\left(R+2\right)}\left(\left(\cos^R\theta-\left(R-1\right)\sin^2\theta\cos^{R-2}\theta\right)\right.\\
&\left.\left[\left(R^2+2R+2\right)-\left(R+1\right)^2\cos^2\theta\right]-2\left(R+1\right)^2\sin^2\theta\cos^R\theta\right),\\
\frac{\partial B_2}{\partial\theta} &= \frac{4\left(\Omega+\omega\right)K}{\left(R+1\right)\left(R+2\right)}\left(\cos^{R+2}\theta\sin\theta-\left(R+1\right)\cos^R\theta\sin^2\theta\right).
\end{aligned}$$

The final derivative is given for C as

$$\begin{aligned}
\frac{\partial^2 C}{\partial\theta^2} &= -\frac{K^2R}{2}\left(\cos^{2R}\theta-\left(2R-1\right)\sin^2\theta\cos^{2R-2}\theta\right)\left[\left(R+1\right)\cos^2\theta-\left(R+2\right)\right]\\
&+ R\left(R+1\right)K^2\sin^2\theta\cos^{2R}\theta-\frac{K^2\left(R+1\right)}{2}\left(\cos^{2R+2}\theta-\left(2R+1\right)\cos^{2R}\theta\sin\theta\right).
\end{aligned}$$